

Penguin Loops for Nonleptonic B -Decays in the Standard Model: Is There a Penguin Puzzle?

Ambar Jain,¹ Ira Z. Rothstein,² and Iain W. Stewart¹

¹*Center for Theoretical Physics, Massachusetts Institute of Technology, Cambridge, MA 02139*

²*Department of Physics, Carnegie Mellon University, Pittsburgh, PA 15213*

We compute standard model penguin amplitudes in nonleptonic B -decays to light charmless mesons using tree amplitude data to fix hadronic parameters. The leading calculation is carried out for the $\alpha_s(m_b)$ penguin contributions from charm quark, up quark, and magnetic penguin loops in the NDR and HV renormalization schemes. Power suppressed penguins that are proportional to the chiral condensate are also computed using a new factorization formula for these terms, which is derived working to all orders in $\alpha_s(\sqrt{m_b\Lambda})$. We demonstrate using SCET₁ that this formula exhibits only small perturbative phases and does not have endpoint singularities. Due to our use of data to fix hadronic parameters we obtain significantly more accurate predictions for the short-distance standard model penguin amplitudes than have been found in the past. Analyzing data in $B \rightarrow \pi\pi$, $B \rightarrow K\pi$, and $B \rightarrow \rho\rho$ for the penguin amplitudes we find that standard model short-distance imaginary parts are an order of magnitude smaller than current measurements, while real parts are up to a factor of two smaller with the correct sign. This difference is most likely a consequence of long-distance charm contributions or new physics. Constraints on the type of new physics that could help explain the data are derived, and used to show that current data favors sizeable long-distance strong phases.

I. INTRODUCTION

B -physics experiments have made considerable progress in improving our understanding of standard model CP violation [1]. Several analyses have fairly small theoretical uncertainty and yield precise results, such as $\sin(2\beta)$ from $B \rightarrow J/\Psi K_s$ or $B \rightarrow \eta' K_s$ type-decays. However, for a large number of observables, extracting short-distance information depends upon our ability to handle QCD effects. Many of these observables are sensitive to new physics, and thus considerable effort has gone into understanding how to calculate strong decay amplitudes with controlled approximations [2]. Examples of the type of observables are the magnitude and relative strong phase of penguin contributions in charmless non-leptonic B -decays, $B \rightarrow \pi\pi, K\pi, \rho\rho$ etc, which have significant contributions from loop-dominated penguin amplitudes.

In this paper we classify standard model contributions to penguin amplitudes using the SCET factorization theorem for nonleptonic decays from Ref. [3], and compute a missing set of $\mathcal{O}(\alpha_s(m_b))$ short-distance perturbative corrections. (These missing corrections were also recently computed in Ref. [35], and we compare results at the end.) In principle these corrections have the potential of making up for an observed shortfall in explaining the penguin amplitude data with leading order strong phases. However, we find that these contributions to the amplitudes are quite small. We also derive a new factorization theorem for “chirally enhanced” penguin amplitudes, which are suppressed by $1/m_b$ but enhanced by the chiral condensate. Our result involves a new generalized form factor $\zeta_\chi^{BM}(z)$ and a single twist-3 meson distribution

$\phi_{pp}^M(u)$, and it does not suffer from endpoint divergences. We find that these contributions also have small imaginary contributions. Indeed, all known imaginary short-distance corrections to the penguin amplitudes are small, roughly an order of magnitude below the experimental values in $B \rightarrow \pi\pi$ decays and $B \rightarrow K\pi$ decays. Explanations for this discrepancy from long-distance standard model contributions are critiqued and weighed against a beyond the standard model explanation.

In the standard model the amplitude for a channel $\bar{B} \rightarrow M_1 M_2$ may be written as

$$A^{M_1 M_2} = \lambda_u^{(f)} T^{M_1 M_2} + \lambda_c^{(f)} P^{M_1 M_2}, \quad (1)$$

with $\lambda_p^{(f)} = V_{pb} V_{pf}^*$, and where we use CKM unitarity to remove $V_{tb} V_{tf}^*$ ($f = d$ or $f = s$). In this paper $T^{M_1 M_2}$ and $P^{M_1 M_2}$ will be called tree and penguin amplitudes respectively. We derive amplitudes for all two-body pseudoscalar and vector modes that do not involve isosinglets in the final state. In comparing with experimental penguin amplitudes extracted from data, we focus on the $B \rightarrow \pi\pi$, $B \rightarrow K\pi$, and $B \rightarrow \rho\rho$ channels.

With the latest data one may extract values for the penguin amplitudes in the $B \rightarrow \pi\pi$ and $B \rightarrow \rho\rho$ channels using isospin symmetry. Isospin implies that $P^{\pi^+\pi^-}$ also appears in the $\pi^0\pi^0$ channel, and is absent for $\pi^0\pi^-$ (up to small electroweak penguin terms [4, 5]). The same is true for $P^{\rho^+\rho^-}$ (using the fact that the ρ 's are measured to be primarily longitudinal, $f_L^{\rho^+\rho^-} \simeq 98\%$ and $f_L^{\rho^0\rho^0} \simeq 91\%$ [6], and neglecting interference due to the large rho width [7]). To quote experimental values for the penguin amplitudes one must pick a phase convention. We take $T^{\pi^+\pi^-}$ and $T^{\rho^+\rho^-}$ to be real and positive, and quote

other phases relative to this. For the penguins we will quote results for

$$P^{\pi\pi} \equiv -P^{\pi^+\pi^-}, \quad P^{K\pi} \equiv -P^{\pi^+K^-}, \quad P^{\rho\rho} \equiv -P^{\rho^+\rho^-}, \quad (2)$$

etc. In addition, we must also fix the value of the well-determined weak phase $\beta = 21.2^\circ$ [1] and the less well determined weak phase γ . The latest global CKM fits give [8, 9]

$$\gamma_{\text{global}}^{\text{CKMfitter}} = 59^\circ_{-3.7^\circ}^{+9.2^\circ}, \quad \gamma_{\text{global}}^{\text{UTFitter}} = 64.6^\circ \pm 4.2^\circ. \quad (3)$$

An alternative method to obtain γ is to use $B \rightarrow \pi\pi$ or $B \rightarrow \rho\rho$ data alone. In principle for $B \rightarrow \pi\pi$ this is possible using only isospin [10], and for $B \rightarrow \rho\rho$ it is possible using isospin, the polarization data, and neglecting the ρ width. However the current experimental uncertainties need information beyond isospin, such as an expansion in Λ_{QCD}/m_b , necessary to obtain results competitive with Eq. (3). An approach with small uncertainties [11], which we label the BRS method, augments the isospin analysis by using the factorization theorem for nonleptonic decays in a specific limited way, namely to use $\text{Im}(T^{\pi^0\pi^0}/T^{\pi^+\pi^-}) \sim \mathcal{O}[\Lambda/E, \mathcal{O}(\alpha_s(m_b))]$. Data on $\text{Br}(\bar{B}^0 \rightarrow \pi^+\pi^-)$, $\text{Br}(B^- \rightarrow \pi^-\pi^0)$, $\text{Br}(\bar{B}^0 \rightarrow \pi^0\pi^0)$, $S_{\pi^+\pi^-}$, and $C_{\pi^+\pi^-}$ or the analogs for $B \rightarrow \rho\rho$ are then used to determine γ . With the latest non-leptonic data [6, 12] as summarized by HFAG [1], this gives

$$\begin{aligned} \gamma_{\pi\pi}^{\text{BRS}} &= 73.9^\circ_{-10.3^\circ}^{+7.5^\circ} \Big|_{\text{exp}}^{+1.0^\circ_{-2.5^\circ}} \Big|_{\text{thy}}, \quad (4) \\ \gamma_{\rho\rho}^{\text{BRS}} &= 77.3^\circ_{-32^\circ}^{+7.6^\circ} \Big|_{\text{exp}}^{+1.0^\circ_{-4.6^\circ}} \Big|_{\text{thy}}, \end{aligned}$$

where we quote the experimental and theory errors separately. With these values of γ , factorization in SCET exactly reproduces the observed $\bar{B}^0 \rightarrow \pi^0\pi^0$ and $\bar{B}^0 \rightarrow \rho^0\rho^0$ branching fractions. There is also a second solution

$$\begin{aligned} (\gamma_{\pi\pi}^{\text{BRS}})^{2\text{nd}} &= 27.7^\circ_{-7.3^\circ}^{+9.9^\circ} \Big|_{\text{exp}}^{+10^\circ_{-4.5^\circ}} \Big|_{\text{thy}}, \quad (5) \\ (\gamma_{\rho\rho}^{\text{BRS}})^{2\text{nd}} &= 52.8^\circ_{-7.7^\circ}^{+32^\circ} \Big|_{\text{exp}}^{+6.7^\circ_{-4.1^\circ}} \Big|_{\text{thy}}, \end{aligned}$$

that is, however, disfavored by the additional piece of information that the form factor parameter $\zeta_J > 0$. The value of γ from $B \rightarrow \rho\rho$ in Eq. (4) has not been quoted earlier in the literature, but the analysis is identical to that for $B \rightarrow \pi\pi$ in Ref. [11]. Currently the global fit values in Eq. (3) and BRS values in Eq. (4) are consistent with each other at the $1\text{-}\sigma$ level. Suppression of $\text{Im}(T^{\pi^0\pi^0}/T^{\pi^+\pi^-})$ can also be studied in a convention where $\lambda_c^{(f)}$ is eliminated from Eq. (1) [13], however in this case charm penguins contribute to the tree amplitudes which can induce contamination by long-distance contributions. We will quote numerical results for the penguin amplitudes using $\gamma = 59^\circ$ and $\gamma = 74^\circ$ to give some indication of the spread of possible values.

With the latest $B \rightarrow \pi\pi$ and $B \rightarrow \rho\rho$ data [6, 12], the isospin formula quoted below in Eq. (15) gives the

penguin amplitudes for $\gamma = 59^\circ$,

$$\begin{aligned} 10^3 \hat{P}^{\pi\pi} &= (1.77 \pm 0.73) - i(2.91 \pm 0.58), \\ 10^3 \hat{P}^{\rho\rho} &= (-2.91 \pm 2.63) - i(0.78 \pm 1.82), \end{aligned} \quad (6)$$

while for $\gamma = 74^\circ$ we find

$$\begin{aligned} 10^3 \hat{P}^{\pi\pi} &= (4.41 \pm 0.61) - i(2.91 \pm 0.58), \\ 10^3 \hat{P}^{\rho\rho} &= (3.81 \pm 2.34) - i(0.78 \pm 1.82). \end{aligned} \quad (7)$$

Here for convenience we pulled out a prefactor to quote a dimensionless penguin amplitude \hat{P} , using

$$\frac{P^{M_1 M_2}}{(1 \text{ GeV})} \equiv \frac{G_F m_B^2}{\sqrt{2}} \hat{P}^{M_1 M_2}. \quad (8)$$

Note that for fixed CP-asymmetries C and S , the extracted real part of $\hat{P}^{\pi\pi}$ and $\hat{P}^{\rho\rho}$ depends fairly strongly on the value of γ , but the imaginary part is completely independent of the choice for γ . (This is demonstrated explicitly in Eq. (15) below.) Neither result depends on the error in $|V_{ub}|$. The experimental errors here have decreased noticeably from early penguin extractions [14]. The challenge for standard model predictions is to reproduce or rule out the values in Eqs. (6-7).

The extraction of both the real and imaginary part of penguin amplitudes in the $K\pi$ system currently requires further theoretical input. In $B \rightarrow K\pi$ decays the penguin amplitudes dominate the tree amplitudes due to CKM suppression, making a precise comparison of their values even more interesting. Both types of amplitudes are important in CP asymmetries. Using a Λ/m_b expansion, the tree amplitude for $\bar{B}^0 \rightarrow K^-\pi^+$ at LO depend only on hadronic parameters $\zeta^{B\pi}$ and $\zeta_J^{B\pi}$ that are fully determined by the tree amplitudes in the $B \rightarrow \pi\pi$ channels, plus the ϕ_K twist-2 distribution function [15]. This allows the phase of the penguin amplitude $P^{K^-\pi^+}$ to be extracted from the data using only factorization for the tree amplitudes (which we will refer to by adding a subscript TF). The tree amplitudes are reliable since a proof of factorization to all orders in α_s was given in Ref. [3, 16], extending the original proposal and one-loop analysis in Ref. [17]. Although factorization has also been demonstrated for light-quark penguin loops (u, d, s), a complete analysis for charm-loops is still lacking. Using the phase convention where $T^{K^-\pi^+}$ is real we find for $\gamma = 59^\circ$

$$10^3 \hat{P}_{\text{TF}}^{K^-\pi^+} = \begin{cases} (4.87 \pm 0.39) - i(2.22 \pm 0.77) \\ -(4.22 \pm 0.36) - i(2.22 \pm 0.34) \end{cases}, \quad (9)$$

while for $\gamma = 74^\circ$

$$10^3 \hat{P}_{\text{TF}}^{K^-\pi^+} = \begin{cases} (4.73 \pm 0.36) - i(2.16 \pm 0.73) \\ -(4.41 \pm 0.34) - i(2.16 \pm 0.68) \end{cases}. \quad (10)$$

The only $B \rightarrow K\pi$ data used here was $\text{Br}(K^-\pi^+)$ and $A_{\text{CP}}(K^-\pi^+)$, and there are two solutions for each γ . Alternatives to the above analysis extract the $K\pi$ penguin amplitudes using a SU(3) based analysis with the $\pi\pi$

data [19] or by a global SU(3) based fit [20], and these yield similar conclusions for the size of the penguin amplitudes. Again the data gives $K\pi$ -penguin amplitudes with large imaginary components which require explanation in the standard model.

To determine penguin amplitudes for charmless B -decays in the standard model it is convenient to organize the relevant mass scales as an expansion in Λ/m_b and Λ/m_c [17]. This can be done from first principles using the effective field theory SCET [21]. In this expansion certain contributions to these amplitudes factorize

allowing them to be parameterized by well defined universal hadronic matrix elements. Since we are interested in the standard model prediction, we also organize the amplitude according to large ($C_{1,2,8g}$) and small (C_{3-10}) Wilson coefficients. To explain which terms will be computed in this paper we schematically give a result \hat{P}_0 for channels $B \rightarrow MM'$ with pseudoscalars, $MM' = PP$, with pseudoscalars and vectors $MM' = PV_0$, and with two longitudinal vectors $MM' = V_0V_0$. For completeness we also quote an analogous result \hat{P}_T for transverse polarizations $MM' = V_TV_T$:

$$\hat{P}_0 \sim \left(C_{3,4} + \frac{\alpha_s(m_b)C_{1,2,8g}}{\pi}\right)\zeta^{BM}\phi^{M'} + \left(C_{3,4} + \frac{\alpha_s(m_b)C_{1,2,8g}}{\pi}\right)\zeta_J^{BM}\phi^{M'} \quad (11)$$

$$+ \left(C_{5,6} + \frac{\alpha_s(m_b)C_{1,2,8g}}{\pi}\right)\left[\frac{\mu_{M'}}{m_b}\zeta^{BM}\phi_{pp}^{M'} + \frac{\mu_{M'}}{m_b}\zeta_J^{BM}\phi_{pp}^{M'}\right] + \left(C_{3,4} + \frac{\alpha_s(m_b)C_{1,2,8g}}{\pi}\right)\frac{\mu_M}{m_b}\zeta_\chi^{BM}\phi^{M'}$$

$$+ C_{1,2}\alpha_s(2m_c)v\hat{A}_{c\bar{c}}^{BMM'} + \frac{\alpha_s(m_b)}{m_b}\left(C_{3,4}f_B\phi^M\phi^{M'} + C_{5,6}f_B\phi_B^+\phi^{3M}\phi^{M'}\right) + C_{5,6}\frac{\alpha_s(m_b)\mu_M}{m_b^2}f_B\phi_{pp}^M\phi^{M'},$$

$$\hat{P}_T \sim \alpha_{em}\frac{m_b}{\Lambda}\hat{A}_{\gamma-\rho}^{BVV} \quad (12)$$

$$+ \left(C_{3,4} + \frac{\alpha_s(m_b)C_{1,2,8g}}{\pi}\right)\left[\frac{1}{m_b}\zeta_\perp^{BV}\phi_{pp\perp}^{V'} + \frac{1}{m_b}\zeta_{J\perp}^{BV}\phi_{pp\perp}^{V'}\right] + \left(C_{5,6} + \frac{\alpha_s(m_b)C_{1,2,8g}}{\pi}\right)\frac{1}{m_b}\zeta_{K\perp}^{BV}\phi_\perp^{V'}$$

$$+ C_{1,2}\alpha_s(2m_c)v\hat{A}_{c\bar{c}}^{BVV'} + C_{5,6}\frac{\alpha_s(m_b)}{m_b^2}\hat{A}_{(2ann-\chi)}^{BVV'}.$$

When coefficients $C_{3,4,5,6}$ appear here we leave implicit the fact that the electroweak penguin coefficients $C_{7,8,9,10}$ can also appear.

The terms on the first line of Eq. (11) for \hat{P}_0 are leading in the $\Lambda/m_{b,c}$ expansion. Working to all orders in $\alpha_s(\mu_i)$ at the intermediate scale $\mu_i \simeq \sqrt{m_b\Lambda}$, they involve a so-called soft form factor ζ^{BM} and a hard form factor ζ_J^{BM} . (Though it should be emphasized these names are somewhat misleading, since both form factors involve hard-collinear exchange, and thus the same length scales.) The terms on the second line of \hat{P}_0 are the ‘‘chirally-enhanced’’ power corrections suppressed by $\mu_{M'}/m_b$. Here $\mu_{M'} \sim \mathcal{O}(\Lambda)$ is a ratio of the squared meson mass to a sum of quark masses, and is important for nonleptonic decays because it is numerically enhanced $\mu_{M'} \simeq 2\text{ GeV}$ [17]. In Eq. (11) we display a new result that we will derive below, namely that to all orders in α_s the chirally enhanced terms in \hat{P}_0 are determined by one new form factor, ζ_χ^{BM} and one twist-3 distribution, ϕ_{pp}^M for longitudinal polarizations/pseudoscalars.

On the third line of Eq. (11) for \hat{P}_0 we have a term $\hat{A}_{c\bar{c}}^{BMM'}$. This is the so-called ‘‘charming penguin’’ due to long-distance charm loop effects [22, 23], whose leading contribution is expected to come from the charm threshold region [3, 24]. It is parametrically down by a power of the non-relativistic velocity v relative to the leading-

power result.

The remaining terms on the third line of Eq. (11) are due to annihilation and are suppressed by one or more powers of Λ/m_b . Terms at order $1/m_b$ contribute only to longitudinal polarizations and include: $f_B\phi^M\phi^{M'}$ which was studied in Refs. [25, 26, 27], and the remaining leading annihilation amplitude $f_B\phi_B^+\phi^{3M}\phi^{M'}$, which was computed recently in Ref. [28]. The $\mu_M f_B\phi_{pp}^M\phi^{M'}$ terms are chirally enhanced annihilation studied in Refs. [27, 29]. At lowest order in the α_s expansion the annihilation terms shown in Eq. (11) are real [29] (using the zero-bin procedure [30]). A nonperturbative complex annihilation amplitude involving soft exchange occurs at order $\alpha_s^2(\mu_i)/m_b$.

The terms shown in the \hat{P}_T amplitude follow a similar notation to that for \hat{P}_0 , but there are no analogs of the LO terms on the first line for \hat{P}_0 [31]. The term shown on the first line of \hat{P}_T comes from γ - ρ conversion [32], and is suppressed by α_{em} , but enhanced by m_b/Λ . \hat{P}_T does not contain chirally enhanced terms, so we show on the second line the terms from the analogous operators, which generate three form factors ζ_\perp^{BV} , $\zeta_{J\perp}^{BV}$, and $\zeta_{K\perp}^{BV}$. In Ref. [31] analogs of the terms on the second line of Eq. (12) were computed with an expansion in $\alpha_s(\mu_i)$, and the penguin annihilation term $\hat{A}_{2ann-\chi}^{BVV'}$ was also treated. Following

Ref. [24] we included a term $\hat{A}_{c\bar{c}}^{B\bar{V}V'}$ in the amplitude to produce transverse vector mesons. This is the most conservative approach given that so little is known about the factorization properties of $\hat{A}_{c\bar{c}}$.

We remark that the second and third lines of Eqs. (11) and (12) do not contain the complete set of $1/m_b$ or $1/m_b^2$ power corrections, but rather a collection of terms that are believed to be important due to numerical enhancement.¹ The additional uncertainty from missing $1/m_b$ corrections will be taken into account in our final error estimates. Also the $C_{3,4}$ and $C_{5,6}$ terms always come together with an $\alpha_s C_{1,2}$ term, which is the matrix element responsible for canceling the largest scheme dependence in these coefficients at next-to-leading-log (NLL) order. Since tree level C_{3-10} terms could compete numerically with $\alpha_s C_{1,2,8g}$ terms, we will require both to be included in what we call our leading order penguin amplitude. In this paper we will neglect $\alpha_s(m_b)C_{3,4}$ terms relative to $\alpha_s(m_b)C_{1,2,8g}$ since numerically they are 6-30 times smaller. This is the same strategy that was adopted for the ‘‘NNLL computations’’ in $B \rightarrow X_s \ell^+ \ell^-$ [33].

Eq. (11) is schematic because we have not yet displayed the precise coefficients in front of each term. The coefficients for the ζ^{BM} terms on the first and second lines were computed in Ref. [17]. To obtain Eq. (11), we expanded in Λ/m and $\alpha_s(m_b)$, but avoided the additional uncertainties from expanding in $\alpha_s(\mu_i)$, where the intermediate scale $\mu_i \simeq \sqrt{E\Lambda} \sim 1.3$ GeV. This is made possible by the fact that the form-factor parameters ζ_J^{BM} and ζ^{BM} are universal hadronic parameters when we distinguish $m^2 \gg E\Lambda \gg \Lambda^2$ [3]. Without expanding in $\alpha_s(\mu_i)$, the third term on line 1 was obtained in Ref. [3]. The third term on line 1 and third and non- $\alpha_s(m_b)$ terms on line 2 were computed at leading order in an expansion in $\alpha_s(\mu_i)$ in Ref. [17].

A main goal of this paper is the computation of the $\alpha_s C_{1,2,8g} \zeta_J^{BM} \phi^{M'}$ terms on line 1 of Eq. (11). Note that this term is a leading-order contribution to the penguin amplitudes due to the hierarchy in the Wilson coefficients. Our other main goal is to derive the factorization theorem for the terms on the second lines of \hat{P}_0 , and compute the corresponding Wilson coefficients. We derive the factorization theorem working to all orders in α_s , and perform tree level matching for all contributions. We also compute the $\alpha_s \zeta^{BM}$ terms, however the perturbative matching computation that determines the $\alpha_s(m_b) \zeta_J^{BM}$ and $\alpha_s(m_b) \zeta_{\chi}^{BM}$ terms on line 2 will not be considered here.

We would like to compute the magnitude and phase of \hat{P} for the $\pi^+ \pi^-$, $K^+ \pi^-$, and $\rho^+ \rho^-$ channels from the

terms in Eq. (11) and compare with Eqs. (6-10). The phase here is that of \hat{P}/\hat{T} . A schematic expression for \hat{T} is given by

$$\begin{aligned} \hat{T} \sim & \left(C_{1,2} + \frac{\alpha_s(m_b) C_{1,2}}{\pi} \right) \zeta^{BM} \phi^{M'} \\ & + \left(C_{1,2} + \frac{\alpha_s(m_b) C_{1,2}}{\pi} \right) \zeta_J^{BM} \phi^{M'} \\ & + C_1 \frac{\alpha_s(m_b)}{m_b} T_{(ann)}^{BMM'} + \dots, \end{aligned} \quad (13)$$

where we suppress terms from Wilson coefficients C_{3-10} and power suppressed terms other than annihilation. For $\hat{T}_{\pi^+ \pi^-}$, $\hat{T}_{\rho^+ \rho^-}$, and $\hat{T}_{K^+ \pi^-}$ the leading term in \hat{T} is real and numerically dominant. Therefore in \hat{P}/\hat{T} the $C_{1,2} \alpha_s$ corrections from \hat{P} are leading, while those from \hat{T} are higher order in α_s . In fact it would be inconsistent to keep the $C_{1,2} \alpha_s$ corrections in \hat{T} without keeping the $C_{3,4} \alpha_s$ terms in \hat{P} , because both of these terms carry μ -dependence that cancels that in ζ^{BM} and ζ_J^{BM} . Thus to compute the imaginary part of \hat{P}/\hat{T} at the order we are working, we can take $\hat{T}^{\pi^+ \pi^-}$ and $\hat{T}^{K^+ \pi^-}$ to be real. Numerically Refs. [34, 35] found that including one and some two-loop corrections gives $10^3 \hat{T}^{\pi\pi} = (31_{-9}^{+7} - i 0.07_{-3}^{+7}) + \hat{T}_{(ann)}^{\pi\pi}$. Thus, the imaginary part is significantly smaller than the real part. Using the zero-bin procedure, the annihilation contributions $T_{(ann)}^{M_1 M_2}$ are also real at leading order in an expansion of α_s at the hard and intermediate scales [28, 29].

Besides $\zeta_J^{BM}(z)$ and ζ^{BM} , the other hadronic parameters in Eq. (11) include the twist-2 distribution $\phi^{M'}$ and twist-3 chirally enhanced distribution $\phi_{pp}^{M'}$ defined below in Eq. (86). In this paper we adopt the point of view that ζ^{BM} and the normalization

$$\zeta_J^{BM} \equiv \int dz \zeta_J^{BM}(z) \quad (14)$$

should be fixed using other data (tree amplitudes and/or form factors) and then used to make predictions for the penguin amplitudes [3]. We will see that, relative to adopting models for all the hadronic parameters, fitting to tree amplitudes removes the dominant hadronic uncertainty in the computation of the short-distance penguin amplitudes. In a generic new physics model, $\hat{P}^{\text{expt}} = \hat{P}^{\text{SM}} + \hat{P}^{\text{BSM}}$, so to test the data for new physics we must have control over \hat{P}^{SM} .

The plan for the paper is as follows. In section II we give formulas for determining the penguin amplitudes and the soft and hard form factor parameters from the data. Section III reviews the leading factorization formula, and section IV discusses the endpoint behavior of $\zeta_J^{BM}(z)$. In section V we give a summary of all $\mathcal{O}(\alpha_s(m_b))$ one-loop hard coefficients at LO, and then in sections VI and VII provide more details of their calculation in the NDR and HV schemes respectively. A factorization theorem for chirally enhanced penguins is derived

¹ Also note that to our knowledge it has not been demonstrated that the chirally enhanced terms shown in Eq. (11) give the complete set of such enhanced contributions at this order in the power expansion. In particular it remains undetermined whether time-ordered product terms appearing at this order are or are not chirally enhanced.

in section VIII working to all orders in α_s at the intermediate scale $\sqrt{m_b \Lambda}$. In section IX we discuss long-distance charm contributions. Penguin annihilation contributions are reviewed in section X. Our analysis strategy is outlined in section XI and input parameters are summarized in section XII.

Our numerical analysis for standard model penguins is taken up in section XIII. This is followed by section XIV where we derive constraints on the effect of new physics contributions, and discuss what is needed to shift the penguin amplitudes closer to the data. Further discussion and conclusions are given in section XV. Several calculational details are relegated to appendices.

II. DETERMINING PENGUIN AMPLITUDES AND THE ζ^{BM} AND ζ_J^{BM} FORM FACTORS WITH NONLEPTONIC DATA

The $B \rightarrow \pi\pi$ data can be used to extract the penguin amplitude $P^{\pi^+\pi^-}$ and the tree amplitudes $T^{\pi^+\pi^-}$ and $T^{\pi^0\pi^-}$, including the strong phase in $P^{\pi^+\pi^-}/T^{\pi^+\pi^-}$. Solving equations in Ref. [11] with our phase convention the penguin amplitude is

$$\begin{aligned} \text{Re}(\hat{P}^{\pi\pi}) &= \frac{N_{\pi^0\pi^-}}{(1 \text{ GeV})} \left\{ \frac{(t_c^{\pi\pi})^2 [\sin 2\beta - \sin(2\beta+2\gamma)] - \bar{R}_c (\sin 2\beta + S_{\pi^+\pi^-})}{|V_{cb}V_{cd}^*| (2t_c^{\pi\pi} \sin \gamma) \cos 2\beta} \right\}, \\ \text{Im}(\hat{P}^{\pi\pi}) &= \frac{N_{\pi^0\pi^-}}{(1 \text{ GeV})} \frac{C_{\pi^+\pi^-} \bar{R}_c}{|V_{cb}V_{cd}^*| (2t_c^{\pi\pi} \sin \gamma)}, \end{aligned} \quad (15)$$

where the parameters on the right-hand-side are determined by nonleptonic data:

$$\begin{aligned} N_{\pi^0\pi^-} &= \left[\frac{64\pi}{m_B^3 G_F^2} \frac{\text{Br}(B^- \rightarrow \pi^0\pi^-)}{\tau_{B^-}} \right]^{1/2}, & t_c^{\pi\pi} &= \frac{1}{\sin \gamma} \left[\frac{\bar{R}_c}{2} \left(1 + B_{\pi\pi} \cos 2\beta + S_{\pi^+\pi^-} \sin 2\beta \right) \right]^{1/2}, \\ \bar{R}_c &= \frac{\text{Br}(\bar{B}^0 \rightarrow \pi^+\pi^-) \tau_{B^-}}{2\text{Br}(B^- \rightarrow \pi^0\pi^-) \tau_{B^0}}, & B_{\pi\pi} &= \sqrt{1 - C_{\pi^+\pi^-}^2 - S_{\pi^+\pi^-}^2}. \end{aligned} \quad (16)$$

Eqs. (15) and (16) also determine the penguin for longitudinal $B \rightarrow \rho\rho$ decays, by simply taking all superscripts and subscripts $\pi \rightarrow \rho$, and were used to determine the numbers quoted in Eqs. (6-7) with $|V_{cb}| = 0.0417$ and $|V_{cd}| = 0.227$. The $\text{Im}(\hat{P})$ is mainly sensitive to the direct CP-asymmetry. Since $(t_c^{\pi\pi} \sin \gamma)$ and $(t_c^{\rho\rho} \sin \gamma)$ do not explicitly depend on the weak phase γ , the same is true for the values extracted for $\text{Im}(P^{\pi\pi})$ and $\text{Im}(P^{\rho\rho})$ (demonstrating the statement we made in the introduction). The amplitude parameter $t_c^{\pi\pi} = |T^{\pi^+\pi^-}|/|T^{\pi^0\pi^+}|$ gives information about the size of the color-suppressed tree amplitude. The results in Eq. (15) and (16) are based on isospin symmetry and neglect small electroweak penguin contributions in $B^- \rightarrow \pi^0\pi^-$. This analysis leaves a \pm sign ambiguity in front of the $B_{\pi\pi}$ dependence in $t_c^{\pi\pi}$, which we resolved in Eq. (16) by taking the “+” solution. This solution is preferred by the standard model and rigorous power counting for the QCD amplitudes. The other experimentally allowed solution, $B_{\pi\pi} \rightarrow -B_{\pi\pi}$, has very large penguin amplitudes, $10^3 |\hat{P}_{\pi\pi}| \sim 11$ and $10^3 |\hat{P}_{\rho\rho}| \sim 24$, which are extremely difficult to accommo-

date in the standard model.

An important question for the phenomenology of charmless nonleptonic B -decays is the relative size of the form factors ζ^{BM} and ζ_J^{BM} (defined below in Eq. (40)). Here we follow Ref. [3] and organize the expansion according to $\zeta_J^{BM} \sim \zeta^{BM}$ which is a natural power counting when factorization is not used at the intermediate scale, and is also the scaling used in the KLS approach [25]. This counting is supported by the $B \rightarrow \pi\pi$ data and factorization with the zero-bin procedure of Ref. [30] (which implies that both of these form factors have an $\alpha_s(\mu_i)$ at leading order in the expansion at the intermediate scale). In the BBNS approach [17], a hierarchy $\zeta_J^{BM} \sim \alpha_s(\mu_i) \zeta^{BM}$ is adopted. This changes the order of terms in the perturbative expansion which we discussed in Eq. (11) by making certain terms higher order in α_s .

At leading order the $B \rightarrow \pi\pi$ factorization theorem for the tree amplitudes can be used to extract the normalization of the soft and hard form factor parameters. Expressed in terms of observables the result is [36]

$$|V_{ub}|(\zeta^{B\pi} + \zeta_J^{B\pi}) = \frac{N_{\pi^0\pi^-}}{f_\pi|V_{ud}|} \left[\frac{(C_1 + C_2)t_c^{\pi\pi} - C_2 - C_3}{C_1^2 - C_2^2 + (C_1 + C_2)(C_4 - C_3)} \right] \left[1 + \mathcal{O}\left(\alpha_s(m_b), \frac{\Lambda}{E}\right) \right], \quad (17)$$

$$|V_{ub}\langle x^{-1} \rangle_\pi \zeta_J^{B\pi} = \frac{N_{\pi^0\pi^-}}{f_\pi|V_{ud}|} \left[\frac{3C_1 + C_2 + C_3 + 3C_4 - 4(C_1 + C_2)t_c^{\pi\pi}}{C_1^2 - C_2^2 + (C_1 + C_2)(C_4 - C_3)} \right] \left[1 + \mathcal{O}\left(\alpha_s(m_b), \frac{\Lambda}{E}\right) \right], \quad (18)$$

where E is the pion energy in the CM frame of the B . On the left-hand-side of Eq. (17) we have the semileptonic $B \rightarrow \pi\ell\bar{\nu}$ form factor at $q^2 \simeq 0$, which is given by $f_+^{B\pi}(0) = \zeta^{B\pi} + \zeta_J^{B\pi}$. The expression for $\langle x^{-1} \rangle_\pi \zeta_J^{B\pi}$ in Eq. (18) follows in a straightforward manner from results in Ref. [3], but to our knowledge has not been presented in this simple closed form in the literature. For the hadronic parameter $\langle x^{-1} \rangle_\pi = \int_0^1 dx \phi_\pi(x)/x$, a fit of the $\gamma\text{-}\pi$ form factor to $\gamma^*\gamma \rightarrow \pi^0$ data gives [37]

$$\langle x^{-1} \rangle_\pi = 2.9 \pm 0.4. \quad (19)$$

Using the latest experimental data [1], $\gamma = 67 \pm 10^\circ$, $|V_{ud}| = 0.9738$, and LL Wilson coefficients, Eq. (17) gives

$$f_+^{B\pi}(0) = \left(0.182 \pm 0.011 \pm 0.036 \right) \frac{4.2 \times 10^{-3}}{|V_{ub}|},$$

$$\langle x^{-1} \rangle_\pi \zeta_J^{B\pi} = \left(0.262 \pm 0.052 \pm 0.052 \right) \frac{4.2 \times 10^{-3}}{|V_{ub}|}. \quad (20)$$

We emphasize that these results do not rely on Eq. (19). In Eq. (20) the first errors are experimental and the second theoretical. Theoretical errors are computed as a generic 20% error on the central value, both here and below in Eq. (23). Setting $|V_{ub}| = 4.2 \times 10^{-3}$ and using $\langle x^{-1} \rangle_\pi = 2.9$ in Eq. (20) gives

$$\zeta^{B\pi} = 0.092 \pm 0.027, \quad \zeta_J^{B\pi} = 0.090 \pm 0.018. \quad (21)$$

These values favor $\zeta_J^{B\pi} \sim \zeta^{B\pi}$. There is a sizeable correlation in their quoted errors, and to take this correlation into account in our numerical analysis we will do Gaussian scans over the range of experimental errors quoted in Eq. (20). A 12% error in $|V_{ub}|$ is also included in our final results.

The same results, Eqs. (15-18) apply for $B \rightarrow \rho\rho$ for longitudinal ρ 's, where now one uses $N_{\rho^0\rho^-}$ and determines $t_c^{\rho\rho}$ from the $B \rightarrow \rho\rho$ branching ratios and CP-asymmetries $S_{\rho^+\rho^-}$ and $C_{\rho^+\rho^-}$. Here the analog of $f_+^{B\pi}(0)$ is the longitudinal $B \rightarrow \rho\ell\bar{\nu}$ form factor at $q^2 \simeq 0$

$$\begin{aligned} A_{\parallel}(0) &= \frac{m_B^2 A_2(0)}{2m_V(m_B + m_V)} - \frac{(m_B + m_V)}{2m_V} A_1(0) \\ &= -\zeta^{B\rho} - \zeta_J^{B\rho}. \end{aligned} \quad (22)$$

Taking $\gamma = 67 \pm 10^\circ$ the nonleptonic data gives

$$\begin{aligned} A_{\parallel}^{B\rho}(0) &= -\left(0.261 \pm 0.022 \pm 0.052 \right) \frac{4.2 \times 10^{-3}}{|V_{ub}|}, \\ \langle x^{-1} \rangle_\rho \zeta_J^{B\rho} &= \left(0.06 \pm 0.11 \right) \frac{4.2 \times 10^{-3}}{|V_{ub}|}. \end{aligned} \quad (23)$$

Again the first errors are experimental and the second theoretical. Due to the large uncertainty in the central value of $\langle x^{-1} \rangle_\rho \zeta_J^{B\rho}$ a 20% theoretical uncertainty would not be noticeable.

It is interesting to make a comparison of the π and ρ parameters, which from the results in Eq. (20) and (23) give

$$R_{\rho\pi} \equiv \frac{\langle x^{-1} \rangle_\rho \zeta_J^{B\rho}}{\langle x^{-1} \rangle_\pi \zeta_J^{B\pi}} = 0.23 \pm 0.42. \quad (24)$$

This large 0.42 experimental error is induced by our current knowledge of the $B \rightarrow \rho\rho$ CP-asymmetries together with greater sensitivity to γ and t_c . Now in SCET_{II} one can derive a factorization theorem for ζ_J^{BM} (discussed in Eq. (46) below) that implies that

$$R_{\rho\pi} = \frac{f_\rho[\langle x^{-1} \rangle_\rho]^2}{f_\pi[\langle x^{-1} \rangle_\pi]^2} \left[1 + \mathcal{O}\left(\alpha_s(\mu_i), \frac{\Lambda}{E}\right) \right]. \quad (25)$$

Here the theoretical errors should be increased to $\simeq 35\%$ to account for the additional expansion in α_s at the intermediate scale μ_i . Using $f_\rho \simeq 1.6 f_\pi$ we find that the nonleptonic data plus factorization at the intermediate scale currently implies

$$\frac{\langle x^{-1} \rangle_\rho}{\langle x^{-1} \rangle_\pi} = 0.38 \pm 0.35 \pm 0.13, \quad (26)$$

where the first error is experimental and the second is the 35% theoretical error.

A result for this ratio can also be obtained from the factorization theorem for the color-suppressed decays $\bar{B}^0 \rightarrow D^0\rho^0$ and $\bar{B}^0 \rightarrow D^0\pi^0$ derived in Eq.(69) of Ref. [38], which gives

$$\frac{\langle x^{-1} \rangle_\rho}{\langle x^{-1} \rangle_\pi} = \frac{f_\pi}{f_\rho} \sqrt{\frac{\text{Br}(\bar{B}^0 \rightarrow D^0\rho^0)}{\text{Br}(\bar{B}^0 \rightarrow D^0\pi^0)}} = 0.62 \pm 0.24. \quad (27)$$

It is quite interesting that this ratio is found to be less than unity, and that the results extracted in Eq. (26) from charmless decays, and in Eq. (27) from charmed final states, agree within errors. The significant range allowed by the errors can be reduced by noting that there is a rigorous lower bound on the inverse moment for positive definite $\phi^M(x)$,

$$\langle x^{-1} \rangle_M = \int_0^1 dx \frac{\phi^M(x)}{x} \geq \int_0^1 dx \phi^M(x) = 1. \quad (28)$$

For $M = \pi$ and $M = \rho$ we have $\phi^M(x) = \phi^M(1-x)$ from isospin and charge conjugation, and this bound can be strengthened:

$$\begin{aligned} \langle x^{-1} \rangle_M &= \int_0^1 dx \frac{\phi^M(x)}{x} = \int_0^{1/2} dx \left(\frac{1}{x} + \frac{1}{1-x} \right) \phi^M(x) \\ &\geq 4 \int_0^{1/2} dx \phi^M(x) = 2. \end{aligned} \quad (29)$$

With the mean value in Eq. (19) this bound is close to the central value in Eq. (27).

For our analysis we take into account the bound and the data in Eqs. (26) and (27), and hence use a model for $\phi_\rho(x)$ that is constrained such $\langle x^{-1} \rangle_\rho = 2.2_{-0.2}^{+0.6}$ which gives $\langle x^{-1} \rangle_\rho / \langle x^{-1} \rangle_\pi \simeq 0.76$. Taking $|V_{ub}| = 4.2 \times 10^{-3}$ we then find using Eq. (23) that

$$\zeta^{B\rho} = 0.234 \pm 0.065, \quad \zeta_J^{B\rho} = 0.027 \pm 0.049. \quad (30)$$

Again we scan over the range of experimental errors in Eq. (23) to take into account the sizeable correlations. Note that $\zeta_J^{B\rho}$ is sensitive to the values of the $B \rightarrow \rho\rho$ branching ratios, which dominate the error and favor a smaller color suppressed amplitude than in $B \rightarrow \pi\pi$. The central values in $B \rightarrow \rho\rho$ are consistent with $\zeta_J^{B\rho} \lesssim \alpha_s(\mu_i)\zeta^{B\rho}$. However, within errors the scaling that we adopt, $\zeta_J^{B\rho} \sim \zeta^{B\rho}$, is also consistent (given that \sim still means that the factors can differ numerically by a factor like 2). As the experimental uncertainties on the nonleptonic decays decrease, we expect the combined analysis of $B \rightarrow \pi\pi, \rho\rho$ introduced in this section to play an important role in furthering our knowledge of hadronic parameters appearing in the factorization theorem for charmless nonleptonic decays.

III. FACTORIZATION AT LEADING POWER

In this section we review the SCET factorization analysis at leading order from [3] to setup our notation. The decays $B \rightarrow M_1 M_2$ are mediated in full QCD by the weak $\Delta B = 1$ Hamiltonian, which for $\Delta S = 0$ reads

$$H_W = \frac{G_F}{\sqrt{2}} \sum_{p=u,c} \lambda_p^{(d)} \left(C_1 O_1^p + C_2 O_2^p + \sum_{i=3}^{10,7\gamma,8g} C_i O_i \right), \quad (31)$$

where the CKM factor is $\lambda_p^{(f)} = V_{pb} V_{pf}^*$ with $f = d$ and at LL order

$$C_{1-10}(m_b) = \{1.107, -.249, .011, -.026, .008, -.031, 4.2 \times 10^{-4}, 4.2 \times 10^{-4}, -9.7 \times 10^{-3}, 1.9 \times 10^{-3}\}. \quad (32)$$

The coefficients in Eq. (31) are known at NLL order [39], and the values we used for our main analysis are pre-

sented in section XII. The basis of operators is

$$\begin{aligned} O_1^p &= (\bar{p}b)_{V-A} (\bar{d}p)_{V-A}, \\ O_2^p &= (\bar{p}_\beta b_\alpha)_{V-A} (\bar{d}_\alpha p_\beta)_{V-A}, \\ O_3 &= (\bar{d}b)_{V-A} (\bar{q}q)_{V-A}, \\ O_4 &= (\bar{d}_\beta b_\alpha)_{V-A} (\bar{q}_\alpha q_\beta)_{V-A}, \\ O_5 &= (\bar{d}b)_{V-A} (\bar{q}q)_{V+A}, \\ O_6 &= (\bar{d}_\beta b_\alpha)_{V-A} (\bar{q}_\alpha q_\beta)_{V+A}, \\ O_7 &= \frac{3e_q}{2} (\bar{d}b)_{V-A} (\bar{q}q)_{V+A}, \\ O_8 &= \frac{3e_q}{2} (\bar{d}_\beta b_\alpha)_{V-A} (\bar{q}_\alpha q_\beta)_{V+A}, \\ O_9 &= \frac{3e_q}{2} (\bar{d}b)_{V-A} (\bar{q}q)_{V-A}, \\ O_{10} &= \frac{3e_q}{2} (\bar{d}_\beta b_\alpha)_{V-A} (\bar{q}_\alpha q_\beta)_{V-A}, \\ O_{8g} &= -\frac{g\bar{m}_b}{4\pi^2} \bar{d}\sigma_{\mu\nu} G^{\mu\nu} P_R b, \\ O_{7\gamma} &= -\frac{e\bar{m}_b}{4\pi^2} \bar{d}\sigma_{\mu\nu} F^{\mu\nu} P_R b. \end{aligned} \quad (33)$$

Here α, β are color indices and e_q are electric charges and the q are summed over the light quarks, $q = u, d, s, c, b$. The $\Delta S = 1$ H_W is obtained by replacing $(f = d) \rightarrow (f = s)$ in Eqs. (31,33). The numerical dominance of C_1, C_2, C_{8g} will allow us to simplify the calculation since we need only include the effects of $O_{1,2,8g}$ at one-loop. Perturbative corrections due to the other operators are numerically tiny. Our sign for g is such that the QCD fermion Feynman rule is $igT^A \gamma^\mu$.

The matching onto SCET occurs in two stages. First one matches onto SCET_I by integrating out fluctuations at the scale m_b . One then matches onto SCET_{II} at the scale $\sqrt{\Lambda m_b}$. For the LO factorization theorem for nonleptonic B-decays this second step of matching can not lead to strong phases, as discussed in [3], and for ζ_J^{BM} is known at one-loop order [40, 41]. In this paper we wish to complete the $\mathcal{O}(\alpha_s)$ matching for the first stage. For tree amplitudes the corresponding computation was carried out in Ref. [42]. Here we consider the result for the penguin amplitudes. In particular we present the short-distance up and charm loop contributions in two different regulation schemes for γ_5 , as well as corresponding contributions from the magnetic gluon operator.

At the scale $\mu \simeq m_b$ the Hamiltonian in Eq. (31) is matched onto operators in SCET. Due to the nature of the matching onto SCET_{II} the first two orders of the power expansion of the Hamiltonian in SCET_I are needed to determine the leading-order amplitudes

$$\begin{aligned} H_W = & \frac{2G_F}{\sqrt{2}} \sum_{n,\bar{n}} \left\{ \sum_i \int [d\omega_j]_{j=1}^3 c_i^{(f)}(\omega_j) Q_{if}^{(0)}(\omega_j) \right. \\ & \left. + \sum_i \int [d\omega_j]_{j=1}^4 b_i^{(f)}(\omega_j) Q_{if}^{(1)}(\omega_j) + \dots \right\}. \end{aligned} \quad (34)$$

The operators for the $\Delta S = 0$ transitions are [3, 16]

$$\begin{aligned} Q_{1d}^{(0)} &= [\bar{u}_{n,\omega_1} \not{P}_L b_v] [\bar{d}_{\bar{n},\omega_2} \not{P}_L u_{\bar{n},\omega_3}], \\ Q_{2d,3d}^{(0)} &= [\bar{d}_{\bar{n},\omega_1} \not{P}_L b_v] [\bar{u}_{\bar{n},\omega_2} \not{P}_{L,R} u_{\bar{n},\omega_3}], \\ Q_{4d}^{(0)} &= [\bar{q}_{\bar{n},\omega_1} \not{P}_L b_v] [\bar{d}_{\bar{n},\omega_2} \not{P}_L q_{\bar{n},\omega_3}], \\ Q_{5d,6d}^{(0)} &= [\bar{d}_{\bar{n},\omega_1} \not{P}_L b_v] [\bar{q}_{\bar{n},\omega_2} \not{P}_{L,R} q_{\bar{n},\omega_3}], \end{aligned} \quad (35)$$

and

$$\begin{aligned} Q_{1d}^{(1)} &= \frac{-2}{m_b} [\bar{u}_{n,\omega_1} ig \not{B}_{n,\omega_4}^\perp P_L b_v] [\bar{d}_{\bar{n},\omega_2} \not{P}_L u_{\bar{n},\omega_3}], \\ Q_{2d,3d}^{(1)} &= \frac{-2}{m_b} [\bar{d}_{\bar{n},\omega_1} ig \not{B}_{n,\omega_4}^\perp P_L b_v] [\bar{u}_{\bar{n},\omega_2} \not{P}_{L,R} u_{\bar{n},\omega_3}], \\ Q_{4d}^{(1)} &= \frac{-2}{m_b} [\bar{q}_{\bar{n},\omega_1} ig \not{B}_{n,\omega_4}^\perp P_L b_v] [\bar{d}_{\bar{n},\omega_2} \not{P}_L q_{\bar{n},\omega_3}], \\ Q_{5d,6d}^{(1)} &= \frac{-2}{m_b} [\bar{d}_{\bar{n},\omega_1} ig \not{B}_{n,\omega_4}^\perp P_L b_v] [\bar{q}_{\bar{n},\omega_2} \not{P}_{L,R} q_{\bar{n},\omega_3}], \\ Q_{7d}^{(1)} &= \frac{-2}{m_b} [\bar{u}_{n,\omega_1} ig \not{B}_{n,\omega_4}^{\perp,\mu} P_L b_v] [\bar{d}_{\bar{n},\omega_2} \not{P}_L \gamma_\mu P_R u_{\bar{n},\omega_3}], \\ Q_{8d}^{(1)} &= \frac{-2}{m_b} [\bar{q}_{\bar{n},\omega_1} ig \not{B}_{n,\omega_4}^{\perp,\mu} P_L b_v] [\bar{d}_{\bar{n},\omega_2} \not{P}_L \gamma_\mu P_R q_{\bar{n},\omega_3}]. \end{aligned} \quad (36)$$

Here $P_L = (1 - \gamma_5)/2$ and $P_R = (1 + \gamma_5)/2$. At lowest order, $Q_{7d,8d}^{(1)}$ give a vanishing contribution to the rates. $Q_{5d,6d}^{(0,1)}$ will not be relevant in our analysis since we will not be considering isosinglet final states. At tree level the matching onto $Q_{5d,6d}^{(0,1)}$ was done in Ref. [43]. From Eqs. (35,36) the $\Delta S = 1$ operators $Q_{is}^{(0)}$ are obtained by swapping $\bar{d} \rightarrow \bar{s}$. The ‘‘quark’’ fields in Eqs. (35,36) with subscripts n and \bar{n} are products of collinear quark fields and Wilson lines with large momenta ω_i . In particular we have defined

$$\begin{aligned} \bar{u}_{n,\omega} &= [\bar{\xi}_n^{(u)} W_n \delta(\omega - \bar{n} \cdot \mathcal{P}^\dagger)], \\ ig \not{B}_{n,\omega}^{\perp,\mu} &= \frac{1}{(-\omega)} [W_n^\dagger [i\bar{n} \cdot D_{c,n}, iD_{n,\perp}^\mu] W_n \delta(\omega - \bar{\mathcal{P}}^\dagger)] \end{aligned} \quad (37)$$

where $\bar{\xi}_n^{(u)}$ creates a n -collinear up quark or annihilates an antiquark. The b_v field is the standard HQET field. For a complete basis we also need operators with octet bilinears, $T^A \otimes T^A$, but their matrix elements vanish at LO.

The leading-order amplitude is generated by time-ordered products of both the operators $Q^{(0)}$ and $Q^{(1)}$ with insertions of a subleading Lagrangians [44, 45]. T-products with $Q^{(0)}$ can be factorized as $T_1^i \tilde{Q}_i^{\bar{n}}$ and contribute to terms with ζ^{BM} , while T-products with $Q^{(1)}$ can be written as $T_2^i \tilde{Q}_i^{\bar{n}}$ and contribute to terms with ζ_J^{BM} . Here

$$\begin{aligned} T_1[\tilde{Q}_i^{(0)}] &\equiv \int d^4y d^4y' T [\tilde{Q}_i^{(0)}(0) i\mathcal{L}_{\xi_n q}^{(1)}(y) i\mathcal{L}_{\xi_n \xi_n}^{(1)}(y')] \\ &\quad + \int d^4y d^4y' T [\tilde{Q}_i^{(0)}(0) i\mathcal{L}_{\xi_n q}^{(1)}(y) i\mathcal{L}_{cg}^{(1)}(y')] \\ &\quad + \int d^4y T [\tilde{Q}_i^{(0)}(0), i\mathcal{L}_{\xi_n q}^{(1,2)}(y)], \\ T_2[\tilde{Q}_i^{(1)}] &\equiv \int d^4y T [\tilde{Q}_i^{(1)}(0), i\mathcal{L}_{\xi_n q}^{(1)}(y)], \end{aligned} \quad (38)$$

and it was convenient to define

$$\begin{aligned} \tilde{Q}_i^{(0)} &= [\bar{q}_{n,\omega_1}^i \not{P}_L b_v], \\ \tilde{Q}_i^{(1)} &= \frac{-2}{m_b} [\bar{q}_{n,\omega_1}^i ig \not{B}_{n,\omega_4}^\perp P_L b_v], \\ \tilde{Q}_i^{\bar{n}} &= \begin{cases} \bar{q}_{\bar{n},\omega_2}^i \not{P}_L q_{\bar{n},\omega_3}^i & i = 1, 2, 4, 5 \\ \bar{q}_{\bar{n},\omega_2}^i \not{P}_R q_{\bar{n},\omega_3}^i & i = 3, 6 \end{cases}. \end{aligned} \quad (39)$$

The Lagrangians in Eq. (38) can be found in Ref. [46]. Note that only the n -collinear fields appear in the T-products T_1^i and T_2^j , which explains why the same $T_{1,2}^i$ appear for heavy-to-light form factors at large meson energies [24]. The form factors simply do not have the extra $\tilde{Q}_i^{\bar{n}}$. In addition we have operators/T-products whose matrix elements give A_{cc} . We refer to section IX below for further discussion of these contributions.

In this paper we use factorization at the scale m_b , where the hadronic parameters are defined by matrix elements of T_1 and T_2 and the \bar{n} -collinear operator, namely

$$\begin{aligned} \langle M_n | T_1 [\bar{q}_{n\omega_1}^L \not{P}_L b_v] | B \rangle &= \mathcal{C}_{qL}^{BM} \bar{\delta}_{\omega_1} m_B \zeta^{BM}, \\ \langle M_n | T_2 [\bar{q}_{n\omega_1}^L ig \not{B}_{n\omega_4}^\perp b_v] | B \rangle &= -\mathcal{C}_{qL}^{BM} \bar{\delta}_{\omega_1\omega_4} \frac{m_B}{2} \zeta_J^{BM}(z), \\ \langle M_{\bar{n}} | \bar{q}_{\bar{n}\omega_2}^{\prime L} \not{P}_L q_{\bar{n}\omega_3}^L | 0 \rangle &= \frac{i}{2} \mathcal{C}_{qLq}^M \bar{\delta}_{\omega_2\omega_3} f_M \phi_M(u), \\ \langle M_{\bar{n}} | \bar{q}_{\bar{n}\omega_2}^{\prime R} \not{P}_R q_{\bar{n}\omega_3}^R | 0 \rangle &= \frac{i}{2} \mathcal{C}_{qRq}^M \bar{\delta}_{\omega_2\omega_3} f_M \phi_M(u), \end{aligned} \quad (40)$$

where $z = \omega_1/m_B$, $u = \omega_2/m_B$ and we have made the momentum-conserving δ -functions explicit, $\bar{\delta}_\omega = \delta(\omega_1 - m_B)$, $\bar{\delta}_{\omega_1\omega_4} = \delta(\omega_1 + \omega_4 - m_B)$, and $\bar{\delta}_{\omega_2\omega_3} = \delta(\omega_2 - \omega_3 - m_B)$. As pictured in Fig. 3, u and $1 - u$ are momentum fractions for the quark and antiquark \bar{n} -collinear fields, and z and $1 - z$ are the momentum fractions carried by the n -collinear quark and gluon field in $\tilde{Q}_i^{(1)}$. Finally, \mathcal{C}_i^{BM} and \mathcal{C}_i^M are Clebsch-Gordan coefficients. We fix the following sign convention for the states

$$\begin{aligned} \pi^+ &= +u\bar{d}, \quad \pi^0 = \frac{1}{\sqrt{2}}(d\bar{d} - u\bar{u}), \quad \pi^- = -d\bar{u}, \\ \bar{K}^0 &= s\bar{d}, \quad K^- = -s\bar{u}, \quad K^+ = u\bar{s}, \quad K^0 = d\bar{s}, \\ \bar{B}^0 &= b\bar{d}, \quad B^- = -b\bar{u}, \quad B^+ = u\bar{b}, \quad B^0 = d\bar{b}, \end{aligned} \quad (41)$$

and take vector meson states to have a negative sign relative to the corresponding pseudoscalar mesons. The over all phase convention is fixed so that the Clebsch-Gordan $\mathcal{C}_{uL}^{\bar{B}^0 \pi^+} = +1$, $\mathcal{C}_{dLu}^{\pi^-} = +1$, $\mathcal{C}_{dRu}^{\pi^-} = -1$, $\mathcal{C}_{uL}^{\bar{B}^0 \rho^+} = +1$, and $\mathcal{C}_{dLu}^{\rho^-} = \mathcal{C}_{dRu}^{\rho^-} = +1$. One can then compute that $\mathcal{C}_{dL}^{\bar{B}^0 \pi^-} = +1$ and $\mathcal{C}_{u,u}^{\pi^0} = -\frac{1}{\sqrt{2}}$, etc. Note that the signs take into account whether the operators have left or right-handed quarks. Putting the pieces together gives the leading order factorization theorem which integrates out

hard $\sim m_b^2$ fluctuations

$$\begin{aligned} A^{LO} &\equiv -i \langle M_1 M_2 | H_W | \bar{B} \rangle \\ &= \frac{G_F m_B^2}{\sqrt{2}} f_{M_1} \left[\int_0^1 du dz T_{1J}(u, z) \zeta_J^{BM_2}(z) \phi^{M_1}(u) \right. \\ &\quad \left. + \zeta^{BM_2} \int_0^1 du T_{1\zeta}(u) \phi^{M_1}(u) \right] + (1 \leftrightarrow 2). \end{aligned} \quad (42)$$

Here the hard coefficients $T_{1\zeta}$ and T_{1J} depend on channel specific linear combinations of the matching coefficients

$$\begin{aligned} T_{1\zeta}(u) &= \mathcal{C}_{uL}^{BM_2} \mathcal{C}_{fLu}^{M_1} c_1^{(f)}(u) + \mathcal{C}_{fL}^{BM_2} \mathcal{C}_{uLu}^{M_1} c_2^{(f)}(u) \\ &\quad + \mathcal{C}_{fL}^{BM_2} \mathcal{C}_{uRu}^{M_1} c_3^{(f)}(u) + \mathcal{C}_{qL}^{BM_2} \mathcal{C}_{fLq}^{M_1} c_4^{(f)}(u), \\ T_{1J}(u, z) &= \mathcal{C}_{uL}^{BM_2} \mathcal{C}_{fLu}^{M_1} b_1^{(f)}(u, z) + \mathcal{C}_{fL}^{BM_2} \mathcal{C}_{uLu}^{M_1} b_2^{(f)}(u, z) \\ &\quad + \mathcal{C}_{fL}^{BM_2} \mathcal{C}_{uRu}^{M_1} b_3^{(f)}(u, z) + \mathcal{C}_{qL}^{BM_2} \mathcal{C}_{fLq}^{M_1} b_4^{(f)}(u, z). \end{aligned} \quad (43)$$

Results for these T 's in different decay channels can be read off of Table I in Ref. [3]. Power counting implies $\zeta^{BM} \sim \zeta_J^{BM} \sim (\Lambda/m_b)^{3/2}$ while $\phi_M \sim 1$. Here the non-perturbative parameters ζ^{BM} , $\zeta_J^{BM}(z)$, and $\phi^M(u)$, all occur in the $B \rightarrow M$ semileptonic and rare form factors. For a model independent analysis they need to be determined from data. Note that in the leading order factorization theorem all terms involve a form factor times a meson distribution function.

Taking the terms proportional to $\lambda_c^{(f)}$ from Eq. (42) generates the penguin amplitude terms on the first line of Eq. (11). Using Eq. (42) still requires matching the full theory O_i 's onto the $Q_{if}^{(0,1)}$ to determine the Wilson coefficients $c_i^{(f)}$ and $b_i^{(f)}$. For the coefficients of $Q_i^{(0)}$ with $f = d, s$ we have

$$\begin{aligned} c_1^{(f)} &= \lambda_u^{(f)} \left(C_1 + \frac{C_2}{N_c} \right) - \lambda_t^{(f)} \frac{3}{2} \left(C_{10} + \frac{C_9}{N_c} \right) + \Delta c_1^{(f)}, \\ c_2^{(f)} &= \lambda_u^{(f)} \left(C_2 + \frac{C_1}{N_c} \right) - \lambda_t^{(f)} \frac{3}{2} \left(C_9 + \frac{C_{10}}{N_c} \right) + \Delta c_2^{(f)}, \\ c_3^{(f)} &= -\lambda_t^{(f)} \frac{3}{2} \left(C_7 + \frac{C_8}{N_c} \right) + \Delta c_3^{(f)}, \\ c_4^{(f)} &= -\lambda_t^{(f)} \left(C_4 + \frac{C_3}{N_c} - \frac{C_{10}}{2} - \frac{C_9}{2N_c} \right) + \Delta c_4^{(f)}, \end{aligned} \quad (44)$$

and for the $Q_i^{(1)}$ we have the coefficients

$$\begin{aligned} b_1^{(f)} &= \lambda_u^{(f)} \left[C_1 + \left(1 + \frac{1}{u} \right) \frac{C_2}{N_c} \right] \\ &\quad - \lambda_t^{(f)} \left[\frac{3}{2} C_{10} + \left(1 + \frac{1}{u} \right) \frac{3C_9}{2N_c} \right] + \Delta b_1^{(f)}, \\ b_2^{(f)} &= \lambda_u^{(f)} \left[C_2 + \left(1 + \frac{1}{u} \right) \frac{C_1}{N_c} \right] \\ &\quad - \lambda_t^{(f)} \left[\frac{3}{2} C_9 + \left(1 + \frac{1}{u} \right) \frac{3C_{10}}{2N_c} \right] + \Delta b_2^{(f)}, \\ b_3^{(f)} &= -\lambda_t^{(f)} \left[\frac{3}{2} C_7 + \left(1 - \frac{1}{u} \right) \frac{3C_8}{2N_c} \right] + \Delta b_3^{(f)}, \\ b_4^{(f)} &= -\lambda_t^{(f)} \left[C_4 - \frac{C_{10}}{2} + \left(1 + \frac{1}{u} \right) \left(\frac{C_3}{N_c} - \frac{C_9}{2N_c} \right) \right] + \Delta b_4^{(f)}, \end{aligned} \quad (45)$$

where $\bar{u} = 1 - u$. The $\Delta c_i^{(f)}$ and $\Delta b_i^{(f)}$ denote terms depending on α_s generated by matching from H_W , and will be considered at $\mathcal{O}(\alpha_s(m_b))$ below. The displayed terms in $c_4^{(f)}$ and $b_4^{(f)}$ correspond to $C_{3,4,9,10}$ terms in the first line of Eq. (11), and $\Delta c_4^{(f)}$ and $\Delta b_4^{(f)}$ include the $\alpha_s C_{1,2,8g}$ terms.

IV. ENDPOINT BEHAVIOR OF $\zeta_J^{BM}(z)$

In order to model the generalized form factors like $\zeta_J^{BM}(z)$ it is useful to know their behavior in the endpoints $z \rightarrow 0$ and $z \rightarrow 1$. This behavior along with that of $\phi^M(u)$ determines whether the convolutions $\int du c_i^{(f)}(u) \phi^M(u)$ and $\int du dz b_i^{(f)}(u, z) \zeta_J^{BM}(z) \phi^M(u)$ in the factorization theorem in Eq. (42) converge naively or require zero-bin subtractions [30]. At tree level $c_i^{(f)}(u) \sim 1$ since it is independent of u , while $b_i^{(f)}(u, z) \sim \bar{u}^{-1}$ is independent of z (for the electroweak coefficient $b_3^{(f)}$ replace the \bar{u}^{-1} by u^{-1}). At one loop the scaling behavior becomes $c_i^{(f)}(u) \sim (u\bar{u})^{-1}$ and $b_i^{(f)}(u, z) \sim (z\bar{u})^{-1}$ as discussed in section V below. Known two-loop corrections do not modify these one-loop scaling results [34].

Using a factorization of the generalized form factor we can connect the scaling of ζ_J^{BM} to that of $\phi^M(u)$. Separating the scales $\Lambda^2 \ll m_b \Lambda$ gives the factorization theorem

$$\zeta_J^{BM}(z) = \frac{f_B f_M}{m_b} \int_0^1 dx \int_0^\infty dk^+ J(z, x, k_+) \phi_B(k_+) \phi^{M_1}(x), \quad (46)$$

where J is a ‘‘jet function’’ that can be determined as a power series in $\alpha_s(\mu_i)$ where $\mu_i \sim \sqrt{m_b \Lambda}$. At tree level J is given by

$$J(z, x, k_+) = \delta(x - z) C_F \frac{\alpha_s(\mu) \pi}{N_c \bar{z} k_+}. \quad (47)$$

Using this result in Eq. (46) gives

$$\zeta_J^{BM}(z) \Big|_{\text{tree}} = 4\pi\alpha_s(\mu) \frac{f_B f_M \beta_B}{3m_B} \frac{\phi^M(z)}{\bar{z}}, \quad (48)$$

which demonstrates that the endpoint scaling $\phi^M(z) \sim (z\bar{z})$ implies $\zeta_J^{BM}(z) \sim z$. Beyond tree level the scaling is determined by corrections to $J(z, x, k_+)$, which is currently known to one-loop order [40, 41] and still yields $\zeta_J^{BM}(z) \sim z$. This scaling is expected to persist to all orders. Evidence for this comes from the argument of Ref. [41] that is based on an assumed correspondence between soft and collinear endpoint singularities in the form factor. A strong argument for why these corresponding contributions must always arise when endpoint singularities appear was given in Ref. [30]. Endpoint singularities are simply an artifact of not properly separating momentum regions in the effective theory, and arise in situations

where a collinear momentum generates a double counting with modes that account for the region where the momentum is soft (and vice versa). In the effective field theory this is avoided by including zero-bin subtractions. Thus zero-bin subtractions are not expected to arise for $\zeta_J^{BM}(z)$, whereas the analogous factorization theorem for ζ^{BM} to Eq. (46), which exhibits endpoint singularities, requires zero-bin subtractions [30].

In Eq. (46) the normalization depends on decay constants and the inverse moment parameter

$$\beta_B \equiv \int dk^+ \phi_B(k^+) / (3k^+) = 1 / (3\lambda_B) \sim \Lambda_{\text{QCD}}^{-1}. \quad (49)$$

Unfortunately, use of Eq. (46) to determine the normalization, ζ_J^{BM} , has a large uncertainty due to the unknown parameter β_B and the $\alpha_s(\mu_i)$ expansion. The μ_i dependence can be reduced by using one-loop results for the jet function, but this introduces additional uncertainty from other moments of $\phi_B(k^+)$.

In this paper we avoid using Eq. (46) and instead reduce the hadronic uncertainties by dealing directly with the normalization parameters ζ^{BM} and ζ_J^{BM} determined from data. The analysis in this section constrains the model that we construct for the shape of $\zeta_J^{BM}(z)$, as discussed in section XI below.

V. SUMMARY OF LEADING-ORDER ONE-LOOP COEFFICIENTS

In this section we summarize the main results of our computation of the fourth term on line one of Eq. (11), while

$$\begin{aligned} \Delta b_4^{(1c)} &= \lambda_c^{(f)} \frac{\alpha_s}{4\pi} \left\{ \frac{h_0^c(u, z, \rho) [3C_2(2z-1) + C_1(7z+1)]}{9\bar{u}z} - \frac{h_1^c(u, z, \rho) \rho C_1 (16\bar{u} + 16z - 27)}{27\bar{u}^2z} + \frac{h_2^c(u, z, \rho) C_1 (1 - 8\bar{u})}{27\bar{u}} \right. \\ &\quad \left. + \frac{h_3^c(u, z, \rho) \{9C_2\bar{u}z + C_1[\bar{u}z(16z-1) + 2(16z^2 - 25z + 27)\rho]\}}{54\bar{u}^2(1-z)z} + \frac{[27C_2(2z-1) + C_1\{(64\bar{u} + 55 + S_{b1}\bar{u} + S_{b2})z - 18\}]}{162\bar{u}z} \right\}, \\ \Delta b_4^{(1u)} &= \lambda_u^{(f)} \frac{\alpha_s}{4\pi} \left\{ \frac{h_2^u(u, z) C_1 (1 - 8\bar{u})}{27\bar{u}} + \frac{h_3^u(u, z) \{9C_2 + C_1(16z-1)\}}{54\bar{u}(1-z)} \right. \\ &\quad \left. + \frac{[27C_2(2z-1) + C_1\{(64\bar{u} + 55 + S_{b1}\bar{u} + S_{b2})z - 18\}]}{162\bar{u}z} \right\}, \\ \Delta b_4^{(1g)} &= -(\lambda_u^{(f)} + \lambda_c^{(f)}) \frac{C_{8g} \bar{m}_b}{m_b} \frac{C_F \alpha_s(\mu)}{2N_c \pi \bar{u}}. \end{aligned} \quad (52)$$

In the NDR scheme the constants $S_{b1}^{\text{NDR}} = S_{b2}^{\text{NDR}} = 0$ while in the HV scheme $S_{b1}^{\text{HV}} = -48$, and $S_{b2}^{\text{HV}} = 6$. The contributions from O_{8g} , $\Delta b_4^{(1g)}$ and $\Delta b_4^{(1g)}$, are generated at tree level and so are scheme independent at this order.

leaving the details to follow in the next two sections. For convenience we will use the following decomposition of the α_s corrections

$$\begin{aligned} \Delta c_4^{(f)} &= \Delta c_4^{(1c)} + \Delta c_4^{(1u)} + \Delta c_4^{(1g)} + \mathcal{O}(\alpha_s^2), \\ \Delta b_4^{(f)} &= \Delta b_4^{(1c)} + \Delta b_4^{(1u)} + \Delta b_4^{(1g)} + \mathcal{O}(\alpha_s^2). \end{aligned} \quad (50)$$

Here superscripts (1c) and (1u) denote the one loop contribution due to charm and up quark loops respectively, while (1g) refers to $\mathcal{O}(\alpha_s)$ corrections due to operator O_{8g} . We summarize the results for these terms in the NDR and HV schemes. For $\Delta c_4^{(f)}$ we have

$$\begin{aligned} \Delta c_4^{(1c)} &= -\lambda_c^{(f)} \frac{C_F C_1 \alpha_s(\mu)}{6N_c \pi} \left\{ \frac{2\rho}{\bar{u}} h_1^c(u, 1, \rho) + h_2^c(u, 1, \rho) - \frac{4}{3} + S_c \right\}, \\ \Delta c_4^{(1u)} &= -\lambda_u^{(f)} \frac{C_F C_1 \alpha_s(\mu)}{6N_c \pi} \left\{ h_2^u(u, 1) - \frac{4}{3} + S_c \right\}, \\ \Delta c_4^{(1g)} &= -(\lambda_u^{(f)} + \lambda_c^{(f)}) \frac{C_{8g} \bar{m}_b}{m_b} \frac{C_F \alpha_s(\mu)}{2N_c \pi \bar{u}}, \end{aligned} \quad (51)$$

which agrees with the computation in Ref. [17] and the verification in Ref. [16]. In the NDR scheme the constant $S_c^{\text{NDR}} = 0$ while in the HV scheme $S_c^{\text{HV}} = 1$. One of our main result is the corresponding corrections for $\Delta b_4^{(f)}$,

In Eqs. (51,52), $\rho = m_c^2/m_b^2$ and

$$\begin{aligned} h_0^c(u, z, \rho) &= \frac{\rho}{\bar{u}z} \left\{ \text{Li}_2 \left[\frac{2}{1 - g(\rho/\bar{u}z)} \right] + \text{Li}_2 \left[\frac{2}{1 + g(\rho/\bar{u}z)} \right] - \text{Li}_2 \left[\frac{2}{1 + g(\rho/\bar{u})} \right] - \text{Li}_2 \left[\frac{2}{1 - g(\rho/\bar{u})} \right] \right\}, \\ h_1^c(u, z, \rho) &= G(\bar{u}z, \rho) - \ln \left(\frac{\mu^2}{m_b^2 \rho} \right), \\ h_2^c(u, z, \rho) &= G(\bar{u}z, \rho). \end{aligned} \quad (53)$$

where we have the usual massive and massless fermion loop functions

$$\begin{aligned}
G(x, \rho) &= \ln\left(\frac{\mu^2}{m_b^2 \rho}\right) - 2\theta(4\rho - x) \bar{g}(\rho/x) \cot^{-1}[\bar{g}(\rho/x)] \\
&\quad + 2 - \theta(x - 4\rho) g(\rho/x) \left\{ \ln\left[\frac{1 + g(\rho/x)}{1 - g(\rho/x)}\right] - i\pi \right\}, \\
G_0(x) &= 2 + \ln\left(\frac{\mu^2}{m_b^2 x}\right) + i\pi,
\end{aligned} \tag{54}$$

with $g(x) = \sqrt{1 - 4x}$ and $\bar{g}(x) = \sqrt{4x - 1}$. The h_i functions are given in terms of loop integrals in Appendix A. The factors of α_s in Eqs. (51,52) should be evaluated at $\mu \simeq m_b$. One can also look at the endpoint power law behavior of these matching coefficients, for which we find $\Delta c_4^{(1c),(1u)} \sim 1$, $\Delta c_4^{(1g)} \sim \Delta b_4^{(1g)} \sim 1/\bar{u}$, and $\Delta b_4^{(1c),(1u)} \sim 1/(\bar{u}z)$.

The SCET Wilson coefficients $c_4^{(f)}$ and $b_4^{(f)}$ should not depend on the γ_5 -scheme choice for H_W . From the point of view of the electroweak Hamiltonian, the scheme dependence in Eqs. (51,52) corresponds to that in matrix elements, and is compensated by scheme dependence of the electroweak Hamiltonian's Wilson coefficients. At lowest order, $c_4^{(f)}$ and $b_4^{(f)}$ in Eqs. (44,45) depend on the penguin coefficients C_3 and C_4 . Since we are calculating $c_4^{(f)}$ and $b_4^{(f)}$ to order α_s we need to take into account the scheme-dependence of $C_{3,4}$ up to order α_s , which for $\mu \simeq m_b$ is given by

$$\begin{aligned}
C_3^{\text{NDR}} &= C_3^{\text{HV}} + \frac{\alpha_s C_1}{36\pi} + \mathcal{O}(\alpha_s^2), \\
C_4^{\text{NDR}} &= C_4^{\text{HV}} - \frac{\alpha_s C_1}{12\pi} + \mathcal{O}(\alpha_s^2).
\end{aligned} \tag{55}$$

Thus at this order the results in Eqs. (44,45) have to be used in the same scheme as the $\Delta c_4^{(f)}$ and $\Delta b_4^{(f)}$ corrections. In $c_4^{(f)}$ and $b_4^{(f)}$ we find that it is only the scheme independent combinations

$$\begin{aligned}
c_4^{(f)} &= -\lambda_t^{(f)} \left[C_4 + \frac{C_3}{3} - \frac{2\alpha_s C_1 S_c}{27\pi} \right] + \dots, \\
b_4^{(f)} &= -\lambda_t^{(f)} \left[C_4 + \frac{1 + \bar{u}}{3\bar{u}} C_3 + \frac{\alpha_s C_1 (S_{b1}\bar{u} + S_{b2})}{648\pi\bar{u}} \right] + \dots
\end{aligned} \tag{56}$$

that occur. This demonstrates that our final results are independent of whether we use the NDR or HV scheme.

VI. CONTRIBUTIONS OF THE CHARM LOOP (NDR SCHEME)

In this section we present the matching calculation in the NDR scheme, where we have an anticommuting γ_5 in $d = 4 - 2\epsilon$ dimensions. For $\Delta c_4^{(f)}$ we calculate the full-theory graphs in Fig. 1a,b,c and match them onto the SCET graph in Fig. 2. In order to ensure that the NDR scheme is consistent, it is important to avoid computing

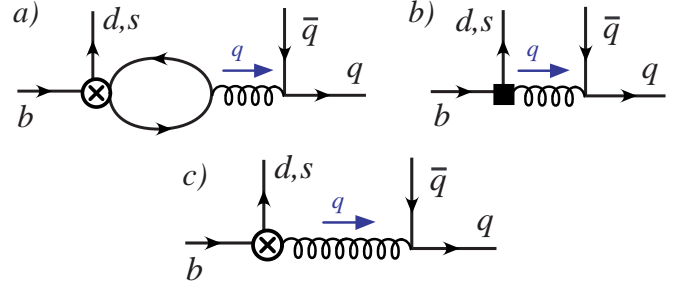


FIG. 1: Full-theory graphs for the matching onto the short-distance penguin coefficient c_4 at $\mathcal{O}(\alpha_s)$. a) loop graph with charm quarks and $C_{1,2}^c$ or up-quarks and $C_{1,2}^u$, b) counterterm graph with O_{DG} , and c) graph with C_{sg} .

Figure 2 shows a SCET Feynman rule diagram. It features a vertex where a b quark line (solid) and a q quark line (dashed) meet. From this vertex, a d,s quark line (dashed) goes up and a q-bar quark line (dashed) goes right. The diagram is equated to the expression $\frac{2G_F}{\sqrt{2}} c_4^{(d,s)} F$.

FIG. 2: SCET Feynman rule for the $Q_{dd}^{(0)}$ operator where the spinors are $F = [\bar{u}_n^{(d)} \not{P}_L u_v^{(b)}][\bar{u}_n^{(q)} \not{P}_L v_n^{(q)}]$.

traces from a closed fermion loop, $\text{tr}[\gamma^\mu \gamma^\nu \gamma^\alpha \gamma^\beta \gamma_5]$ (see Ref. [47] for a review). In the basis shown in Eq. (33) the charm fields are not in the same bilinear, so Fig. 1a does not involve a trace. Since we are treating $m_c \sim m_b$, there are no corresponding loop graphs in the effective theory. Possible loop corrections stemming from NRQCD loops vanish at leading order in the power counting, as discussed later in section IX on long-distance charm contributions.

To renormalize Fig. 1a we use the operator

$$O_{DG} = \bar{d}[D_\mu, g G^{\mu\nu}] \gamma_\nu (1 - \gamma_5) b, \tag{57}$$

which appears in the electro-weak Hamiltonian as

$$H_{c.t.} = \frac{G_F}{\sqrt{2}} \sum_{p=u,c} \lambda_p^{(d)} C_{DG} O_{DG}. \tag{58}$$

In the standard basis for H_W given in Eq. (33) the operator O_{DG} is redundant and has been removed using the gluon equation of motion (corresponding to an on-shell basis of operators). For our computation we keep O_{DG} with a pure counterterm coefficient, δC_{DG} , and use it for renormalization. This has the advantage that the counterterm graphs maintain their topological correspondence with the divergent loops (when the divergent loop is shrunk to a point). Furthermore, it allows us to obtain the desired matching results while avoiding the use of d -dimensional Fierz relations with evanescent operators. At the end of the computation we remove O_{DG} following Ref. [48], by writing it in terms of four-quark operators and an operator that vanishes by the equations of motion, $[D_\mu, G^{\mu\nu}] = -gT^a \sum_q \bar{q} \gamma^\nu T^a q$, and transforming the two-loop anomalous dimension back to that for the standard basis. As shown in Ref. [48] this gives the usual

two-loop anomalous dimension in the NDR scheme [39]. Thus our NDR scheme coefficients are the standard ones.

The graph in Fig. 1b involves an insertion of the operator O_{DG} with counterterm coefficient δC_{DG} , where

$$C_{DG}^{\text{bare}} O_{DG}[\psi^0, A^0] = C_{DG} O_{DG}^{\text{ren}} + \delta C_{DG} O_{DG}^{\text{ren}}.$$

Thus δC_{DG} corresponds to a combination of a counterterm for composite operator renormalization, and wavefunction renormalization, which for our purposes are not required separately. The choice $\delta C_{DG} = -4C_1/(3(4\pi)^2\epsilon)$ cancels the $1/\epsilon$ divergence in Fig. 1a. The same value for δC_{DG} will be used to renormalize the H_W graphs needed for the matching computation for $\Delta b_4^{(f)}$ below.

At this order in α_s we only have the tree level graph shown in Fig. 2 on the SCET_I side. Matching Fig. 1 and Fig. 2 gives the following contribution to the SCET coefficient $c_4^{(f)}$ in the notation of Eq. (50):

$$\begin{aligned} \Delta c_4^{(1c)} &= -\lambda_c^{(f)} \frac{C_F \alpha_s C_1}{6\pi N_c} \left\{ \frac{2m_c^2}{q^2} [I_0(q^2) - I_0] + I_0(q^2) - \frac{1}{\epsilon} - \frac{4}{3} \right\} \\ \Delta c_4^{(1u)} &= -\lambda_u^{(f)} \frac{C_F \alpha_s C_1}{6\pi N_c} \left\{ I_0^{(u)}(q^2) - \frac{1}{\epsilon} - \frac{4}{3} \right\}, \\ \Delta c_4^{(1g)} &= -(\lambda_u^{(f)} + \lambda_c^{(f)}) \frac{C_{8g} \bar{m}_b}{m_b} \left(\frac{2\alpha_s}{9\pi \bar{u}} \right), \end{aligned} \quad (59)$$

where definitions for the loop integrals $I_0(q^2)$ etc. are given in the appendix. The explicit $1/\epsilon$ comes from the counterterm graph and cancels the divergence in $I_0(q^2)$. In terms of momentum fractions Eq. (59) yields the NDR result given above in Eq. (51).

Next consider the computation of $\Delta b_4^{(f)}$ which comes from matching the full theory loop graphs in Fig. 3 and counterterm diagrams with O_{DG} shown in Fig. 4, onto the tree level SCET graph in Fig. 5. We refer to the graphs in Fig. (3) as G_a, G_b etc. and those in Fig. (4) as $\delta G_{ab}, \delta G_c$ etc.

The results for the graphs with quark-loops, Fig. 3a-f, are

$$\begin{aligned} G_a &= \frac{ig^3}{q^2} \frac{i}{(4\pi)^2} [\bar{q}_n \gamma_{\perp\mu} T^b q_{\bar{n}}] \left[\bar{d}_{\bar{n}} \not{\epsilon} \left(\frac{\bar{n} \cdot f_1}{2} \gamma_{\perp}^{\lambda} \gamma_{\perp}^{\mu} + \frac{\bar{n} \cdot f_2}{2} \gamma_{\perp}^{\mu} \gamma_{\perp}^{\lambda} \right) \left(C_1 T^b T^a + \frac{C_2}{2} \delta^{ab} \right) P_L b_v \right], \\ G_b &= \frac{-ig^3}{q^2} \frac{i}{(4\pi)^2} [\bar{q}_n \gamma_{\perp\mu} T^b q_{\bar{n}}] \left[\bar{d}_{\bar{n}} \not{\epsilon} \left(\frac{\bar{n} \cdot f_2}{2} \gamma_{\perp}^{\lambda} \gamma_{\perp}^{\mu} + \frac{\bar{n} \cdot f_1}{2} \gamma_{\perp}^{\mu} \gamma_{\perp}^{\lambda} \right) \left(C_1 T^a T^b + \frac{C_2}{2} \delta^{ab} \right) P_L b_v \right], \\ \delta G_{ab} &= \frac{2iC_1 g^3 f^{abc}}{3(4\pi)^2 q^2 \epsilon} [\bar{q}_n \gamma_{\perp}^{\lambda} T^b q_{\bar{n}}] [\bar{d}_{\bar{n}} (\not{\epsilon} - \not{p}) P_L T^c b_v], \\ G_c + \delta G_c &= \frac{-2g^3 (2C_1) f^{abc}}{3q^2 (p+q)^2} [\bar{d}_{\bar{n}} \gamma_{\alpha} P_L T^c b_v] [\bar{q}_n \gamma_{\perp}^{\lambda} T^b q_{\bar{n}}] \frac{i}{(4\pi)^2} \left\{ \frac{2m_c^2}{(p+q)^2} (I_0((p+q)^2) - I_0) + I_0((p+q)^2) - \frac{1}{\epsilon} - \frac{4}{3} \right\} \\ &\quad \times \{q^2 p^{\alpha} + p \cdot q (p^{\alpha} - q^{\alpha})\}, \\ G_d + \delta G_d &= \frac{ig^3 (2C_1)}{6m_b u} [\bar{d}_{\bar{n}} \not{\epsilon} \gamma_{\perp}^{\lambda} \gamma_{\perp}^{\mu} T^a T^b P_L b_v] [\bar{q}_n \gamma_{\perp\mu} T^b q_{\bar{n}}] \frac{i}{(4\pi)^2} \left\{ \frac{2m_c^2}{q^2} (I_0(q^2) - I_0) + I_0(q^2) - \frac{1}{\epsilon} - \frac{4}{3} \right\}, \\ G_e + \delta G_e &= \frac{ig^3 (2C_1)}{6m_b} [\bar{d}_{\bar{n}} \not{\epsilon} \gamma_{\perp}^{\mu} \gamma_{\perp}^{\lambda} T^b T^a P_L b_v] [\bar{q}_n \gamma_{\perp\mu} T^b q_{\bar{n}}] \frac{i}{(4\pi)^2} \left\{ \frac{2m_c^2}{q^2} (I_0(q^2) - I_0) + I_0(q^2) - \frac{1}{\epsilon} - \frac{4}{3} \right\}, \\ G_f + \delta G_f &= \frac{ig^3 (2C_1)}{6m_b (1-u)} [\bar{d}_{\bar{n}} \not{\epsilon} T^b P_L b_v] [\bar{q}_n \gamma_{\perp}^{\lambda} T^b T^a q_{\bar{n}}] \frac{i}{(4\pi)^2} \left\{ \frac{2m_c^2}{(p+q)^2} (I_0((p+q)^2) - I_0) + I_0((p+q)^2) - \frac{1}{\epsilon} - \frac{4}{3} \right\}, \\ G_g + \delta G_g &= \frac{ig^3 (2C_1)}{6m_b (1-u)} [\bar{d}_{\bar{n}} \not{\epsilon} T^b P_L b_v] [\bar{q}_n \gamma_{\perp}^{\lambda} T^a T^b q_{\bar{n}}] \frac{i}{(4\pi)^2} \left\{ \frac{2m_c^2}{(p+q)^2} (I_0((p+q)^2) - I_0) + I_0((p+q)^2) - \frac{1}{\epsilon} - \frac{4}{3} \right\}. \end{aligned} \quad (60)$$

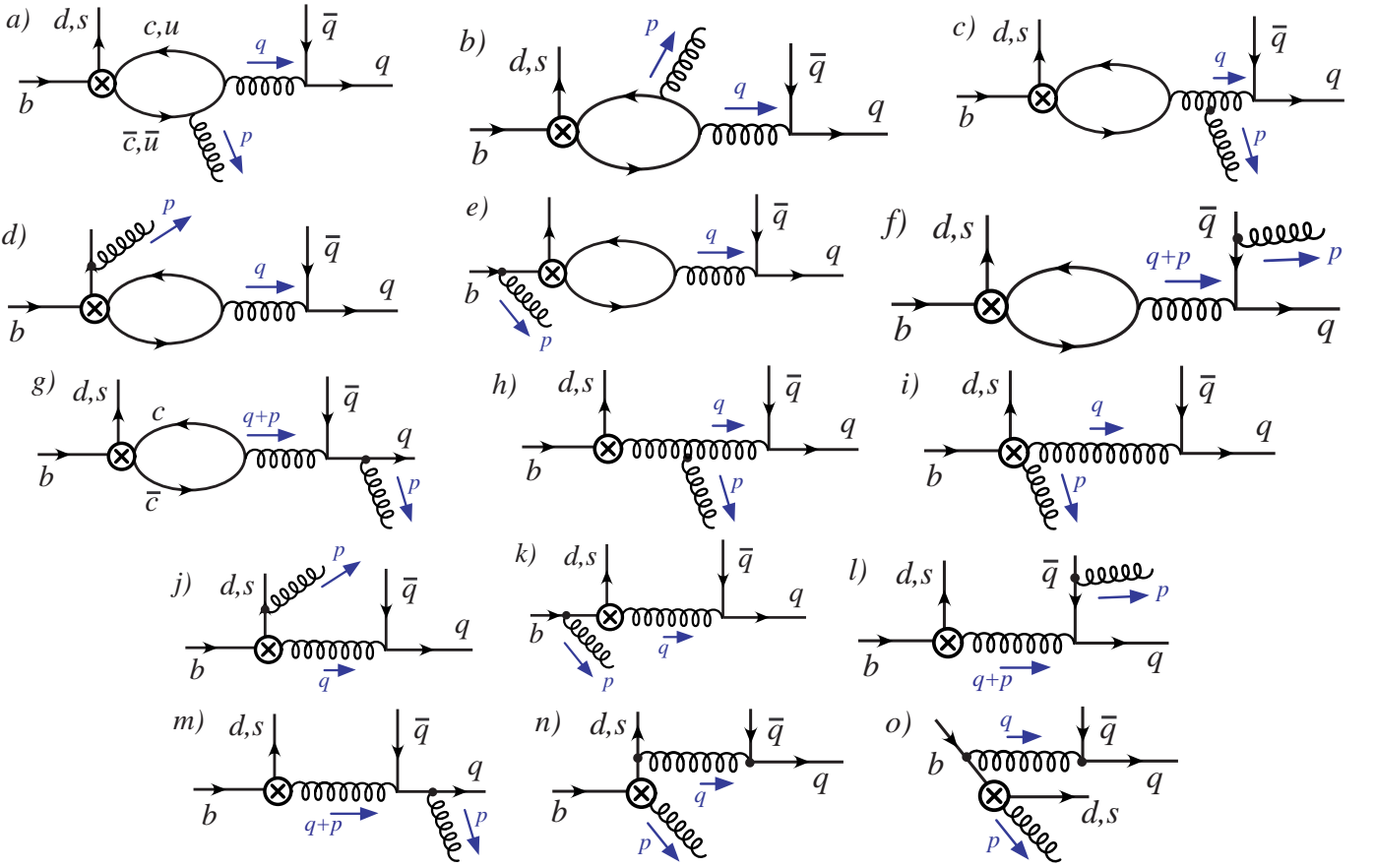


FIG. 3: Graphs for the matching onto the penguin coefficient b_4 at $\mathcal{O}(\alpha_s)$. Not drawn are i) graphs with no gluon attached to the quark loop, which vanish in the NDR and HV schemes due to the chirality, and ii) graphs with only the gluon of momentum p radiated from the quark loop which also vanish. Here the momentum fraction of the gluon is \bar{z} with $\bar{n} \cdot p = m_b \bar{z}$, the q -quark has fraction z , with $\bar{n} \cdot q = m_b z$, the \bar{q} -quark has momentum fraction \bar{u} , so $n \cdot q = m_b \bar{u}$, and the d or s quark has fraction u .

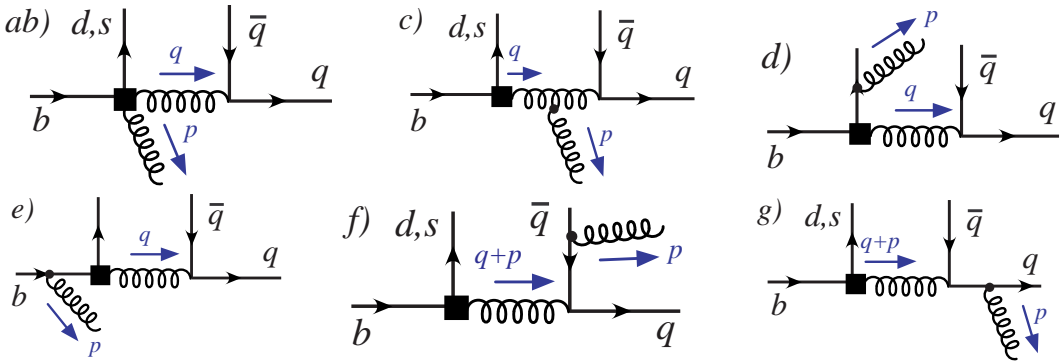


FIG. 4: Counterterm graphs for Fig. 3 involving the operator O_{DG} . The graph labeled ab) is the counterterm for the sum of graphs a) and b) in Fig. 3.

In G_a and G_b we have objects f_1^α and f_2^α which are defined by

$$\begin{aligned}
f_1^\alpha(p, q, m_c) &= \left\{ 2m_c^2 \left(q^\alpha - p^\alpha - \frac{q^2 p^\alpha}{2p \cdot q} \right) J_0 + \left(\frac{q^2 q^\alpha}{3p \cdot q} + \frac{2m_c^2 q^\alpha}{3p \cdot q} + \frac{q^2 p^\alpha}{2p \cdot q} - \frac{2m_c^2 q^2 p^\alpha}{3(p \cdot q)^2} - \frac{q^4 p^\alpha}{12(p \cdot q)^2} \right) [I_0((p+q)^2) - I_0(q^2)] \right. \\
&\quad \left. - \frac{2m_c^2 p^\alpha}{3p \cdot q} [I_0((p+q)^2) - I_0] - \frac{(q^\alpha - p^\alpha)}{3} I_0((p+q)^2) + \left(\frac{10}{9} (q^\alpha - p^\alpha) - \frac{q^2 p^\alpha}{6p \cdot q} \right) \right\}, \\
f_2^\alpha(p, q, m_c) &= \left\{ -m_c^2 \left(\frac{q^2 p^\alpha}{p \cdot q} \right) J_0 + \left(-\frac{q^2 q^\alpha}{6p \cdot q} + \frac{2m_c^2 q^\alpha}{3p \cdot q} - \frac{2m_c^2 q^2 p^\alpha}{3(p \cdot q)^2} - \frac{q^4 p^\alpha}{12(p \cdot q)^2} \right) [I_0((p+q)^2) - I_0(q^2)] \right. \\
&\quad \left. - \frac{2m_c^2 p^\alpha}{3p \cdot q} [I_0((p+q)^2) - I_0] - \frac{(q^\alpha - p^\alpha)}{3} I_0((p+q)^2) + \left(\frac{1}{9} (q^\alpha - p^\alpha) - \frac{q^2 p^\alpha}{6p \cdot q} \right) \right\}. \tag{61}
\end{aligned}$$

Results for the loop integrals I_0 and J_0 are given in appendix A. Note that the only contributions from the δG -counterterm graphs are explicit $1/\epsilon$'s, which exactly cancel divergences due to the loop integrals. We have made some simplifications in the expressions for the last four graphs, where u is the momentum fraction of the d-quark in M_1 and z is the momentum fraction of the quark in M_2 . The result $G_g + \delta G_g$ corresponds to the contribution of the expansion of the external full QCD q -quark field onto the n -collinear quark field in SCET. For $\Delta S = 1$ decays with $f = s$ one makes the replacement $\bar{d}_n \rightarrow \bar{s}_n$ in Eq. (60).

Next we sum the graphs in Eq. (60) and Fierz them to match onto the SCET operator $Q_{4f}^{(1)}$, and thus obtain $\Delta b_4^{(f)}$. The results for $G_a + G_b + \delta G_{ab}$, $G_c + \delta G_c$, etc. are finite as $\epsilon \rightarrow 0$, so we can Fierz them in 4-dimensions,

and then read off the prefactor of the spinors $P^{\lambda a}$ shown in Fig. 5 to obtain $\Delta b_4^{(f)}$. A few useful Fierz formulas are listed in appendix A. The definitions for all momentum fractions are summarized in the caption of Fig. 3. The result in the NDR scheme is

$$= \frac{-4gG_F \epsilon_\lambda^\alpha}{\sqrt{2}m_b} b_4^{(d,s)} P^{\lambda a}$$

FIG. 5: SCET Feynman rule for the $Q_{4d}^{(1)}$ operator where the spinor product is $P^{\lambda a} = [\bar{u}_n^{(d)} T^a \gamma_\perp^\mu P_L u_v^{(b)}][\bar{u}_n^{(q)} \not{P} P_L v_n^{(q)}]$.

$$\begin{aligned}
\Delta b_4^{(1c)} &= \lambda_c^{(f)} \frac{\alpha_s}{4\pi} \left\{ \frac{m_c^2 J_0 [3C_2(2z-1) + C_1(7z+1)]}{9\bar{u}z} - \frac{(I_0(q^2) - I_0)\rho C_1(16\bar{u} + 16z - 27)}{27\bar{u}^2 z} \right. \\
&\quad + \frac{(I_0(q^2) - \frac{1}{\epsilon}) C_1(1-8\bar{u})}{27\bar{u}} + \frac{(I_0((p+q)^2) - I_0(q^2))\{9C_2\bar{u}z + C_1[\bar{u}z(16z-1) + 2(16z^2 - 25z + 27)\rho]\}}{54\bar{u}^2(1-z)z} \\
&\quad \left. + \frac{[27C_2(2z-1) + C_1\{(64\bar{u} + 55)z - 18\}]}{162\bar{u}z} \right\}. \tag{62}
\end{aligned}$$

The result for the up-quark penguin loops is simply obtained by taking $m_c \rightarrow 0$ which gives

$$\begin{aligned}
\Delta b_4^{(1u)} &= \lambda_u^{(d)} \frac{\alpha_s}{4\pi} \left\{ \frac{(I_0^{(u)}(q^2) - \frac{1}{\epsilon}) C_1(1-8\bar{u})}{27\bar{u}} + \frac{(I_0^{(u)}((p+q)^2) - I_0^{(u)}(q^2))\{9C_2 + C_1(16z-1)\}}{54\bar{u}(1-z)} \right. \\
&\quad \left. + \frac{[27C_2(2z-1) + C_1\{(64\bar{u} + 55)z - 18\}]}{162\bar{u}z} \right\}. \tag{63}
\end{aligned}$$

These results for $\Delta b_4^{(1c)}$ and $\Delta b_4^{(1u)}$ in NDR are summarized in a more compact notation in Eq. (52).

Next we quote the results for contributions of the graphs with the operator O_{8g} , Fig. 3h-m give

$$\begin{aligned}
G_h &= \frac{-ig^3 C_{8g} \bar{m}_b}{8\pi^2 m_b^2} \left(\frac{\bar{z}}{\bar{u}z} \right) f^{abc} [\bar{d}_{\bar{n}} P_R T^c b_v] [\bar{q}_n \gamma_{\perp}^{\lambda} T^b q_{\bar{n}}] \\
G_i &= \frac{-ig^3 C_{8g} \bar{m}_b}{16\pi^2 m_b^2} \left(\frac{1}{\bar{u}z} \right) f^{abc} [\bar{d}_{\bar{n}} (\gamma_{\perp}^{\lambda} \gamma_{\perp}^{\mu} - \gamma_{\perp}^{\mu} \gamma_{\perp}^{\lambda}) P_R T^c b_v] [\bar{q}_n \gamma_{\perp}^{\mu} T^b q_{\bar{n}}] \\
G_j &= \frac{-g^3 C_{8g} \bar{m}_b}{8\pi^2 m_b^2} \left(\frac{1}{uz} \right) [\bar{d}_{\bar{n}} \gamma_{\perp}^{\lambda} \gamma_{\perp}^{\mu} P_R T^a T^b b_v] [\bar{q}_n \gamma_{\perp \mu} T^b q_{\bar{n}}] \\
G_l &= \frac{-g^3 C_{8g} \bar{m}_b}{8\pi^2 m_b^2} \left(\frac{1}{\bar{u}} \right) [\bar{d}_{\bar{n}} P_R T^b b_v] [\bar{q}_n \gamma_{\perp}^{\lambda} T^b T^a q_{\bar{n}}] \\
G_m &= \frac{-g^3 C_{8g} \bar{m}_b}{8\pi^2 m_b^2} \left(\frac{1}{\bar{u}} \right) [\bar{d}_{\bar{n}} P_R T^b b_v] [\bar{q}_n \gamma_{\perp}^{\lambda} T^a T^b q_{\bar{n}}] \\
G_o &= \frac{g^3 C_{8g} \bar{m}_b}{8\pi^2 m_b^2} \left(\frac{\bar{z}}{z(z + \bar{u}\bar{z})} \right) [\bar{d}_{\bar{n}} \gamma_{\perp}^{\lambda} \gamma_{\perp}^{\mu} P_R T^a T^b b_v] [\bar{q}_n \gamma_{\perp \mu} T^b q_{\bar{n}}] \\
G_k &= G_n = 0.
\end{aligned} \tag{64}$$

Here \bar{m}_b is the $\overline{\text{MS}}$ mass which always accompanies C_{8g} , while m_b is a short-distance threshold mass (for which we will use the 1S-mass). For $f = s$ we take $\bar{d}_{\bar{n}} \rightarrow \bar{s}_{\bar{n}}$. Fierzing the results in Eq. (64) and matching onto Fig. 5 we obtain the contribution to $\Delta b_4^{(d)}$ due to O_{8g} ,

$$\Delta b_4^{(1g)} = -(\lambda_u^{(f)} + \lambda_c^{(f)}) \frac{C_{8g} \bar{m}_b}{m_b} \left(\frac{2\alpha_s}{9\pi\bar{u}} \right), \tag{65}$$

which turns out to be identical to the matching result for $\Delta c_4^{(1g)}$.

VII. CONTRIBUTIONS OF THE CHARM LOOP (HV SCHEME)

Next we repeat the calculation of the previous section using the HV scheme. In the HV scheme, γ_5 anticommutes with Dirac matrices in 4-dimensions, and commutes with the Dirac matrices in the remaining (-2ϵ) -dimensions. Here we can consistently handle traces with γ^5 in $d \neq 4$ dimensions. In the HV scheme the Dirac matrices in the $(V - A)$ interactions in the weak Hamiltonian are taken in four-dimensions, while all γ -matrices from the QCD and QED Lagrangians are in d -dimensions

(see Ref. [47] for a review of the HV scheme). We will perform the computation in two operator bases, namely the original one $O_{1,2}^p$ in Eq. (33) and a different basis given by

$$\begin{aligned}
\tilde{O}_1^p &= [\bar{d}b]_{V-A} [\bar{p}p]_{V-A}, \\
\tilde{O}_2^p &= [\bar{d}T^a b]_{V-A} [\bar{p}T^a p]_{V-A},
\end{aligned} \tag{66}$$

with Wilson coefficients \tilde{C}_1 and \tilde{C}_2 . Notice that in addition to the different Fierz order, the $\tilde{O}_{1,2}^p$ basis is also color Fierzed with respect to the $O_{1,2}^p$ basis. In the $\tilde{O}_{1,2}^p$ basis we need to evaluate fermion traces like $\text{tr}[\gamma^{\mu} \gamma^{\nu} \gamma^{\alpha} \gamma^{\beta} \gamma_5]$. As we explain below, the answer for the matching computation in either of these bases is the same in the HV-scheme. Renormalization with the operator O_{DG} goes the same way as in the NDR scheme except that we replace $C_1 = \tilde{C}_2/2$.

The result for the charm and up-quark loop in the HV scheme is well known, see e.g. Ref. [39], and with either basis gives the same result for $\Delta c_4^{(1c)}$ and $\Delta c_4^{(1u)}$ as the NDR scheme but with $S_c^{\text{HV}} = +1$ in Eq. (51).

For Δb_4 we start with the computation in the $\tilde{O}_{1,2}^p$ basis. The graphs in Figs. 3 and 4 give

$$\begin{aligned}
G_a + G_b + \delta G_{ab} &= \frac{2i\tilde{C}_1 g^3}{(4\pi)^2} \epsilon^{\alpha\lambda\mu\rho} \left[\frac{(p_\rho - q_\rho)}{q^2} \left(m_c^2 J_0 + \frac{1}{2} \right) - (q_\rho + p_\rho) \frac{1}{4p \cdot q} (I_0((p+q)^2) - I_0(q^2)) \right] [\bar{d}_{\bar{n}} \gamma_\alpha P_L b_v] [\bar{q}_n \gamma_{\perp\mu} T^a q_{\bar{n}}] \\
&+ \frac{i\tilde{C}_2 g^3}{(4\pi)^2} \left\{ d^{abc} \epsilon^{\alpha\lambda\mu\rho} \left[\frac{(p_\rho - q_\rho)}{q^2} \left(m_c^2 J_0 + \frac{1}{2} \right) - (q_\rho + p_\rho) \frac{1}{4p \cdot q} (I_0((p+q)^2) - I_0(q^2)) \right] [\bar{d}_{\bar{n}} \gamma_\alpha P_L T^c b_v] [\bar{q}_n \gamma_{\perp\mu} T^b q_{\bar{n}}] \right. \\
&\quad + \frac{f^{abc}}{q^2} \left[\left(\frac{q^2}{4p \cdot q} (p^\alpha + q^\alpha) + \frac{2m_c^2}{3p \cdot q} q^\alpha - \frac{q^2}{6p \cdot q} q^\alpha - \frac{2m_c^2 q^2}{3(p \cdot q)^2} p^\alpha - \frac{q^4}{12(p \cdot q)^2} p^\alpha \right) (I_0((p+q)^2) - I_0(q^2)) \right. \\
&\quad + \frac{1}{3} (p^\alpha - q^\alpha) \left(I_0((p+q)^2) - \frac{1}{\epsilon} \right) - \frac{2m_c^2 p^\alpha}{3p \cdot q} (I_0((p+q)^2) - I_0) - \left(m_c^2 (p^\alpha - q^\alpha) + \frac{m_c^2 q^2}{p \cdot q} p^\alpha \right) J_0 \\
&\quad \left. \left. - p^\alpha \frac{q^2}{6p \cdot q} - \frac{5}{18} (p^\alpha - q^\alpha) \right] [\bar{d}_{\bar{n}} \gamma_\alpha P_L T^c b_v] [\bar{q}_n \gamma_{\perp}^\lambda T^b q_{\bar{n}}] \right\}, \tag{67}
\end{aligned}$$

where we use $\epsilon^{0123} = +1$. In Figs. 3c-g only \tilde{O}_2^p contributes, and we have

$$\begin{aligned}
G_c + \delta G_c &= \frac{-2\tilde{C}_2 g^3 f^{abc}}{3q^2(p+q)^2} [\bar{d}_{\bar{n}} \gamma_\alpha P_L T^c b_v] [\bar{q}_n \gamma_{\perp}^\lambda T^b q_{\bar{n}}] \frac{i}{(4\pi)^2} \left\{ \frac{2m_c^2}{(p+q)^2} (I_0((p+q)^2) - I_0) + I_0((p+q)^2) - \frac{1}{\epsilon} - \frac{1}{3} \right\} \\
&\quad \times \{q^2 p^\alpha + p \cdot q (p^\alpha - q^\alpha)\}, \\
G_d + \delta G_d &= \frac{i\tilde{C}_2 g^3}{6m_b u} [\bar{d}_{\bar{n}} \not{k} \gamma_{\perp}^\lambda \gamma_{\perp}^\mu T^a T^b P_L b_v] [\bar{q}_n \gamma_{\perp\mu} T^b q_{\bar{n}}] \frac{i}{(4\pi)^2} \left\{ \frac{2m_c^2}{q^2} (I_0(q^2) - I_0) + I_0(q^2) - \frac{1}{\epsilon} - \frac{1}{3} \right\}, \\
G_e + \delta G_e &= \frac{i\tilde{C}_2 g^3}{6m_b} [\bar{d}_{\bar{n}} \not{k} \gamma_{\perp}^\mu \gamma_{\perp}^\lambda T^b T^a P_L b_v] [\bar{q}_n \gamma_{\perp\mu} T^b q_{\bar{n}}] \frac{i}{(4\pi)^2} \left\{ \frac{2m_c^2}{q^2} (I_0(q^2) - I_0) + I_0(q^2) - \frac{1}{\epsilon} - \frac{1}{3} \right\}, \\
G_f + \delta G_f &= \frac{i\tilde{C}_2 g^3}{6m_b(1-u)} [\bar{d}_{\bar{n}} \not{k} T^b P_L b_v] [\bar{q}_n \gamma_{\perp}^\lambda T^b T^a q_{\bar{n}}] \frac{i}{(4\pi)^2} \left\{ \frac{2m_c^2}{(p+q)^2} (I_0((p+q)^2) - I_0) + I_0((p+q)^2) - \frac{1}{\epsilon} - \frac{1}{3} \right\}, \\
G_g + \delta G_g &= \frac{i\tilde{C}_2 g^3}{6m_b(1-u)} [\bar{d}_{\bar{n}} \not{k} T^b P_L b_v] [\bar{q}_n \gamma_{\perp}^\lambda T^a T^b q_{\bar{n}}] \frac{i}{(4\pi)^2} \left\{ \frac{2m_c^2}{(p+q)^2} (I_0((p+q)^2) - I_0) + I_0((p+q)^2) - \frac{1}{\epsilon} - \frac{1}{3} \right\}.
\end{aligned} \tag{68}$$

Results for I_0 and J_0 can be found in appendix A. Again we are free to Fierz these finite results in 4-dimensions. Computing $\Delta c_4^{(f)}$ and $\Delta b_4^{(f)}$ from these expressions gives the results summarized in Eq. (52).

Alternatively one can do the HV scheme calculation in the same basis $O_{1,2}^p$ as the NDR scheme calculation. Although there are no fermion loops in this basis the HV scheme computation does differ from the NDR scheme. For each graph the results differ due to an extra $\mathcal{O}(\epsilon)$ term generated in manipulating the Dirac matrices. Therefore it is easy to quote the HV scheme results obtained in this basis, as replacements to be made in the in NDR result. For f_1^α in Eq. (61) we should replace

$$\left(\frac{10}{9} (q^\alpha - p^\alpha) - \frac{q^2 p^\alpha}{6p \cdot q} \right) \rightarrow \left(\frac{7}{9} (q^\alpha - p^\alpha) - \frac{q^2 p^\alpha}{6p \cdot q} \right), \tag{69}$$

and for f_2^α the HV scheme result is obtained by replacing

$$\left(\frac{1}{9} (q^\alpha - p^\alpha) - \frac{q^2 p^\alpha}{6p \cdot q} \right) \rightarrow \left(\frac{-2}{9} (q^\alpha - p^\alpha) - \frac{q^2 p^\alpha}{6p \cdot q} \right). \tag{70}$$

For graphs $G_c + \delta G_c$ to $G_g + \delta G_g$ in Eq. (60) and for $\Delta c_4^{(1p)}$ in Eq. (59) we replace

$$-\frac{4}{3} \rightarrow -\frac{1}{3}. \tag{71}$$

Finally the HV scheme result for $\Delta b_4^{(1p)}$ in Eqns. (62) and (63) is obtained by the replacement

$$\begin{aligned}
&\frac{[27C_2(2z-1) + C_1\{(64\bar{u}+55)z-18\}]}{162\bar{u}z} \\
&\rightarrow \frac{[27C_2(2z-1) + C_1\{(16\bar{u}+61)z-18\}]}{162\bar{u}z}. \tag{72}
\end{aligned}$$

This is same as the result that we obtained from the HV scheme calculation in the $\tilde{O}_{1,2}^p$ basis. As discussed earlier in section V, the scheme dependence in C_3 and C_4 which appear at tree level accounts for the shifts in $\Delta c_4^{(f)}$ and $\Delta b_4^{(f)}$ given by Eqs. (71) and (72), thus leaving the SCET Wilson coefficients independent of choice of NDR or HV scheme. The calculation in the HV scheme in the $\tilde{O}_{1,2}^p$ basis differs from that in the NDR scheme, and provides a non-trivial cross-check on our results.

VIII. CHIRALY ENHANCED PENGUINS

It is well known that certain power corrections have the potential to be numerically enhanced in penguin amplitudes. In particular the so-called chirally enhanced terms [17], which are formally down by a factor of Λ/m_b , but are numerically of order μ_P/m_b .² For the pion $\mu_\pi(2\text{ GeV}) = 1.7\text{ GeV}$, and this can be understood from the fact that $\mu_\pi \propto \Lambda_\chi$ rather than Λ_{QCD} , where Λ_χ is the scale of chiral symmetry breaking. Thus relative to the other power corrections these terms have the possibility of being magnified by a numerical factor of $\mu_\pi/\Lambda \sim 3-4$. A valid factorization theorem for the complete set of chirally enhanced corrections has not yet been derived, because previous attempts encountered endpoint singularities [17]. In this section we derive a factorization theorem for chirally enhanced tree and penguin amplitudes that does not suffer from endpoint singularities. Our analysis uses factorization in SCET_I and the complete result involves only one additional generalized form factor and one light-cone meson distribution beyond those occurring at leading order.

To consider chirally enhanced operators in SCET we can work with a complete basis of operators suppressed by one power of Λ/m_b , and then look for all operators with a \mathcal{P}_\perp in the light-quark bilinear as explained in Ref. [29]. This provides a unique way to determine the contributions that are chirally enhanced, without invoking the Wandzura-Wilczek (WW) approximation [49] as was done in Ref. [17].

We therefore construct a complete basis of operators with one P_\perp^α , starting with the field structures:

$$\begin{aligned} Q_A^{(1\chi)} &= (\bar{\xi}_n \Gamma_n h_v) (\bar{\xi}_{\bar{n}} \Gamma_{\bar{n}} \mathcal{P}_\perp^\beta \xi_{\bar{n}}), \\ Q_{B1}^{(2\chi)} &= (\bar{\xi}_n i g \mathcal{B}_{n\perp}^\alpha \Gamma_n h_v) (\bar{\xi}_{\bar{n}} \Gamma_{\bar{n}} \mathcal{P}_\perp^\beta \xi_{\bar{n}}), \\ Q_{B2}^{(2\chi)} &= (\bar{\xi}_n \mathcal{P}_\perp^{\dagger\beta} i g \mathcal{B}_{n\perp}^\alpha \Gamma_n h_v) (\bar{\xi}_{\bar{n}} \Gamma_{\bar{n}} \xi_{\bar{n}}). \end{aligned} \quad (73)$$

Only the color structures shown are required at this order. Operators with a $i g \mathcal{B}_{n\perp}^\alpha$ are needed at the same order as operators without, because of the additional suppression of the non- $\mathcal{B}_{n\perp}^\alpha$ operators in the matrix element of the required time-ordered products. This is the same situation which we described already at leading order in Λ/m_b in Eq. (38). Note that in Eq. (73) we do not consider other operators with \mathcal{P}_\perp or ∂_\perp since they are not chirally enhanced. To perform the matching we work with a basis of four-quark operators of definite chirality, where the possibilities are inherited from the full electroweak Hamiltonian: $(LH)(LL)$, $(LH)(RR)$, or $(RH)(LR)$. Here the order corresponds to the quark fields in Eq. (73) and we do not assign a chirality to the

heavy quark denoted by H . With definite chirality a complete basis of Dirac structures includes

$$\Gamma_n \in \{1, \gamma_\perp^\mu\}, \quad \Gamma_{\bar{n}} \in \{\not{n}, \not{n} \gamma_\perp^\nu\}, \quad (74)$$

where $\Gamma_{\bar{n}} = \not{n}$ contributes only to $(LH)(LL)$ and $(LH)(RR)$, while $\Gamma_{\bar{n}} = \not{n} \gamma_\perp^\nu$ contributes only to $(RH)(LR)$.

First let's construct a complete basis of the $Q_A^{(1\chi)}$ -type operators in Eq. (73). Here $\Gamma_n \otimes \Gamma_{\bar{n}}$ must have a \perp β index, and we find the basis

$$\begin{aligned} Q_{1(qfq)}^{(1\chi)} &= \frac{1}{m_b} [\bar{q}_{n\omega_1}^R b_v] [\bar{f}_{\bar{n}\omega_2}^L \not{n} \mathcal{P}_\perp q_{\bar{n}\omega_3}^R], \\ Q_{2(qfq)}^{(1\chi)} &= Q_{3(qfq)}^{(1\chi)} \frac{3}{2} e_q, \\ Q_{3(qfq)}^{(1\chi)} &= \frac{1}{m_b} [\bar{q}_{n\omega_1}^L \gamma_\perp^\beta b_v] [\bar{f}_{\bar{n}\omega_2}^L \not{n} \mathcal{P}_\perp^\beta q_{\bar{n}\omega_3}^L], \\ Q_{4(fuu)}^{(1\chi)} &= \frac{1}{m_b} [\bar{f}_{n\omega_1}^L \gamma_\perp^\beta b_v] [\bar{u}_{\bar{n}\omega_2}^R \not{n} \mathcal{P}_\perp^\beta u_{\bar{n}\omega_3}^R], \end{aligned} \quad (75)$$

where we have $f = d, s$. The (qfq) subscripts on the operators indicate the flavors of the light quarks, and the basis has in addition the operators $Q_{3(fuu)}^{(1\chi)}$ and $Q_{3(ufu)}^{(1\chi)}$. Whenever a flavor label q appears we implicitly sum over $q = u, d, s$. The operators $Q_{1,2}^{(1\chi)}$ give contributions to PP , PV , and V_0V_0 final states, whereas $Q_{3,4}^{(1\chi)}$ only contribute for transversely polarized vector mesons. If operators that produce \bar{n} -isosinglet mesons are included, we have in addition $Q_{3(fqq)}^{(1\chi)}$ and $Q_{4(fqq)}^{(2\chi)}$. Since the $Q_{1,2,4}^{(1\chi)}$ operators have right-handed quarks, only $O_{5,6,7,8}$ in the electroweak Hamiltonian can contribute to their matching at tree level, while other operators start contributing at one-loop.

Next we construct a complete basis for the $Q_{B1}^{(2\chi)}$ and $Q_{B2}^{(2\chi)}$ -type operators. For chirality $(LH)(LL)$ we must have $\Gamma_n = 1$ and $\Gamma_{\bar{n}} = \not{n}$ and we have two choices for contracting the \perp indices, $g_\perp^{\alpha\beta}$ or $i\epsilon_\perp^{\alpha\beta}$. To avoid having the epsilon symbol in our basis we trade $i\epsilon_\perp^{\alpha\beta}$ for a pair of γ_\perp^\perp 's. Here the possible flavor structures are (qfq) , (ufu) , (fuu) , and (fqq) from matching the operators in the original H_W . For chirality $(LH)(RR)$ the same Dirac basis applies, with flavor choices (fuu) and (fqq) . The latter flavor structure only produces \bar{n} -collinear isosinglet mesons. Finally for $(RH)(LR)$ we must have $\Gamma_n = \gamma_\perp^\mu$ and $\Gamma_{\bar{n}} = \not{n} \gamma_\perp^\nu$ and there are only two inequivalent ways of contracting the \perp indices ($\alpha\beta\mu\nu$). This follows since contractions with an $i\epsilon_\perp$ do not lead to independent structures because of the fixed chirality, and the identity $\not{n} \gamma_\perp^\mu P_L \otimes \not{n} \gamma_\perp^\nu P_R = 0$ which allows an additional contraction to be eliminated. For $(RH)(LR)$ only the flavor structure (qfq) contributes. All together these results

² Although chirally enhanced penguin contributions are large, for tree amplitudes they are numerically the same size as other expected power corrections as emphasized in Ref. [24].

lead us to define the basis

$$\begin{aligned}
Q_{1(qfq)}^{(2\chi)} &= \frac{-1}{m_b} \left[\bar{q}_{n\omega_1}^L \frac{1}{\bar{n} \cdot \mathcal{P}} \mathcal{P}_\perp \cdot ig \mathcal{B}_{n\perp} b_v \right] [\bar{f}_{\bar{n}\omega_2}^L \not{q} q_{\bar{n}\omega_3}^L], \\
Q_{2(fuu)}^{(2\chi)} &= \frac{-1}{m_b} \left[\bar{f}_{n\omega_1}^L \frac{1}{\bar{n} \cdot \mathcal{P}} \mathcal{P}_\perp \cdot ig \mathcal{B}_{n\perp} b_v \right] [\bar{u}_{\bar{n}\omega_2}^R \not{u} u_{\bar{n}\omega_3}^R], \\
Q_{3(qfq)}^{(2\chi)} &= \frac{-1}{m_b^2} [\bar{q}_{n\omega_1}^R ig \mathcal{B}_{n\perp} b_v] [\bar{f}_{\bar{n}\omega_2}^L \not{q} \mathcal{P}_\perp q_{\bar{n}\omega_3}^R], \\
Q_{4(qfq)}^{(2\chi)} &= \frac{3}{2} e_q Q_{3(qfq)}^{(2\chi)}, \\
Q_{5(qfq)}^{(2\chi)} &= \frac{-1}{m_b} \left[\bar{q}_{n\omega_1}^L \frac{1}{\bar{n} \cdot \mathcal{P}} ig \mathcal{B}_{n\perp}^\alpha b_v \right] [\bar{f}_{\bar{n}\omega_2}^L \not{q} \mathcal{P}_\alpha^\perp q_{\bar{n}\omega_3}^L], \\
Q_{6(fuu)}^{(2\chi)} &= \frac{-1}{m_b} \left[\bar{f}_{n\omega_1}^L \frac{1}{\bar{n} \cdot \mathcal{P}} ig \mathcal{B}_{n\perp}^\alpha b_v \right] [\bar{u}_{\bar{n}\omega_2}^R \not{u} \mathcal{P}_\alpha^\perp u_{\bar{n}\omega_3}^R], \\
Q_{7(qfq)}^{(2\chi)} &= \frac{-1}{m_b^2} [\bar{q}_{n\omega_1}^R \mathcal{P}_\perp^\dagger ig \mathcal{B}_{n\perp} b_v] [\bar{f}_{\bar{n}\omega_2}^L \not{q} \gamma_\alpha^\perp q_{\bar{n}\omega_3}^R], \\
Q_{8(qfq)}^{(2\chi)} &= \frac{3}{2} e_q Q_{7(qfq)}^{(2\chi)}, \tag{76}
\end{aligned}$$

plus operators with the same Dirac structure but different flavors, $Q_{i(ufu)}^{(2\chi)}$ and $Q_{i(fuu)}^{(2\chi)}$ for $i = 1$ and 5 . The operators in Eq. (76) also incorporate electroweak penguins, since we can write $e_q q \bar{q} = u \bar{u} - 1/3 q \bar{q}$. Operators $Q_{1-4}^{(2\chi)}$, contribute for $B \rightarrow PP$, $B \rightarrow PV$, and $B \rightarrow V_0 V_0$ decays, whereas the operators $Q_{5-8}^{(2\chi)}$ only contribute for decays with transverse vectors in the final state, $B \rightarrow VT V_T$. If \bar{n} -isosinglet operators are included we have in addition the operators $Q_{i(fqq)}^{(2\chi)}$ where $i = 1, 2, 5, 6$.

For the basis in Eq. (76) we have only written operators that contribute to B decays. The remaining operators which only contribute for weak B^* decays are

$$\begin{aligned}
Q_{1(qfq)}^{(2\chi)*} &= \frac{-1}{m_b^2} [\bar{q}_{n\omega_1}^L \mathcal{P}_\alpha^\dagger ig \mathcal{B}_{n\perp} \gamma_\perp^\alpha b_v] [\bar{f}_{\bar{n}\omega_2}^L \not{q} q_{\bar{n}\omega_3}^L], \\
Q_{2(fuu)}^{(2\chi)*} &= \frac{-1}{m_b^2} [\bar{f}_{n\omega_1}^L \mathcal{P}_\alpha^\dagger ig \mathcal{B}_{n\perp} \gamma_\perp^\alpha b_v] [\bar{u}_{\bar{n}\omega_2}^R \not{u} u_{\bar{n}\omega_3}^R], \\
Q_{3(qfq)}^{(2\chi)*} &= \frac{-1}{m_b^2} [\bar{q}_{n\omega_1}^R \gamma_\perp^\beta ig \mathcal{B}_{n\perp}^\alpha b_v] [\bar{f}_{\bar{n}\omega_2}^L \not{q} \gamma_\alpha^\perp \mathcal{P}_\beta^\perp q_{\bar{n}\omega_3}^R] \\
&\quad + \frac{1}{m_b^2} [\bar{q}_{n\omega_1}^R ig \mathcal{B}_{n\perp} b_v] [\bar{f}_{\bar{n}\omega_2}^L \not{q} \mathcal{P}_\perp q_{\bar{n}\omega_3}^R], \\
Q_{5(qfq)}^{(2\chi)*} &= \frac{-1}{m_b^2} [\bar{q}_{n\omega_1}^L ig \mathcal{B}_{n\perp} \gamma_\alpha^\perp b_v] [\bar{f}_{\bar{n}\omega_2}^L \not{q} \mathcal{P}_\perp^\alpha q_{\bar{n}\omega_3}^L], \\
Q_{6(fuu)}^{(2\chi)*} &= \frac{-1}{m_b^2} [\bar{f}_{n\omega_1}^L ig \mathcal{B}_{n\perp} \gamma_\alpha^\perp b_v] [\bar{u}_{\bar{n}\omega_2}^R \not{u} \mathcal{P}_\perp^\alpha u_{\bar{n}\omega_3}^R], \\
Q_{7(qfq)}^{(2\chi)*} &= \frac{-1}{m_b^2} [\bar{q}_{n\omega_1}^R \mathcal{P}_\perp^\dagger ig \mathcal{B}_{n\perp}^\alpha b_v] [\bar{f}_{\bar{n}\omega_2}^L \not{q} \gamma_\alpha^\perp q_{\bar{n}\omega_3}^R] \\
&\quad + \frac{1}{m_b^2} [\bar{q}_{n\omega_1}^R \mathcal{P}_\perp^\dagger ig \mathcal{B}_{n\perp} b_v] [\bar{f}_{\bar{n}\omega_2}^L \not{q} \gamma_\alpha^\perp q_{\bar{n}\omega_3}^R], \tag{77}
\end{aligned}$$

and $Q_{4,8(qfq)}^{(2\chi)*} = \frac{3}{2} e_q Q_{3,7(qfq)}^{(2\chi)*}$. Taken together the results in Eqs. (76) and (77) form a complete basis for decays

to non-isosinglet final states. We demonstrate that the $Q_{i(F)}^{(2\chi)*}$ only contribute for B^* decays in appendix B.

The Hamiltonian for the full basis of (1χ) and (2χ) type-operators contributing to B -decays is

$$\begin{aligned}
H &= \frac{4G_F}{\sqrt{2}} \sum_{i,F} \left[\int [d\omega_{1,2,3}] c_{i(F)}^X(\omega_j) Q_{i(F)}^{(1\chi)}(\omega_j) \right. \\
&\quad \left. + \int [d\omega_{1-4}] b_{i(F)}^X(\omega_j) Q_{i(F)}^{(2\chi)}(\omega_j) \right], \tag{78}
\end{aligned}$$

where the indices run over the operator number i and possibilities for the flavors F for the $Q_{i(F)}$'s shown in Eqs. (75) and (76), and $c_{i(F)}^X$ and $b_{i(F)}^X$ are short-distance Wilson coefficients.

Next we match from H_W onto the operators in Eqs. (75) and (76) to determine the Wilson coefficients $c_{i(F)}^X$ and $b_{i(F)}^X$ at lowest order in the $\alpha_s(m_b)$ expansion. At lowest order $c_{i(F)}^X$ are simply given by the matrix elements of the O_i 's expanded to next-to-leading order in the λ power counting with

$$q = \left(1 + \frac{1}{\bar{n} \cdot \mathcal{P}} \not{\mathcal{P}}_\perp \frac{\not{\bar{n}}}{2} \right) q_n. \tag{79}$$

For the $(LH)(LL)$ and $(LH)(RR)$ chirality only the expansion of the \bar{n} -bilinear contributes, and for the non-isosinglet operators we find

$$\begin{aligned}
c_{3(ufu)}^X &= -\frac{1}{\bar{u}} \left[\lambda_u^{(f)} \left(C_1 + \frac{C_2}{N_c} \right) - \lambda_t^{(f)} \frac{3}{2} \left(C_{10} + \frac{C_9}{N_c} \right) \right] \\
&\quad + \Delta c_{3(ufu)}^X, \\
c_{3(fuu)}^X &= -\frac{1}{\bar{u}} \left[\lambda_u^{(f)} \left(C_2 + \frac{C_1}{N_c} \right) - \lambda_t^{(f)} \frac{3}{2} \left(C_9 + \frac{C_{10}}{N_c} \right) \right] \\
&\quad + \Delta c_{3(fuu)}^X, \\
c_{3(qfq)}^X &= \lambda_t^{(f)} \frac{1}{\bar{u}} \left[C_4 + \frac{C_3}{N_c} - \frac{C_{10}}{2} - \frac{C_9}{2N_c} \right] + \Delta c_{3(qfq)}^X, \\
c_{4(fuu)}^X &= -\lambda_t^{(f)} \frac{3}{2\bar{u}} \left(C_7 + \frac{C_8}{N_c} \right) + \Delta c_{4(fuu)}^X. \tag{80}
\end{aligned}$$

As usual the $\Delta c_{i(F)}^X$ terms denote perturbative corrections. Numerically they will not always be suppressed due to the competition between $C_{3,4}$ and $\alpha_s(m_b)C_1$. For the operators $Q_{1,2(F)}^{(1\chi)}$ only O_{5-8} from H_W contribute at tree-level since the operator involves right handed quarks. We find

$$\begin{aligned}
c_{1(qfq)}^X &= \lambda_t^{(f)} \left(C_6 + \frac{C_5}{N_c} \right) \frac{1}{u\bar{u}} + \Delta c_{1(qfq)}^X, \\
c_{2(qfq)}^X &= \lambda_t^{(f)} \left(C_8 + \frac{C_7}{N_c} \right) \frac{1}{u\bar{u}} + \Delta c_{2(qfq)}^X. \tag{81}
\end{aligned}$$

We find that the loop and magnetic penguin graphs in Fig. 1 can only contribute to the matching when a factor of \perp -momentum is generated by expanding the spinors.

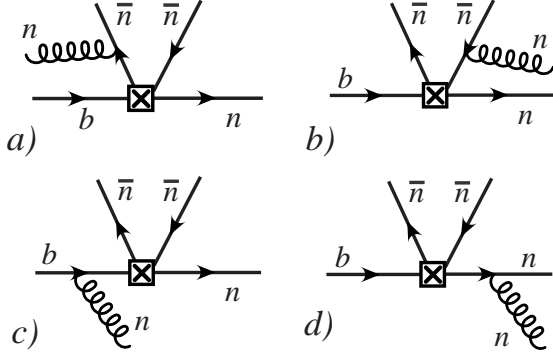


FIG. 6: Full theory graphs for the matching onto the short-distance penguin coefficients for the Q_{B1} and Q_{B2} type operators.

They give the following $\mathcal{O}(\alpha_s)$ corrections to the matching

$$\begin{aligned} \Delta c_{1(qfq)}^X &= \frac{C_F \alpha_s(\mu)}{6N_c \pi} \left\{ \frac{\lambda_u^{(f)} C_1}{u\bar{u}} \left[h_2^u(u, 1) - \frac{4}{3} + S_c \right] \right. \\ &\quad + \frac{\lambda_c^{(f)} C_1}{u\bar{u}} \left[\frac{2\rho}{\bar{u}} h_1^c(u, 1, \rho) + h_2^c(u, 1, \rho) - \frac{4}{3} + S_c \right] \\ &\quad \left. + (\lambda_u^{(f)} + \lambda_c^{(f)}) \frac{3C_{8g} \bar{m}_b}{m_b u\bar{u}} \right\}, \\ \Delta c_{3(qfq)}^X &= \frac{C_F \alpha_s(\mu)}{6N_c \pi} \left\{ \lambda_u^{(f)} C_1 \frac{1}{\bar{u}} \left[h_2^u(u, 1) - \frac{4}{3} + S_c \right] \right. \\ &\quad \left. + \lambda_c^{(f)} C_1 \frac{1}{\bar{u}} \left[\frac{2\rho}{\bar{u}} h_1^c(u, 1, \rho) + h_2^c(u, 1, \rho) - \frac{4}{3} + S_c \right] \right\}, \end{aligned} \quad (82)$$

where the other $\Delta c_{i(F)}$ coefficients are zero at this level, and $S_c = 0$ for the NDR scheme while $S_c = 1$ for the HV scheme. The scheme dependence in these results cancels against that in the tree level $C_{3,4}$ terms in $c_{3(qfq)}^X$ just as for the LO $c_4^{(f)}$ Wilson coefficient, and also in an identical manner against the scheme dependence in the tree-level $C_{5,6}$ terms in $c_{1(qfq)}^X$.

Next consider the matching calculation which determines $b_{i(F)}^X$. At tree-level this involves computing the graphs in Fig. 6, and involves non-zero contributions from expanding the propagators in graphs a), b), and c), and from expanding the spinors with Eq. (79) for graphs a),

b), and d). We find

$$\begin{aligned} b_{1(qfq)}^X &= 2\lambda_t^{(f)} \left[\frac{(1+uz)}{uz} \left(\frac{C_3}{N_c} - \frac{C_9}{2N_c} \right) + C_4 - \frac{C_{10}}{2} \right] \\ &\quad + \Delta b_{1(qfq)}^X, \\ b_{2(fuu)}^X &= 3\lambda_t^{(f)} \left[C_7 + \frac{C_8}{N_c} - \frac{1}{\bar{u}z} \frac{C_8}{N_c} \right] + \Delta b_{2(fuu)}^X, \\ b_{3(qfq)}^X &= \lambda_t^{(f)} \frac{1}{u\bar{u}} \left(C_6 + \frac{C_5}{N_c} \right) + \Delta b_{3(qfq)}^X, \\ b_{4(qfq)}^X &= \lambda_t^{(f)} \frac{1}{u\bar{u}} \left(C_8 + \frac{C_7}{N_c} \right) + \Delta b_{4(qfq)}^X, \\ b_{5(qfq)}^X &= -\lambda_t^{(f)} \frac{2}{u\bar{u}} \left(\frac{C_3}{N_c} - \frac{C_9}{2N_c} \right) + \Delta b_{5(qfq)}^X, \\ b_{6(fuu)}^X &= -\lambda_t^{(f)} \frac{3C_8}{N_c} \frac{1}{u\bar{u}} + \Delta b_{6(fuu)}^X, \\ b_{7(qfq)}^X &= \lambda_t^{(f)} \frac{1}{u\bar{u}z} \frac{C_5}{N_c} + \Delta b_{7(qfq)}^X, \\ b_{8(qfq)}^X &= \lambda_t^{(f)} \frac{1}{u\bar{u}z} \frac{C_7}{N_c} + \Delta b_{8(qfq)}^X, \end{aligned} \quad (83)$$

and

$$\begin{aligned} b_{1(ufu)}^X &= \frac{2(1+uz)}{uz} \left(-\frac{C_2}{N_c} \lambda_u^{(f)} + \frac{3C_9}{2N_c} \lambda_t^{(f)} \right) \\ &\quad - \left(2C_1 \lambda_u^{(f)} - 3C_{10} \lambda_t^{(f)} \right) + \Delta b_{1(ufu)}^X, \\ b_{5(ufu)}^X &= \frac{2}{u\bar{u}} \left(\frac{C_2}{N_c} \lambda_u^{(f)} - \frac{3C_9}{2N_c} \lambda_t^{(f)} \right) + \Delta b_{5(ufu)}^X, \\ b_{1(fuu)}^X &= \frac{2(1+uz)}{uz} \left(-\lambda_u^{(f)} \frac{C_1}{N_c} + \lambda_t^{(f)} \frac{3C_{10}}{2N_c} \right) \\ &\quad - \left(2C_2 \lambda_u^{(f)} - 3C_9 \lambda_t^{(f)} \right) + \Delta b_{1(fuu)}^X, \\ b_{5(fuu)}^X &= \frac{2}{u\bar{u}} \left(\frac{C_1}{N_c} \lambda_u^{(f)} - \frac{3C_{10}}{2N_c} \lambda_t^{(f)} \right) + \Delta b_{5(fuu)}^X. \end{aligned} \quad (84)$$

Results for the Wilson coefficients for cases with isosinglet \bar{n} -mesons can be determined in an analogous way, but in this case operators with gluons also become necessary. We leave this for future work.

Since we are only using factorization of effects at $\mu \sim m_b$ the matrix elements of the operators $Q_{i(F)}^{(1\chi)}$ and $Q_{i(F)}^{(2\chi)}$ give hadronic parameters. For the \bar{n} -collinear field we need the matrix elements in Eq. (40), and the corresponding results with right-handed light quarks and Clebsch-Gordan coefficients

$$\begin{aligned} \langle M_n | T_1 [\bar{q}_{n\omega_1}^R \not{v} b_v] | B \rangle &= C_{qR}^{BM} \bar{\delta}_{\omega_1} m_B \zeta^{BM}, \quad (85) \\ \langle M_n | T_2 [\bar{q}_{n\omega_1}^R i g \not{B}_{n\omega_4}^\perp b_v] | B \rangle &= -C_{qR}^{BM} \bar{\delta}_{\omega_1 \omega_4} \frac{m_B}{2} \zeta_J^{BM}(z). \end{aligned}$$

We also need a new form factor $\zeta_X^{BM}(z)$ and the chiral-

$M_1 M_2$	R_1	R_2	R_1^X	R_2^X
$\pi^- \pi^+, \rho^- \pi^+$	$c_{1(qfq)}^X + c_{2(qfq)}^X$	0	$b_{1(qfq)}^X + b_{1(ufu)}^X$	0
$\pi^- \rho^+$	$-c_{1(qfq)}^X - c_{2(qfq)}^X$	0	$b_{1(qfq)}^X + b_{1(ufu)}^X$	0
$\pi^- \pi^0$	$\frac{1}{\sqrt{2}} [c_{1(qfq)}^X + c_{2(qfq)}^X]$	$\frac{-1}{\sqrt{2}} [c_{1(qfq)}^X - \frac{1}{2} c_{2(qfq)}^X]$	$\frac{1}{\sqrt{2}} [b_{1(ufu)}^X + b_{1(qfq)}^X]$	$\frac{1}{\sqrt{2}} [b_{1(fuu)}^X - b_{2(fuu)}^X - b_{1(qfq)}^X]$
$\rho^- \pi^0$	$\frac{1}{\sqrt{2}} [c_{1(qfq)}^X + c_{2(qfq)}^X]$	$\frac{1}{\sqrt{2}} [c_{1(qfq)}^X - \frac{1}{2} c_{2(qfq)}^X]$	$\frac{1}{\sqrt{2}} [b_{1(ufu)}^X + b_{1(qfq)}^X]$	$\frac{1}{\sqrt{2}} [b_{1(fuu)}^X - b_{2(fuu)}^X - b_{1(qfq)}^X]$
$\pi^- \rho^0$	$\frac{-1}{\sqrt{2}} [c_{1(qfq)}^X + c_{2(qfq)}^X]$	$\frac{-1}{\sqrt{2}} [c_{1(qfq)}^X - \frac{1}{2} c_{2(qfq)}^X]$	$\frac{1}{\sqrt{2}} [b_{1(ufu)}^X + b_{1(qfq)}^X]$	$\frac{1}{\sqrt{2}} [b_{1(fuu)}^X + b_{2(fuu)}^X - b_{1(qfq)}^X]$
$\pi^0 \pi^0$	$-\frac{1}{2} c_{1(qfq)}^X + \frac{1}{4} c_{2(qfq)}^X$	$\frac{-1}{2} c_{1(qfq)}^X + \frac{1}{4} c_{2(qfq)}^X$	$\frac{1}{2} [b_{1(fuu)}^X - b_{2(fuu)}^X - b_{1(qfq)}^X]$	$\frac{1}{2} [b_{1(fuu)}^X - b_{2(fuu)}^X - b_{1(qfq)}^X]$
$\rho^0 \pi^0$	$-\frac{1}{2} c_{1(qfq)}^X + \frac{1}{4} c_{2(qfq)}^X$	$\frac{1}{2} c_{1(qfq)}^X - \frac{1}{4} c_{2(qfq)}^X$	$\frac{1}{2} [b_{1(fuu)}^X + b_{2(fuu)}^X - b_{1(qfq)}^X]$	$\frac{1}{2} [b_{1(fuu)}^X - b_{2(fuu)}^X - b_{1(qfq)}^X]$
$K^{(*)0} K^-, K^{(*)0} \bar{K}^0$	$-c_{1(qfq)}^X + \frac{1}{2} c_{2(qfq)}^X$	0	$-b_{1(qfq)}^X$	0
$K^0 K^{*-}, K^0 \bar{K}^{*0}$	$c_{1(qfq)}^X - \frac{1}{2} c_{2(qfq)}^X$	0	$-b_{1(qfq)}^X$	0
$K^{(*)-} K^{(*)+}$	—	—	—	—
$\pi^+ K^{(*)-}$	0	$c_{1(qfq)}^X + c_{2(qfq)}^X$	0	$b_{1(ufu)}^X + b_{1(qfq)}^X$
$\rho^+ K^-$	0	$-c_{1(qfq)}^X - c_{2(qfq)}^X$	0	$b_{1(ufu)}^X + b_{1(qfq)}^X$
$\pi^0 K^{(*)-}$	0	$\frac{1}{\sqrt{2}} [c_{1(qfq)}^X + c_{2(qfq)}^X]$	$\frac{1}{\sqrt{2}} [b_{1(fuu)}^X - b_{2(fuu)}^X]$	$\frac{1}{\sqrt{2}} [b_{1(ufu)}^X + b_{1(qfq)}^X]$
$\rho^0 K^-$	0	$\frac{-1}{\sqrt{2}} [c_{1(qfq)}^X + c_{2(qfq)}^X]$	$\frac{1}{\sqrt{2}} [b_{1(fuu)}^X + b_{2(fuu)}^X]$	$\frac{1}{\sqrt{2}} [b_{1(ufu)}^X + b_{1(qfq)}^X]$
$\pi^- \bar{K}^{(*)0}$	0	$-c_{1(qfq)}^X + \frac{1}{2} c_{2(qfq)}^X$	0	$-b_{1(qfq)}^X$
$\rho^- \bar{K}^0$	0	$c_{1(qfq)}^X - \frac{1}{2} c_{2(qfq)}^X$	0	$-b_{1(qfq)}^X$
$\pi^0 \bar{K}^{(*)0}$	0	$\frac{-1}{\sqrt{2}} [c_{1(qfq)}^X - \frac{1}{2} c_{2(qfq)}^X]$	$\frac{1}{\sqrt{2}} [b_{1(fuu)}^X - b_{2(fuu)}^X]$	$-\frac{1}{\sqrt{2}} b_{1(qfq)}^X$
$\rho^0 \bar{K}^0$	0	$\frac{1}{\sqrt{2}} [c_{1(qfq)}^X - \frac{1}{2} c_{2(qfq)}^X]$	$\frac{1}{\sqrt{2}} [b_{1(fuu)}^X + b_{2(fuu)}^X]$	$-\frac{1}{\sqrt{2}} b_{1(qfq)}^X$

TABLE I: Hard functions for the chirally enhanced amplitudes in Eq. (87) for \bar{B}^0 and B^- decays to PP and PV channels. We have not listed results for $R_{1,2}^J$, but they have the same Clebsch-Gordan coefficients as $R_{1,2}$ and so can be simply obtained by the replacements $c_{1(qfq)}^X \rightarrow b_{3(qfq)}^X$ and $c_{2(qfq)}^X \rightarrow b_{4(qfq)}^X$ in the columns above.

enhanced function $\phi_{pp}^P(x)$ defined by

$$\begin{aligned}
\langle M | T_2 \left[\bar{q}_{n\omega_1}^L \frac{1}{\bar{n} \cdot \mathcal{P}} \mathcal{P}_\perp \cdot i g B_{n\omega_4}^\perp b_v \right] | B \rangle & \quad (86) \\
= -\mathcal{C}_{qL}^{BM} \bar{\delta}_{\omega_1 \omega_4} \frac{\mu_M}{12} \zeta_\chi^{BM}(z), \\
\langle P(p) | \bar{q}_{n\omega_2}^L \bar{\eta} \mathcal{P}_\perp q_{n\omega_3}^R | 0 \rangle & = -\frac{i}{6} \mathcal{C}_{qLq'}^P \bar{\delta}_{\omega_2 \omega_3} f_P \mu_P \phi_{pp}^P(x),
\end{aligned}$$

where $\bar{\delta}_{\omega\omega'} = \delta(\omega - \omega' - m_B)$ and the momentum fractions $z = \omega_1 / \bar{n} \cdot p_M$ and $x = \omega_2 / \bar{n} \cdot p_P$. where \mathcal{C}_{qL}^{BM} and $\mathcal{C}_{qLq'}^M$ are the same Clebsch-Gordan coefficients that appeared already at leading order in Eq. (43). For the chirally-enhanced distribution function ϕ_{pp}^M we used the definition in Ref. [29], and take the other twist-3 meson distribution to be the three-body $\phi^{3M}(x, \bar{x})$ which does not generate chirally enhanced contributions. In a more traditional basis there is a redundancy at this order in $1/m_b$ (see for example [50]), and $\phi_{pp}^P(x) = 3x[\phi_p^P(x) + \phi_\sigma^{P'}(x)]/6 + 2f_{3P}/(f_P \mu_P) \int dy' / y' \phi_{3P}(y - y', y)$. In the Wandzura-Wilczek approximation one would set $\phi_{pp}(x) = 6x(1-x)$.

Taking the matrix element of the above operators leads to a factorization theorem for the chirally enhanced amplitude for non-isosinglet charmless B -decays to PP and

PV channels

$$\begin{aligned}
A^X(\bar{B} \rightarrow M_1 M_2) & = \frac{G_F m_B^2}{\sqrt{2}} \left\{ \quad (87) \\
& - \frac{\mu_{M_1} f_{M_1}}{3m_B} \zeta^{BM_2} \int_0^1 du R_1(u) \phi_{pp}^{M_1}(u) + (1 \leftrightarrow 2) \\
& - \frac{\mu_{M_1} f_{M_1}}{3m_B} \int_0^1 du dz R_1^J(u, z) \zeta_J^{BM_2}(z) \phi_{pp}^{M_1}(u) + (1 \leftrightarrow 2) \\
& - \frac{\mu_{M_2} f_{M_1}}{6m_B} \int_0^1 du dz R_1^X(u, z) \zeta_\chi^{BM_2}(z) \phi^{M_1}(u) + (1 \leftrightarrow 2) \left. \right\}.
\end{aligned}$$

This amplitude only includes the chirally-enhanced power corrections where factors of μ_M are generated by pseudo-scalars, and so for vectors we define $\mu_V = 0$. (Note that we include the symmetry factor of 1/2 in the branching ratio prefactor for $B \rightarrow \pi^0 \pi^0$ rather than the amplitude.) In terms of Clebsch-Gordan coefficients for the different final states, the hard functions R_i , R_i^J , and R_i^X for the

chirally enhanced amplitudes are

$$\begin{aligned}
R_1(u) &= C_{qR}^{BM_2} C_{fLq}^{M_1} \left[c_{1(qfq)}^X + \frac{3}{2} e_q c_{2(qfq)}^X \right], \quad (88) \\
R_1^J(u, z) &= C_{qR}^{BM_2} C_{fLq}^{M_1} \left[b_{3(qfq)}^X + \frac{3}{2} e_q b_{4(qfq)}^X \right], \\
R_1^X(u, z) &= C_{qL}^{BM_2} C_{fLq}^{M_1} b_{1(qfq)}^X + C_{uL}^{BM_2} C_{fLu}^{M_1} b_{1(ufu)}^X \\
&\quad + C_{fL}^{BM_2} C_{uLu}^{M_1} b_{1(fuu)}^X + C_{fL}^{BM_2} C_{uRu}^{M_1} b_{2(fuu)}^X.
\end{aligned}$$

Summation over $q = u, d, s$ is implicit. Results for these hard functions in different channels are listed in Table I. Equation (87) with Eq. (88) corresponds to the contributions given in the second line of Eq. (11) (when we extract the coefficients of the $\lambda_c^{(f)}$ terms).

From the matching results we find that the endpoint behavior of the Wilson coefficients is $c_{i(F)}^X \sim 1/(u\bar{u})$ and $b_{i(F)}^X \sim 1/(zu\bar{u})$. Since we know the endpoint behavior $\phi_{pp}(u) \sim u\bar{u}$ and $\zeta_J(z) \sim z$, it remains to determine the behavior of $\zeta_\chi(z)$. The operator defining $\zeta_\chi(z)$ has an extra $\mathcal{P}_\perp/\bar{n} \cdot \mathcal{P}$ relative to the operator defining the distribution $\zeta_J(z)$. Now from the collinear power counting $\mathcal{P}_\perp \ll \bar{n} \cdot \mathcal{P}$, so consistency of the power counting in SCET_I implies that the scaling of $\zeta_\chi(z)$ as $z \rightarrow 0$ and $z \rightarrow 1$ can be no worse than $\zeta_J(z)$. Thus we take $\zeta_\chi(z) \sim z$. This demonstrates that all the terms in the factorization theorem for chirally enhanced penguin and tree contributions given in Eq. (87) converge, just like the leading order factorization theorem in Eq. (42). In appendix B we argue that the same conclusion about the z -convolution is obtained if one considers the direct computation of $\zeta_\chi(z)$ in SCET_{II}.

As already noted, the operators in Eqs. (75) and (76) also generate contributions with two transverse vectors in the final state. To take the matrix element of these terms requires

$$\begin{aligned}
\langle V | \bar{q}_{n\omega_1}^L \not{n} \gamma_\perp^\alpha q_{n\omega_2}^R | 0 \rangle &= C_{qLq}^V \bar{\delta}_{\omega_1\omega_2} f_T^V \phi_\perp^V(u) \epsilon_\perp^\alpha, \\
\langle V | \bar{q}_{n\omega_1}^{L,R} \not{n} \mathcal{P}_\perp^\alpha q_{n\omega_2}^{L,R} | 0 \rangle &= C_{qL,Rq}^V \bar{\delta}_{\omega_1\omega_2} f_{pp}^V \phi_{pp\perp}^V(u) \epsilon_\perp^\alpha, \quad (89)
\end{aligned}$$

where $u = \omega_1/m_b$ and three form factors

$$\begin{aligned}
\langle V | \bar{q}_{n\omega_1}^L \gamma_\perp^\alpha b_v | B \rangle &= C_{qL}^{BV} \bar{\delta}_{\omega_1} m_B \zeta_\perp^{BV} \epsilon_{L\perp}^\alpha, \quad (90) \\
\langle V | \bar{q}_{n\omega_1}^L i g \mathcal{B}_{n\omega_4}^{\perp\alpha} b_v | B \rangle &= -C \bar{\delta}_{\omega_1\omega_4} m_B \zeta_{J\perp}^{BV}(z) \epsilon_\perp^\alpha, \\
\langle V | \bar{q}_{n\omega_1}^R \mathcal{P}_\perp^{\dagger\alpha} i g \mathcal{B}_{n\omega_4}^\perp b_v | B \rangle &= -C' \bar{\delta}_{\omega_1\omega_4} m_B \zeta_{K\perp}^{BV}(z) \epsilon_\perp^\alpha,
\end{aligned}$$

where $z = \omega_1/m_b$. Thus, our complete basis of operators with \mathcal{P}^α terms generates a contribution to the amplitude to produce two transverse vector mesons that involve two types of light-cone meson distributions, and three types of form-factors. These analogs of the chirally enhanced terms were displayed as the contributions on the second line of Eq. (12). Our analysis demonstrates that only these terms will be generated from the \mathcal{P}_\perp operators considered in this section, however a full analysis of these terms will not be given here. Hence we have not bothered to specify the Clebsch-Gordan coefficients \mathcal{C} and \mathcal{C}' relative to our other conventions.

IX. LONG-DISTANCE CHARM

In order to properly determine the short-distance coefficients by matching we must make sure that we subtract any effective theory diagrams. Earlier we stated that there were no SCET loop graphs to subtract. In this section we further justify this claim and discuss long-distance charm contributions. We take $m_c \sim m_b$ and so do not have collinear charm quarks. Furthermore, graphs with collinear or soft up quarks are power suppressed. The only remaining term to consider are soft non-relativistic charm that propagate in the EFT. While a factorization theorem for this type of long distance charm effect has not yet been derived, we may nevertheless match systematically by including in the effective theory the proper SCET-NRQCD hybrid operators as discussed in [24].

We begin by showing that non-zero contributions from the hybrid operators requires a non-zero residual momentum and hence do not affect the matching computations in earlier sections. We may write the momenta of the charm quarks as

$$\begin{aligned}
p_1^\mu &= \frac{q^\mu}{2} + L_i^\mu r^i, \\
p_2^\mu &= \frac{q^\mu}{2} - L_i^\mu r^i, \quad (91)
\end{aligned}$$

where q^μ is the total momentum of the charm quark pair and r^i is the relative 3-momentum in the $c\bar{c}$ rest frame. $L_\mu^\nu(q)$ is the Lorentz boost from the center-of-mass frame to the B rest frame and has components

$$\begin{aligned}
L_0^0 &= 1 + \frac{\vec{q}^2}{4m_c^2}, \quad L_i^0 = \frac{q_i}{2m_c}, \\
L_i^j &= \delta_i^j + \left(\frac{E_q}{2m_c} - 1 \right) \frac{q^j q_i}{\vec{q}^2}. \quad (92)
\end{aligned}$$

When matching onto NRQCD at lowest order in α_s we generate a generic set of the four quark operators. As with the operators in Eqs. (35,36) there will be a set of operators with and without gluon external lines. Thus there will be two generic forms of the operators

$$\begin{aligned}
O_{prod}^a &= (\eta^\dagger L(\Gamma_{NR})\chi)(\bar{f}_{\bar{n},\omega_1} \Gamma_{hl} b_v), \\
O_{prod}^b &= (\eta^\dagger L(\Gamma_{NR})\chi)(\bar{f}_{\bar{n},\omega_1} B_n^\perp \Gamma_{hl} b_v), \quad (93)
\end{aligned}$$

Γ_{NR}, Γ_{hl} are the possible bilinear Dirac structures for NRQCD and a heavy-light bilinear in SCET. The gluon field B_\perp has a four vector index that is either contracted with Γ_{hl} or $L(\Gamma_{NR})$. For O^a the only possible structure is

$$L(\Gamma_{NR}) \otimes \Gamma_{hl} = \sigma^i L_\mu^i \otimes \gamma_\perp^\mu P_L \quad (94)$$

For the O^b operators the possible structures are

$$L(\Gamma_{NR}) \otimes \Gamma_{hl} = \{1 \otimes \mathcal{B}_n^\perp P_L, \sigma^i L_0^i \otimes \mathcal{B}_n^\perp P_L\} \quad (95)$$

In addition we have four quark operators that are generated by integrating out one hard gluon exchange. They have the general form

$$\begin{aligned} O_{ann}^a &= \frac{\alpha_s(2m_c)}{4m_c^2} (\eta^\dagger L(\Gamma_{NR})\chi)(\bar{q}_{\bar{n},\omega_1}\Gamma_{n\bar{n}}q_{n,\omega_3}), \\ O_{ann}^b &= \frac{\alpha_s(2m_c)}{4m_c^2} (\eta^\dagger L(\Gamma_{NR})\chi)(\bar{q}_{\bar{n},\omega_1}B_n^\perp\Gamma_{n\bar{n}}q_{n,\omega_3}). \end{aligned} \quad (96)$$

For the O_{ann}^a operators the possible structures are

$$L(\Gamma_{NR}) \otimes \Gamma_{n\bar{n}} = \{1 \otimes 1, \sigma^i L_0^i \otimes 1, \sigma^i L_\mu^i \otimes \gamma_\perp^\mu\} \quad (97)$$

while for the O_{ann}^b operators the possible structures are

$$L(\Gamma_{NR}) \otimes \Gamma_{n\bar{n}} = \{1 \otimes \mathcal{B}_n^\perp, \sigma^i L_0^i \otimes \mathcal{B}_n^\perp, \sigma^i L_\mu^i \otimes \mathcal{B}_{n\perp}^\mu\}. \quad (98)$$

In general both $1 \otimes 1$ and $T \otimes T$ color structures are allowed in the operators $O_{prod}^{a,b}$ and $O_{ann}^{a,b}$.

$A_{c\bar{c}}$ then follows from the time ordered products of the form

$$\begin{aligned} T_1^{c\bar{c}} &\equiv \int d^4z d^4y d^4y' T [O_{prod}^a(0)O_{ann}^a(z) i\mathcal{L}_{\xi_n q}^{(1)}(y) i\mathcal{L}_{\xi_n \xi_n}^{(1)}(y')] \\ &+ \int d^4z d^4y d^4y' T [O_{prod}^a(0)O_{ann}^a(z) i\mathcal{L}_{\xi_n q}^{(1)}(y) i\mathcal{L}_{c\bar{g}}^{(1)}(y')] \\ &+ \int d^4z d^4y T [O_{prod}^a(0)O_{ann}^a(z), i\mathcal{L}_{\xi_n q}^{(1,2)}(y)], \\ T_2^{c\bar{c}} &\equiv \int d^4z d^4y T [O_{prod}^b(0)O_{ann}^b(z), i\mathcal{L}_{\xi_n q}^{(1)}(y)] \\ &+ T [O_{prod}^a(0)O_{ann}^b(z), i\mathcal{L}_{\xi_n q}^{(1)}(y)]. \end{aligned} \quad (99)$$

These operators could be factored into soft and collinear components, however the details of this factorization will not be carried out here. The factorization for semi-inclusive decays was discussed in Ref. [51].

Now let us review some aspects of the power counting for these terms (referring to the appendix of Ref. [24] for further details). First note that implicit in these operators is a label conserving delta function. Recall that the NRQCD fields have two large labels [52] $\chi_{\gamma, m, v}$ which have been suppressed in these operators. For instance, reinstating the momentum conserving delta function and momentum labels for O_{prod}^a , we write

$$\begin{aligned} O_{prod}^a &= (\eta_{mv}^\dagger T^A(\sigma^i L_0^i)\chi_{-mv})(\bar{q}_{\bar{n},\omega_1}\not{P}_L T^A b_v) \\ &\delta(m_b - \omega_1 - n_\mu L_0^\mu(2m_c)). \end{aligned} \quad (100)$$

Note that these delta functions do not imply that we are only including a single point in the phase space, since the residual momenta of the HQET and SCET field in the operator may flow through the charm loop. Furthermore since the residual momentum scales as $\Lambda \sim mv^2$, the fluctuations in the external momenta effectively smear over the non-relativistic region.

The delta function constraint simplifies the matching since the contribution of these hybrid operators to the

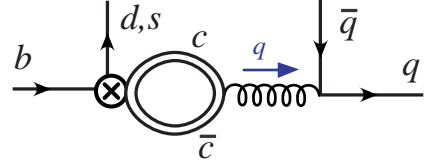


FIG. 7: Charm loop contribution from the non-relativistic region.

matching vanishes at the lowest order in v . To see this, we may work slightly away from threshold, by giving the heavy quark (without loss of generality) some small residual momentum $k \sim \Lambda$, such that the invariant mass of the charm quark pair is

$$q^2 = (m_b v + k - p)^2 = 4m_c^2 - \frac{4m_c^2}{m_b} \bar{n} \cdot k, \quad (101)$$

where $\bar{n} \cdot k \sim \Lambda$ and p is the momentum of the d, s quark. In deriving Eq. (101) we used the heavy quark equation of motion, $v \cdot k = 0$, and expanded about the threshold, $m_b - n \cdot p \simeq 4m_c^2/m_b$. An explicit calculation of the one loop diagram shown in Fig. 7, shows that this contribution is proportional to

$$\sqrt{q^2 - 4m_c^2} \sim \sqrt{\Lambda m_b}. \quad (102)$$

Given our scaling, $mv^2 \sim \Lambda$ we find that this contribution is order v as anticipated by power counting arguments. Hence, only if we were interested in matching explicitly onto v -suppressed corrections would be need to include these hybrid operator diagrams. Since the suppression by v leaves these terms larger than other Λ/m_b power corrections it is quite feasible that long-distance charm contributions are numerically relevant.

Finally, we explain why in general we expect these long distance charm contributions to be complex. As was shown in Ref. [38] a sufficient condition for the generation of a complex phase is the presence of soft Wilson lines in both the n and \bar{n} directions. In most observables these Wilson lines cancel, however, it is clear that this will not be the case for the long-distance charm contribution. The underlying reason for the lack of such a cancellation is the fact that the charm quark propagate over long distances. Thus when we rescale the light quark fields

$$q_n(x) \rightarrow Y_n(x)q_n(x), \quad q_{\bar{n}}(y) \rightarrow Y_{\bar{n}}(y)q_{\bar{n}}(y), \quad (103)$$

the argument of the Wilson lines will be at different positions. Furthermore in general the charmed quarks will not decouple from the B meson, thus the soft matrix element will be of the form

$$\begin{aligned} \langle 0 | [\eta^\dagger \chi](0) [\chi^\dagger \eta](y) [\bar{q} Y_n](z^-) [Y_n^\dagger b_v](0) \\ Y_n(y) Y_n^\dagger(z^-) Y_{\bar{n}}(0) Y_{\bar{n}}^\dagger(y) | B \rangle, \end{aligned} \quad (104)$$

where the spin contractions and the color contractions of the fields and Wilson lines have been suppressed. Note

that since the charm quark pair propagates over long distances the point y^μ is displaced away from zero along the light cone as well as transverse directions. Since this matrix element for long-distance charm knows about the two final state hadrons, it can have a nonperturbative complex phase.

X. PENGUIN ANNIHILATION

In this section we review the penguin annihilation contributions occurring on the third lines of Eqs. (11) and (12). For our purposes they are defined as the $\lambda_c^{(f)}$ terms in the amplitude obtained when the spectator quark is annihilated by the weak operator. These contributions start at $\mathcal{O}(\Lambda/m_b)$ relative to the leading power penguin terms. They include the well known terms $f_B \phi^M \phi^{M'}$ from spectator annihilation with a subsequent pair creation [25, 27], as well as terms of the same parametric size $f_B \phi_B^+ \phi^{3M} \phi^{M'}$ where the spectator emits an energetic collinear gluon prior to its annihilation [28]. The former require zerobin subtractions to obtain finite convolutions [29], while the latter do not. With these subtractions the leading penguin annihilation contribution to the amplitude is real. The scheme dependence of the zerobin procedure is compensated by terms involving the exchange of a soft quark in the annihilation process, $A_{Tann}^{(1)}$, which come from time-ordered products in SCET_I. These time-ordered product terms start at order α_s^2/m_b and have a nonperturbative strong rescattering phase. At $\mathcal{O}(\Lambda^2/m_b^2)$ one also has chiral-enhanced penguin annihilation terms $f_B \mu_M \phi_{pp}^M \phi^{M'}$ [27] which can also be factorized with zerobin subtractions as in Ref. [28].

The annihilation terms $f_B \phi^M \phi^{M'}$ and $f_B \mu_M \phi_{pp}^M \phi^{M'}$ do not involve a hard-collinear propagator and so appear to be insensitive to the intermediate scale $\mu_i \simeq \sqrt{m_b \Lambda}$. However the zero-bin subtraction procedure is needed to distinguish soft and collinear regions, and so they are not defined independent of $A_{Tann}^{(1)}$ at $\mathcal{O}(\alpha_s^2(\mu_i))$. Since this procedure has an $\alpha_s(\mu_i)$ expansion we consider all penguin annihilation contributions with an expansion at the intermediate scale, unlike our analysis of amplitudes in earlier sections. This increases the theoretical uncertainty, and will be accounted for in our error analysis.

From Refs. [29] and [28] the penguin annihilation amplitudes at $\mathcal{O}(\alpha_s)$ for $B \rightarrow M_1 M_2$ are

$$\begin{aligned} \hat{A}_{Lann}^{(1)} &= -\frac{\hat{f}_B f_{M_1} f_{M_2}}{m_B^2} \langle H_c^{M_1 M_2} \rangle, \\ \hat{A}_{hcann}^{(1)} &= -\frac{\hat{f}_B \beta_B}{m_B m_b} \left[f_{3M_1} f_{M_2} \langle H_{hc1}^{M_1 M_2} \rangle \right. \\ &\quad \left. + \eta_{M_1} f_{M_1} f_{3M_2} \langle H_{hc1}^{M_1 M_2} \rangle \right], \\ \hat{A}_{Lann}^{(2\chi)} &= -\frac{\hat{f}_B f_{M_1} f_{M_2}}{m_B^2} \left[\frac{\mu_{M_1}}{m_b} \langle H_{\chi^1}^{M_1 M_2} \rangle + \frac{\mu_{M_2}}{m_b} \langle H_{\chi^2}^{M_1 M_2} \rangle \right]. \end{aligned} \quad (105)$$

Here we have the inverse moment of the B light-cone distribution

$$\beta_B = \int_0^\infty \frac{dk}{3k} \phi_B^+(k) = \frac{\lambda_B^{-1}}{3}, \quad (106)$$

and the five factors $\langle H_c^{M_1 M_2} \rangle$, $\langle H_{hc1}^{M_1 M_2} \rangle$, $\langle H_{hc1}^{M_1 M_2} \rangle$, $\langle H_{\chi^1}^{M_1 M_2} \rangle$, and $\langle H_{\chi^2}^{M_1 M_2} \rangle$ are linear combinations of the moment parameters

$$\begin{aligned} \beta_{ic}^{M_1 M_2} &= \oint_0^1 dx dy (a_{ic} + a_{i+4})(x, y) \phi^{M_1}(y) \phi^{M_2}(x), \\ \beta_{hc1,3}^{M_1 M_2} &= \int_0^1 dx dy d\bar{y} \frac{a_{1,3}^{hc}(x, y, \bar{y})}{1-y-\bar{y}} \phi^{3M_1}(y, \bar{y}) \phi^{M_2}(x), \\ \beta_{hc2,4}^{M_1 M_2} &= \int_0^1 dx d\bar{x} dy \frac{a_{2,4}^{hc}(x, \bar{x}, y)}{1-x-\bar{x}} \phi^{M_1}(y) \phi^{3M_2}(x, \bar{x}), \\ \beta_{\chi^{1,5}}^{M_1 M_2} &= \frac{1}{6} \oint_0^1 dx dy a_{1,5}^\chi(x, y) \phi_{pp}^{M_1}(y) \phi^{M_2}(x), \\ \beta_{\chi^{2,6}}^{M_1 M_2} &= \frac{1}{6} \oint_0^1 dx dy a_{2,6}^\chi(x, y) \phi^{M_1}(y) \phi_{pp}^{M_2}(x), \end{aligned} \quad (107)$$

respectively. The appropriate linear combinations for each channel are given by the entries in Tables II, III, IV, and V of Ref. [29] for $\hat{A}_{Lann}^{(1)}$ and $\hat{A}_{Lann}^{(2\chi)}$, and in Table I of Ref. [28] for $\hat{A}_{hcann}^{(1)}$. The distribution functions ϕ^M and ϕ_{pp}^M appearing in Eq. (107) were defined above in Eqs. (40) and (86), while the three-body distribution is defined by the matrix element

$$\langle M | \bar{q}'^L \not{n} i g \not{B}_{n\omega_3}^{\perp} q_{n\omega_2}^R | 0 \rangle = \frac{iC_{q_L q}^M}{\omega_3} \bar{\delta}_{\omega_1 \omega_3}^{\omega_2} f_{3P} \phi_{3P}(y, \bar{y}), \quad (108)$$

where $\bar{\delta}_{\omega_1 \omega_3}^{\omega_2} = \delta(\omega_1 + \omega_3 - \omega_2 - m_b)$, $y = \omega_1/m_b$, and $\bar{y} = -\omega_2/m_b$. The circle on some of the integrations in Eq. (107) indicates the terms which require zero-bin subtractions. These subtractions modify the hadronic distributions by inducing dependence on a rapidity parameter, which increases the uncertainty from these terms. For our numerical analysis we adopt the models used in Refs. [29] and [28] to determine the β 's in section XII below.

XI. ANALYSIS STRATEGY AND MODELS FOR THE SHAPE OF $\zeta_J^{BM}(z)$ AND $\zeta_\chi^{BM}(z)$

To make predictions for the $P^{M_1 M_2}$ penguins at leading order we need values for the twist-2 meson distribution $\phi_M(u)$ and the form factors ζ^{BM} , $\zeta_J^{BM}(z)$. To compute the Λ/m_b suppressed chiral-enhanced amplitudes we need in addition the twist-3 distribution $\phi_{pp}^M(u)$ and the form factor $\zeta_\chi^{BM}(z)$.

A common model for ϕ^M and ϕ_{pp}^M capturing the essential features is given by the first few terms in the Gegen-

bauer series

$$\begin{aligned}\phi^M(x) &= 6x(1-x)\{1 + a_1^M(6x-3) + 6a_2^M(1-5x+5x^2) \\ &\quad + 15a_4^M(1-14x+56x^2-84x^3+42x^4)\}, \\ \phi_{pp}^M(x) &= 6x(1-x)\{a_{0pp}^M + a_{1pp}^M(6x-3) \\ &\quad + 6a_{2pp}^M(1-5x+5x^2)\},\end{aligned}\quad (109)$$

where x corresponds to the momentum fraction for the quark field (dressed by a Wilson line). Our ranges for the model parameters a_i^M and a_{ipp}^M are summarized in the next section. Note that we include both a_2^M and a_4^M in $\phi^M(x)$. This allows us to account for data on $\langle x^{-1} \rangle_\pi$ which constrains $a_2^M + a_4^M$, while varying $a_2^M - a_4^M$ to obtain a range of models. From charge conjugation and isospin, $\phi^{\pi,\rho}(x) = \phi^{\pi,\rho}(1-x)$. Thus we will set $a_1^\pi = a_1^\rho = 0$. With SU(3) flavor symmetry $a_1^K = 0$, so smaller values are adopted for this parameter than are used for a_2^K (we keep a non-zero a_1^M for SU(3) violation, but do not include a non-zero a_3^M or any other odd-moment parameter). These restrictions from charge conjugation also apply to the distribution ϕ_{pp}^M . To see this we follow the same argument given in Ref. [53] but for the matrix element defining the chiral-enhanced distribution:

$$\begin{aligned}\langle \pi^0 | C^\dagger C \bar{\xi}_n W_n C^\dagger C \bar{\eta} \gamma_5 \mathcal{P}_\perp \delta(\omega - \bar{\mathcal{P}}_+) W_n^\dagger \xi_n C^\dagger C | 0 \rangle \\ = (+1) \langle \pi^0 | (C W_n^\dagger \xi_n)^T \bar{\eta} \gamma_5 \mathcal{P}_\perp \delta(\omega - \bar{\mathcal{P}}_+) (\bar{\xi}_n W_n C)^T | 0 \rangle \\ = + \langle \pi^0 | \bar{\xi}_{n,p'} W_n \bar{\eta} \gamma_5 \mathcal{P}_\perp \delta(\omega + \bar{\mathcal{P}}_+) W_n^\dagger \xi_{n,p} | 0 \rangle.\end{aligned}\quad (110)$$

Here $\bar{\mathcal{P}}_+ = \bar{\mathcal{P}}^\dagger + \bar{\mathcal{P}}$, C is the charge-conjugation operator and \mathcal{C} is the charge-conjugation matrix. To obtain the last line we note that the sign from $\mathcal{P}_\perp^\alpha \bar{\xi}_n = -\bar{\xi}_n \mathcal{P}_\perp^{\alpha\dagger}$ cancels the sign from $\mathcal{C}^\dagger(\gamma_\alpha^\perp)^T \mathcal{C} = \gamma_\mu^\perp$. Hence the matrix element is even under $\omega = (1-2x)\bar{n} \cdot p_\pi \rightarrow -\omega$, which implies $\phi_{pp}^{\pi^0}(x) = \phi_{pp}^{\pi^0}(1-x)$. Hence we have $a_{1pp}^\pi = a_{1pp}^\rho = 0$ and small values of a_{1pp}^K . Note that in Wandzura-Wilczek approximation $a_{0pp}^M = 1$ and $a_{1,2pp}^M = 0$.

Potentially larger uncertainty comes from the values for ζ^{BM} and $\zeta_J^{BM}(z)$. At lowest order the $b_i(u, z)$ coefficients in Eq. (42) are independent of z and thus only ζ^{BM} and the zeroth z -moment, ζ_J^{BM} , from Eq. (14) are required. This yields two form factor parameters to be fit to tree amplitude data. For convolutions with the $\alpha_s \Delta b_i(u, z)$ terms we need more information about the z -dependence. However it is still very useful to fit the norm ζ_J^{BM} to the nonleptonic tree amplitude data. In particular, by only modeling the shape of $\zeta_J(z)$ we reduce the model uncertainty considerably. The fit to nonleptonic decay data currently provides the most accurate way of determining the normalization of $\zeta_J^{BM}(z)$. Thus, our strategy allows us to make predictions for the penguin amplitudes based on input about the parameters from the tree amplitudes, while avoiding expanding in $\alpha_s(\mu_i)$.

We adopt a polynomial model for the z -dependence by

using the parameterization

$$\begin{aligned}\zeta_J^{BM}(z) \\ = z\{A_0^{BM} + A_1^{BM}(6z-3) + A_2^{BM}(1-5z+5z^2)\}.\end{aligned}\quad (111)$$

One of these parameters is then eliminated by constraining $\zeta_J^{BM} = \int dz \zeta_J^{BM}(z)$ to its central value obtained from experiment. We then eliminate $A_0^{B\pi}$ in favor of $\zeta_J^{B\pi}$ to obtain

$$\begin{aligned}\zeta_J^{BM}(x) &= 2x \zeta_J^{BM} - A_1^{BM}(4x-6x^2) \\ &\quad + \frac{5}{6} A_2^{BM}(x-6x^2+6x^3).\end{aligned}\quad (112)$$

Note that the remaining A_i^{BM} terms in Eq. (112) must integrate to zero. As we will see in the next section, this considerably reduces the uncertainty generated by these form factor parameters. For $M = \pi$ we will simply set $A_1^{B\pi} = 0$, thus leaving $A_2^{B\pi}$ as the remaining parameter.³

The polynomial form in Eq. (111) could be justified by the SCET_{II} factorization theorem in Eq. (46), where it is inherited from that in Eq. (109) at lowest order. However we do not view our model in this context, and thus do not fix the coefficients A_i^M to values determined by a_i^M . Instead we consider Eq. (112) as a model specified in SCET_I without reference to SCET_{II}-factorization, and take A_i^M as parameters to be varied in a suitably large range. This ensures that our model for ζ_J^{BM} covers a wider range of z -dependence than the restrictive approximation in Eq. (48) would.

Similar to $\zeta_J^{BM}(z)$ we write a model for $\zeta_\chi^{BM}(z)$ as

$$\begin{aligned}\zeta_\chi^{B\pi}(x) &= 2x \zeta_\chi^{B\pi} - A_{\chi 1}^{B\pi}(4x-6x^2) \\ &\quad + \frac{5}{6} A_{\chi 2}^{B\pi}(x-6x^2+6x^3),\end{aligned}\quad (113)$$

We have taken $\zeta_\chi^{BM}(0) = 0$ due to the constraint on this function derived in section VIII.

For $M = \rho$, the simple polynomial model of Eq. (109) does not support the value of $\langle x^{-1} \rangle_\rho = 2.2_{-0.2}^{+0.6}$ obtained from data in section II, unless we include higher order polynomial terms in Gegenbauer expansion. Values of $\langle x^{-1} \rangle_M$ close to 2.0 require $\phi^M(x)$ to peak around $x = 1/2$ with smaller widths. Therefore we choose the following model for $\phi^\rho(x)$, which has all the desired properties

$$\phi^\rho(x) = N(a_\rho) x(1-x) \operatorname{sech}\left(\frac{x-1/2}{a_\rho}\right).\quad (114)$$

Here a^ρ is a parameter whose value is motivated by the inverse moment $\langle x^{-1} \rangle_\rho$ determined from data in section II, and $N(a^\rho)$ is chosen to normalize $\phi^\rho(x)$ to 1.

³ The choice $A_1^{B\pi} = 0$ can be justified by isospin and tree-level SCET_{II} factorization, but we instead view this choice as part of the model. The value of A_1^{BK} then parameterizes SU(3) violation.

For $\zeta_J^{B\rho}$ we will use a polynomial model like Eq. (112)

$$\zeta_J^{B\rho}(x) = 2x \zeta_J^{B\rho} + \frac{5}{6} A_2^{B\rho} (x - 6x^2 + 6x^3), \quad (115)$$

where for simplicity we take $A_1^{B\rho} = 0$. Alternatively we could have based our model for $\zeta_J^{B\rho}(x)$ on Eqs. (114) and (48) where it would inherit features of the sech function, however we find that using this alternative functional form does not significantly change our error analysis. Therefore we adhere to the simple polynomial model of Eq. (115). Numerical estimates for the model parameters introduced in this section are presented in the next section.

XII. INPUT PARAMETERS

Several well determined parameters that are needed for our analysis include [54] $m_b^{1S} = 4.7 \text{ GeV}$, $\bar{m}_b(4.7 \text{ GeV}) = 4.1 \text{ GeV}$, $m_c^{1S} = 1.4 \text{ GeV}$, $\alpha_s(m_b) = 0.22$, $\mu_\pi(m_b) = 2.5 \text{ GeV}$, and $\mu_K(m_b) = 2.8 \text{ GeV}$. Defining $\hat{f}_M = f_M/(1 \text{ GeV})$ we take $\hat{f}_\pi = 0.131$, $\hat{f}_K = 0.160$, $\hat{f}_\rho = 0.209$, and from recent lattice data [55] $\hat{f}_B = 0.22$. We also require the Wilson coefficients of the weak effective Hamiltonian, which are known at NLL order [39]. In the NDR scheme taking $\alpha_s(m_Z) = 0.118$, $m_t = 170.9 \text{ GeV}$, and $m_b = 4.7 \text{ GeV}$ gives $C_{7\gamma}(m_b) = -.316$, $C_{8g}(m_b) = -0.149$ and the NLL results

$$C_{1-10}(m_b) = \{1.080, -.179, .012, -.033, .0096, -.040, 4.2 \times 10^{-4}, 4.2 \times 10^{-4}, -9.7 \times 10^{-3}, 1.9 \times 10^{-3}\}. \quad (116)$$

In varying μ to estimate uncertainties we will also need

$$\begin{aligned} C_{1-10}(2m_b) &= \{1.04, -.104, .0080, -.023, .0074, -.026, 4.2 \times 10^{-4}, 2.8 \times 10^{-4}, -9.3 \times 10^{-3}, 1.3 \times 10^{-3}\}, \\ C_{7\gamma}(2m_b) &= -0.281, \quad C_{8G}(2m_b) = -0.135, \\ C_{1-10}(m_b/2) &= \{1.13, -.279, .019, -.047, .012, -.061, 5.7 \times 10^{-4}, 7.1 \times 10^{-4}, -10.0 \times 10^{-3}, 2.8 \times 10^{-3}\}, \\ C_{7\gamma}(m_b/2) &= -0.358, \quad C_{8G}(m_b/2) = -0.166. \end{aligned} \quad (117)$$

With 2-loop running the $\overline{\text{MS}}$ mass $\overline{m}_b(2m_b) = 3.7 \text{ GeV}$, $\overline{m}_b(m_b/2) = 4.7 \text{ GeV}$, and the chiral-enhancement parameters $\mu_\pi(2m_b) = 2.8 \text{ GeV}$, $\mu_\pi(m_b/2) = 2.2 \text{ GeV}$, $\mu_K(2m_b) = 3.1 \text{ GeV}$, and $\mu_K(m_b/2) = 2.5 \text{ GeV}$.

The $\gamma^*\gamma \rightarrow \pi^0$ data constrains the inverse pion moment, and based on the analysis in Ref. [37] gives

$$a_2^\pi + a_4^\pi = -0.03 \pm 0.14. \quad (118)$$

For the other linear combination we take $a_2^\pi - a_4^\pi = 0.2 \pm 0.3$. In our error analysis we do a Gaussian scan over these ranges in order to properly take into account the correlation in the individual errors of a_2^π and a_4^π , which is large. Based on recent lattice data for moments of the π and K distributions [56] we take $a_2^K = 0.2 \pm 0.2$ and set $a_4^K = 0$. Here the lattice error on a_2^K was doubled to give an estimate for higher moments. For $M = \pi$ isospin and charge conjugation imply $a_1^\pi = a_{1pp}^\pi = 0$, while for $M = K$ we use [56] $a_1^K = -0.05 \pm 0.02$. For simplicity we take $a_{0pp}^{\pi,K} = 1$. We also take $a_{2pp}^{\pi,K} = 0.1 \pm 0.3$ and $a_{1pp}^K = 0.0 \pm 0.1$. For our model of $\phi^\rho(x)$ in Eq. (114) we use $a^\rho = 0.1_{-0.1}^{+0.3}$.

In section II we obtained values for the nonleptonic form factors $\zeta^{B\pi}$, $\zeta_J^{B\pi}$, $\zeta^{B\rho}$, $\zeta_J^{B\rho}$, from a fit to nonleptonic data for the tree amplitudes. Because the uncertainty in these parameters are highly correlated we scan over their values by doing a Gaussian scan over the range specified by the experimental errors in Eqs. (20) and (23) and for the form factors and $\langle x^{-1} \rangle_M \zeta_J^{BM}$ with $M = \pi, \rho$. Since data is being used for these normalization parameters this does not introduce model uncertainty. The choice of the remaining parameters A_i introduces model dependence to $\zeta_J(z)$. We take $A_1^{\pi,\rho} = 0$, $A_2^\pi = (0.25 \pm 0.30)$ and $A_2^\rho = -(0.05 \pm 0.05)$. We also will use $\zeta_\chi^{B\pi} = 0.0 \pm 0.2$ and set $A_{\chi 1}^\pi = 0$, and $A_{\chi 2}^\pi = (0.0 \pm 0.5)$. Note that to predict the $\hat{P}^{K\pi}$ amplitudes we do not need values of ζ^{BK} and ζ_J^{BK} , since only pion form factors appear in the $B \rightarrow K\pi$ amplitudes. The kaon form factors are needed for $B \rightarrow K\bar{K}$.

Finally we will need values for the model parameters appearing in the annihilation amplitudes in section XII. The three-body decay constants are taken as $f_{3\pi} \simeq 4.5 \times 10^{-3} \text{ GeV}^2$, $f_{3K} \simeq 4.5 \times 10^{-3} \text{ GeV}^2$, and $f_{3\rho} \simeq 0.13 \text{ GeV}^2$ from recent QCD sum rule results [57, 58], where $f_{3\rho} = m_\rho f_\rho^T$. For the B -meson inverse moment appearing in the the three-body annihilation amplitude, $\hat{A}_{hcann}^{(1)}$, we take $\beta_B = (2.5 \pm 1.0) \text{ GeV}^{-1}$, where the central value is consistent with our value for $\zeta_J^{B\pi}$ using Eq. (48) and (109), and the error takes into account the uncertainty from the $\alpha_s(\mu_i)$ expansion. For the remaining ingredients we simply quote results for the necessary moments at $\mu = m_b$

$$\begin{aligned}
\beta_{1c}^{\pi\pi} &= (-3.0 \pm 1.6) \times 10^{-2}, & \beta_{3c}^{\pi\pi} &= 0.63 \pm 0.32, & \beta_{4c}^{\pi\pi} &= -0.15 \pm 0.09, & (119) \\
\beta_{hc1}^{\pi\pi} &= -1.32 \pm 0.42, & \beta_{hc2}^{\pi\pi} &= 0.13 \pm 0.12, & \beta_{hc3}^{\pi\pi} &= (-2.4 \pm 2.2) \times 10^{-3}, & \beta_{hc4}^{\pi\pi} &= (-4.9 \pm 1.6) \times 10^{-2}, \\
\beta_{\chi1}^{\pi\pi} &= 0.0 \pm 5.1, & \beta_{\chi2}^{\pi\pi} &= 0.0 \pm 4.7, & \beta_{\chi5}^{\pi\pi} &= 0.0 \pm 0.067, & \beta_{\chi6}^{\pi\pi} &= 0.0 \pm 0.084, \\
\beta_{4c}^{\pi K} &= -0.159 \pm 0.087, & & & & & & \\
\beta_{hc1}^{\pi K} &= -1.37 \pm 0.44, & \beta_{hc2}^{\pi K} &= 0.13 \pm 0.12, & \beta_{hc3}^{\pi K} &= (-2.3 \pm 2.3) \times 10^{-3}, & \beta_{hc4}^{\pi K} &= (-4.9 \pm 1.5) \times 10^{-2}, \\
\beta_{\chi1}^{\pi K} &= 0.0 \pm 6.4, & \beta_{\chi2}^{\pi K} &= 0.0 \pm 5.8, & \beta_{\chi5}^{\pi K} &= 0.0 \pm 0.085, & \beta_{\chi6}^{\pi K} &= 0.0 \pm 0.10, \\
\beta_{1c}^{\rho\rho} &= (5.1^{+4.2}_{-1.4}) \times 10^{-3}, & \beta_{3c}^{\rho\rho} &= -0.11^{+0.09}_{-0.03}, & \beta_{4c}^{\rho\rho} &= (2.5^{+2.1}_{-0.7}) \times 10^{-2}, & & \\
\beta_{hc1}^{\rho\rho} &= (-3.9^{+3.4}_{-3.0}) \times 10^{-2}, & \beta_{hc2}^{\rho\rho} &= (-1.7^{+2.9}_{-1.6}) \times 10^{-3}, & \beta_{hc3}^{\rho\rho} &= (-1.6 \pm 1.2) \times 10^{-4}, & \beta_{hc4}^{\rho\rho} &= (1.5^{+1.3}_{-1.1}) \times 10^{-3}.
\end{aligned}$$

The values are computed as in Refs. [29] and [28] with inputs for C_i , μ_π , and μ_K consistent with those given above. For the case of $\beta_{hci}^{\rho\rho}$ we used $\phi_{3\rho}(x, \bar{x}) = 360x\bar{x}(1 - \bar{x} - x)^2(x - \bar{x})w_3^\rho$, where $w_3^\rho = -0.20 \pm 0.15$ is taken from QCD sum-rules [59] with an inflated error to account for higher Gegenbauer terms (the relation between our notation and theirs is $\phi_{3\rho} = -\Phi_{3;\rho}^\perp/2$). Note that our central value of 0.0 for the $\beta_{\chi i}$ terms in Eq. (119) indicates that we do not have information on the sign of these terms. Results for the β 's at $\mu = m_b/2$ and $\mu = 2m_b$ are quoted in appendix C.

XIII. NUMERICAL ANALYSIS

In this section we make predictions for the penguin amplitudes $\hat{P}_{M_1 M_2}$ in the standard model, focusing on $\pi^+\pi^-$, $K^+\pi^-$, and $\rho^+\rho^-$ final states. Our sign convention for the penguin amplitudes was given in Eqs. (1) and (2). To facilitate comparing the size of various contributions we introduce the notation

$$\begin{aligned}
\hat{P}_{MM'} &= (\hat{P}_{MM'}^\zeta + \hat{P}_{MM'}^{\zeta J}) + (\hat{P}_{MM'}^{\chi\zeta} + \hat{P}_{MM'}^{\chi\zeta J} + \hat{P}_{MM'}^{\chi\chi_\chi}) \\
&\quad + \hat{P}_{c\bar{c}} + (\hat{P}_{MM'}^{Lann} + \hat{P}_{MM'}^{Gann} + \hat{P}_{MM'}^{Lann\chi}). \quad (120)
\end{aligned}$$

The two terms in the first parentheses correspond to the leading power terms in line 1 of Eq. (11), the second parentheses to the chirally enhanced terms in line 2, and $\hat{P}_{c\bar{c}}$ corresponds to the long-distance charm penguin in line 3. In the last parentheses the first two are LO annihilation terms from local annihilation and hard-collinear annihilation respectively, while the term $\hat{P}_{MM'}^{Lann\chi}$ stands for chiral-enhanced annihilation.

The leading power terms can be written as moments

over the distribution functions

$$\begin{aligned}
\hat{P}_{\pi\pi}^\zeta &= -\hat{f}_\pi \langle c_1^c + c_4^c \rangle_\pi \zeta^{B\pi}, \\
\hat{P}_{\pi\pi}^{\zeta J} &= -\hat{f}_\pi \langle (b_1^c + b_4^c) \zeta_J^{B\pi} \rangle_\pi, \\
\hat{P}_{K\pi}^\zeta &= -\hat{f}_K \langle c_1^c + c_4^c \rangle_K \zeta^{B\pi}, \\
\hat{P}_{K\pi}^{\zeta J} &= -\hat{f}_K \langle (b_1^c + b_4^c) \zeta_J^{B\pi} \rangle_K, \\
\hat{P}_{\rho\rho}^\zeta &= -\hat{f}_\rho \langle c_1^c + c_4^c \rangle_\rho \zeta^{B\rho}, \\
\hat{P}_\rho^{\zeta J} &= -\hat{f}_\rho \langle (b_1^c + b_4^c) \zeta_J^{B\rho} \rangle_\rho, \quad (121)
\end{aligned}$$

where $\hat{f}_\pi = f_\pi/(1 \text{ GeV})$ and $\hat{f}_K = f_K/(1 \text{ GeV})$. In an analogous fashion we can define moments for the chirally enhanced penguin amplitudes. For $B \rightarrow \pi\pi$ and $B \rightarrow K\pi$ we obtain from Eq. (87) and Table I

$$\begin{aligned}
\hat{P}_{\pi\pi}^{\chi\zeta} &= \frac{\hat{f}_\pi \mu_\pi}{3m_B} \zeta^{B\pi} \langle c_{1(qf q)}^{\chi c} + c_{2(qf q)}^{\chi c} \rangle_\pi^{pp}, \\
\hat{P}_{\pi\pi}^{\chi\zeta J} &= \frac{\hat{f}_\pi \mu_\pi}{3m_B} \langle [b_{3(qf q)}^{\chi c} + b_{4(qf q)}^{\chi c}] \zeta_J^{B\pi} \rangle_\pi^{pp}, \\
\hat{P}_{\pi\pi}^{\chi\chi_\chi} &= \frac{\hat{f}_\pi \mu_\pi}{6m_B} \langle [b_{1(qf q)}^{\chi c} + b_{1(uf u)}^{\chi c}] \zeta_{\chi}^{B\pi} \rangle_\pi, \\
\hat{P}_{K\pi}^{\chi\zeta} &= \frac{\hat{f}_K \mu_K}{3m_B} \zeta^{B\pi} \langle c_{1(qf q)}^{\chi c} + c_{2(qf q)}^{\chi c} \rangle_K^{pp}, \\
\hat{P}_{K\pi}^{\chi\zeta J} &= \frac{\hat{f}_K \mu_K}{3m_B} \langle [b_{3(qf q)}^{\chi c} + b_{4(qf q)}^{\chi c}] \zeta_J^{B\pi} \rangle_K^{pp}, \\
\hat{P}_{K\pi}^{\chi\chi_\chi} &= \frac{\hat{f}_K \mu_K}{6m_B} \langle [b_{1(qf q)}^{\chi c} + b_{1(uf u)}^{\chi c}] \zeta_{\chi}^{B\pi} \rangle_K. \quad (122)
\end{aligned}$$

In Eq. (121) we have decomposed the leading Wilson coefficients into terms proportional to the two CKM structures,

$$\begin{aligned}
c_i^{(f)} &= \lambda_u^{(f)} c_i^u + \lambda_t^{(f)} c_i^t = \lambda_u^{(f)} \tilde{c}_i^u + \lambda_c^{(f)} c_i^c, \\
b_i^{(f)} &= \lambda_u^{(f)} \tilde{b}_i^u + \lambda_t^{(f)} b_i^t = \lambda_u^{(f)} \tilde{b}_i^u + \lambda_c^{(f)} b_i^c, \quad (123)
\end{aligned}$$

where some coefficients (such as c_1^c and b_1^c) are purely from electroweak penguins [60]. Similarly we split the Wilson coefficients $c_{i(F)}^\chi$ and $b_{i(F)}^\chi$ for the chirally en-

hanced amplitudes in Eqs. (81-84) as

$$\begin{aligned} c_{i(F)}^X &= \lambda_u^{(f)} c_{i(F)}^{Xu} + \lambda_c^{(f)} c_{i(F)}^{Xc}, \\ b_{i(F)}^X &= \lambda_u^{(f)} b_{i(F)}^{Xu} + \lambda_c^{(f)} b_{i(F)}^{Xc}. \end{aligned} \quad (124)$$

The moments appearing in Eqs. (121) and (122) are

$$\begin{aligned} \langle c_i \rangle_M &= \int_0^1 du c_i(u) \phi^M(u), \\ \langle b_i \zeta_J^{BM_2} \rangle_{M_1} &= \int_0^1 du \int_0^1 dz b_i(u, z) \phi^{M_1}(u) \zeta_J^{BM_2}(z), \\ \langle c_i \rangle_M^{pp} &= \int_0^1 du c_i(u) \phi_{pp}^M(u), \\ \langle b_i \zeta_J^{BM_2} \rangle_{M_1}^{pp} &= \int_0^1 du \int_0^1 dz b_i(u, z) \phi_{pp}^{M_1}(u) \zeta_J^{BM_2}(z), \\ \langle b_i \zeta_\chi^{BM_2} \rangle_{M_1} &= \int_0^1 du \int_0^1 dz b_i(u, z) \phi^{M_1}(u) \zeta_\chi^{BM_2}(z). \end{aligned} \quad (125)$$

Generically power counting alone gives $\hat{P}^\zeta \sim \hat{P}^{\zeta_J}$, where the exact size is modified by numerical coefficients. For the chirally enhanced moments the power counting is $\hat{P}_{M_1 M_2}^{\chi \zeta} \sim \hat{P}_{M_1 M_2}^{\zeta_J} \sim \hat{P}_{M_1 M_2}^{\chi \zeta_\chi}$ since $\zeta \sim \zeta_J \sim \zeta_\chi$.

The penguin annihilation amplitudes can also be written in terms of moments of distributions. Using the notation in Refs. [29] and [28] the necessary amplitudes are

$$\begin{aligned} \hat{P}_{\pi\pi}^{\text{Lann}} &= -\frac{\hat{f}_B f_\pi^2}{m_B^2} \left(\beta_{1c}^{\pi\pi} + 2\beta_{3c}^{\pi\pi} + \beta_{4c}^{\pi\pi} \right), \\ \hat{P}_{\pi\pi}^{\text{Gann}} &= -\frac{\hat{f}_B \beta_B f_{3\pi} f_\pi}{m_B m_b} \left(\beta_{hc1}^{\pi\pi} + \beta_{hc2}^{\pi\pi} - \frac{1}{2}\beta_{hc3}^{\pi\pi} - \frac{1}{2}\beta_{hc4}^{\pi\pi} \right), \\ \hat{P}_{\pi\pi}^{\text{Lann}\chi} &= -\frac{\hat{f}_B f_\pi^2 \mu_\pi}{m_B^2 m_b} \left(\beta_{\chi 1}^{\pi\pi} - \beta_{\chi 2}^{\pi\pi} - \frac{1}{2}\beta_{\chi 5}^{\pi\pi} + \frac{1}{2}\beta_{\chi 6}^{\pi\pi} \right), \\ \hat{P}_{K\pi}^{\text{Lann}} &= -\frac{\hat{f}_B f_\pi f_K}{m_B^2} \beta_{4c}^{\pi K}, \\ \hat{P}_{K\pi}^{\text{Gann}} &= -\frac{\hat{f}_B \beta_B}{m_B m_b} \left[f_{3\pi} f_K \left(\beta_{hc1}^{\pi K} - \frac{1}{2}\beta_{hc3}^{\pi K} \right) \right. \\ &\quad \left. + f_{3K} f_\pi \left(\beta_{hc2}^{\pi K} - \frac{1}{2}\beta_{hc4}^{\pi K} \right) \right], \\ \hat{P}_{K\pi}^{\text{Lann}\chi} &= -\frac{\hat{f}_B f_\pi f_K}{m_B^2} \left[\frac{\mu_\pi}{m_b} \left(\beta_{\chi 1}^{\pi K} - \frac{1}{2}\beta_{\chi 5}^{\pi K} \right) \right. \\ &\quad \left. + \frac{\mu_K}{m_b} \left(-\beta_{\chi 2}^{\pi K} + \frac{1}{2}\beta_{\chi 6}^{\pi K} \right) \right], \\ \hat{P}_{\rho\rho}^{\text{Lann}} &= -\frac{\hat{f}_B f_\rho^2}{m_B^2} \left(\beta_{1c}^{\rho\rho} + 2\beta_{3c}^{\rho\rho} + \beta_{4c}^{\rho\rho} \right), \\ \hat{P}_{\rho\rho}^{\text{Gann}} &= -\frac{\hat{f}_B \beta_B f_{3\rho} f_\rho}{m_B m_b} \left(\beta_{hc1}^{\rho\rho} - \beta_{hc2}^{\rho\rho} - \frac{1}{2}\beta_{hc3}^{\rho\rho} + \frac{1}{2}\beta_{hc4}^{\rho\rho} \right), \end{aligned} \quad (126)$$

where the β -moment parameters were defined above in Eq. (107) and numerical values were given in Eq. (119).

To evaluate the remaining penguin amplitudes in Eqs. (121) and (122) we use the form of the distributions

from section XI. It is useful to write Eq. (125) as integrals over short-distance coefficients, i_α and $j_{\alpha\beta}$, multiplying model parameters a_α and A_β :

$$\begin{aligned} \langle c_4^c \rangle_M &= i_0^{(4c)} + \sum_{\alpha \neq 0} i_\alpha^{(4c)} a_\alpha^M, \\ \langle c_1^c \rangle_M &= i_0^{(1c)} + \sum_{\alpha \neq 0} i_\alpha^{(1c)} a_\alpha^M, \\ \langle b_{4\zeta_J}^{cBM_2} \rangle_{M_1} &= j_{00}^{(4c)} \zeta_J^{BM_2} + \sum_{(\alpha, \beta) \neq (0,0)} j_{\beta\alpha}^{(4c)} A_\beta^{BM_2} a_\alpha^{M_1}, \\ \langle b_{1\zeta_J}^{cBM_2} \rangle_{M_1} &= j_{00}^{(1c)} \zeta_J^{BM_2} + \sum_{(\alpha, \beta) \neq (0,0)} j_{\beta\alpha}^{(1c)} A_\beta^{BM_2} a_\alpha^{M_1}, \end{aligned} \quad (127)$$

where $\alpha = 0, 1, 2, 4$ with $a_\alpha^M = (1, a_1^M, a_2^M, a_4^M)$, and $\beta = 0, 1, 2$ with $A_\beta^{BM} = (\zeta_J^{BM}, A_1^{BM}, A_2^{BM})$. This step is useful because the short-distance coefficients, i_α , $j_{\alpha\beta}$ are integrals which can be evaluated numerically independent of the choice of the model parameters. This makes it easier to propagate errors from parameter uncertainties into the final amplitude predictions. It also makes it possible to study the short-distance uncertainties (such as the μ -dependence) directly in terms of i_α and $j_{\beta\alpha}$. In Eq. (127) we have separated out the dominant term from the sum. Since our values of $\zeta_J^{B\pi}$ and $\zeta^{B\pi}$ are extracted from independent experimental data, these dominant terms in the penguin amplitudes become model independent. For the chiral enhanced amplitudes the analog of Eq. (127) is

$$\begin{aligned} \langle c_{1(qf q)}^{\chi c} \rangle_M^{pp} &= k_0^{(1c)} + \sum_{\gamma \neq 0} k_\gamma^{(1c)} p_\gamma^M, \\ \langle c_{2(qf q)}^{\chi c} \rangle_M^{pp} &= k_0^{(2c)} + \sum_{\gamma \neq 0} k_\gamma^{(2c)} p_\gamma^M, \\ \langle b_{3(qf q)}^{\chi c} \zeta_J^{BM_2} \rangle_{M_1}^{pp} &= \ell_{00}^{(3c)} \zeta_J^{BM_2} + \sum_{(\gamma, \beta) \neq (0,0)} \ell_{\gamma\beta}^{(3c)} A_\gamma^{BM_2} p_\beta^{M_1}, \\ \langle b_{4(qf q)}^{\chi c} \zeta_J^{BM_2} \rangle_{M_1}^{pp} &= \ell_{00}^{(4c)} \zeta_J^{BM_2} + \sum_{(\gamma, \beta) \neq (0,0)} \ell_{\gamma\beta}^{(4c)} A_\gamma^{BM_2} p_\beta^{M_1}, \\ \langle b_{1(qf q)}^{\chi c} \zeta_\chi^{BM_2} \rangle_{M_1} &= \ell_{00}^{(1c)} \zeta_\chi^{BM_2} + \sum_{(\alpha, \beta) \neq (0,0)} \ell_{\beta\alpha}^{(1c)} A_{\chi\beta}^{BM_2} a_\alpha^{M_1}, \\ \langle b_{1(uf u)}^{\chi c} \zeta_\chi^{BM_2} \rangle_{M_1} &= \ell_{00}^{(2c)} \zeta_\chi^{BM_2} + \sum_{(\alpha, \beta) \neq (0,0)} \ell_{\beta\alpha}^{(2c)} A_{\chi\beta}^{BM_2} a_\alpha^{M_1}, \end{aligned} \quad (128)$$

where $\beta, \gamma = 0, 1, 2$, $p_\gamma^M = \{1, a_{1pp}^M, a_{2pp}^M\}$ and $A_{\chi\beta}^{BM} = \{\zeta_\chi^{BM}, A_{\chi 1}^{BM}, A_{\chi 2}^{BM}\}$. In terms of the i, j, k, ℓ coefficients,

Eqs. (121) and (122) are given by

$$\begin{aligned}
\hat{P}_{\pi\pi}^\zeta &= -\hat{f}_\pi [i_\alpha^{(4c)} + i_\alpha^{(1c)}] \zeta^{B\pi} a_\alpha^\pi, \\
\hat{P}_{\pi\pi}^{\zeta_j} &= -\hat{f}_\pi [j_{\beta\alpha}^{(4c)} + j_{\beta\alpha}^{(1c)}] A_\beta^{B\pi} a_\alpha^\pi, \\
\hat{P}_{\pi\pi}^{\chi\zeta} &= \frac{\hat{f}_\pi \mu_\pi}{3m_B} [k_\gamma^{(1c)} + k_\gamma^{(2c)}] \zeta^{B\pi} p_\gamma^\pi, \\
\hat{P}_{\pi\pi}^{\chi\zeta_j} &= \frac{\hat{f}_\pi \mu_\pi}{3m_B} [\ell_{\gamma\beta}^{(3c)} + \ell_{\gamma\beta}^{(4c)}] A_\gamma^{B\pi} p_\beta^\pi, \\
\hat{P}_{\pi\pi}^{\chi\zeta_\chi} &= \frac{\hat{f}_\pi \mu_\pi}{3m_B} [\ell_{\beta\alpha}^{(1c)} + \ell_{\beta\alpha}^{(2c)}] A_{\chi\beta}^{B\pi} a_\alpha^\pi,
\end{aligned} \tag{129}$$

and

$$\begin{aligned}
\hat{P}_{K\pi}^\zeta &= -\hat{f}_K [i_\alpha^{(4c)} + i_\alpha^{(1c)}] a_\alpha^K \zeta^{B\pi}, \\
\hat{P}_{K\pi}^{\zeta_j} &= -\hat{f}_K [j_{\beta\alpha}^{(4c)} + j_{\beta\alpha}^{(1c)}] A_\beta^{B\pi} a_\alpha^K, \\
\hat{P}_{K\pi}^{\chi\zeta} &= \frac{\hat{f}_K \mu_K}{3m_B} [k_\gamma^{(1c)} + k_\gamma^{(2c)}] \zeta^{B\pi} p_\gamma^\pi, \\
\hat{P}_{K\pi}^{\chi\zeta_j} &= \frac{\hat{f}_K \mu_K}{3m_B} [\ell_{\gamma\beta}^{(3c)} + \ell_{\gamma\beta}^{(4c)}] A_\gamma^{B\pi} p_\beta^K, \\
\hat{P}_{K\pi}^{\chi\zeta_\chi} &= \frac{\hat{f}_K \mu_\pi}{3m_B} [\ell_{\beta\alpha}^{(1c)} + \ell_{\beta\alpha}^{(2c)}] A_{\chi\beta}^{B\pi} a_\alpha^K,
\end{aligned} \tag{130}$$

where a sum over $\alpha = 0, 1, 2, 4$ and $\beta, \gamma = 0, 1, 2$ is understood.

Evaluating the short-distance integrals at zeroth order in α_s with the C_i 's in Eq. (116) the i 's and j 's are

$$\begin{aligned}
i^{(4c)} \times 10^3 &= (-28.4, 0, 0, 0), \\
i^{(1c)} \times 10^3 &= (-1.96, 0, 0, 0), \\
j^{(4c)} \times 10^3 &= \begin{bmatrix} -11.1 & 17.3 & 17.3 & 17.3 \\ 0 & 0 & 0 & 0 \\ 0 & 0 & 0 & 0 \end{bmatrix}, \\
j^{(1c)} \times 10^3 &= \begin{bmatrix} -16.4 & -14.5 & -14.5 & -14.5 \\ 0 & 0 & 0 & 0 \\ 0 & 0 & 0 & 0 \end{bmatrix}.
\end{aligned} \tag{131}$$

At the scale $\mu = m_b$ we find

$$\begin{aligned}
i^{(4c)} \times 10^3 &= (-36.2 - i9.58, 4.49 + i8.12, 10.5 + i2.06, 4.42 - i2.36), \\
j^{(4c)} \times 10^3 &= \begin{bmatrix} -14.0 - i4.52 & 27.6 + i4.47 & 28.1 - i0.15 & 25.8 - i0.55 \\ -1.05 - i3.63 & -2.30 + i2.10 & 1.32 + i1.95 & -0.20 - i1.64 \\ 0.15 + i0.04 & -0.10 - i0.08 & 0.08 - i0.14 & -0.07 + i0.14 \end{bmatrix}, \\
k^{(1c)} \times 10^3 &= (281 + i54.7, 8.6 - i69.1, 240 + i41.1).
\end{aligned} \tag{132}$$

Note that the short-distance “ i ” coefficients for ζ^{BM} are comparable in size to the short-distance “ j ” coefficients for $\zeta_J^{BM}(z)$. For the chirally enhanced integrals we find

$$\begin{aligned}
k^{(1c)} \times 10^3 &= (218, 0, 218), \\
k^{(2c)} \times 10^3 &= (-3.38, 0, -3.38), \\
\ell^{(1c)} \times 10^3 &= \begin{bmatrix} -12.3 & 69.1 & -69.1 & -69.1 \\ 34.5 & -34.5 & 34.5 & 34.5 \\ 0 & 0 & 0 & 0 \end{bmatrix}, \\
\ell^{(2c)} \times 10^3 &= \begin{bmatrix} 61.9 & -57.9 & 57.9 & 57.9 \\ -29.0 & 29.0 & -29.0 & -29.0 \\ 0 & 0 & 0 & 0 \end{bmatrix}, \\
\ell^{(3c)} \times 10^3 &= \begin{bmatrix} 218 & 0 & 218 \\ 0 & 0 & 0 \\ 0 & 0 & 0 \end{bmatrix}, \\
\ell^{(4c)} \times 10^3 &= \begin{bmatrix} -3.38 & 0 & -3.38 \\ 0 & 0 & 0 \\ 0 & 0 & 0 \end{bmatrix}.
\end{aligned} \tag{132}$$

Relative to the size of $i^{(4c)}$ and $j^{(1c,4c)}$ the enhanced size of the $k^{(1c)}$ and the $\ell^{(ic)}$ short-distance coefficients is quite striking. Comparing the matching coefficients in Eqs. (44,45) and (81,83) we see that the combinations of coefficients from H_W are similar in size ($C_{3,4}$ versus $C_{5,6}$). However, the $k^{(1c)}$ and $\ell^{(ic)}$ moments are enhanced by a factor of $\simeq 6$ due to the inverse moment fraction factor $1/u\bar{u}$. This numerical factor provides additional enhancement beyond the numerical enhancement in μ_M/m_b , and is the essential reason why the chirally enhanced penguin amplitudes are numerically important.

Next we evaluate the short-distance integrals $i^{(4c)}$, $j^{(4c)}$, and $k^{(1c)}$ up to order α_s , by including the one-loop results for $b_4^{(f)}$ and $c_4^{(f)}$ given earlier in section V. Where known we also evaluate the chiral enhanced short-distance integrals up to $\mathcal{O}(\alpha_s)$ (from Eq.(82)).

We will also analyze how stable our results are to variations in μ . For the LO results in Eqs. (131) and (132) a change in μ simply reflects changes in the $C_i(\mu)$ and so will not be shown. At NLO in the perturbative expansion we find for

$$\mu = m_b/2 = 2.35 \text{ GeV}$$

$$\begin{aligned} i^{(4c)} \times 10^3 &= (-38.9 - i12.3, 7.46 + i10.5, 15.2 + i2.65, 7.37 - i3.05), \\ j^{(4c)} \times 10^3 &= \begin{bmatrix} -12.6 - i6.67 & 34.6 + i6.12 & 36.3 + i0.45 & 33.1 - i1.23 \\ -0.92 - i4.01 & -2.51 + i2.30 & 1.40 + i2.14 & -0.13 - i1.82 \\ 0.20 + i0.09 & 0.17 + i0.09 & 0.08 - i0.21 & -0.08 + i0.20 \end{bmatrix}, \\ k^{(1c)} \times 10^3 &= (359 + i70.6, 11.1 - i89.2, 306 + i53.0), \end{aligned} \quad (134)$$

while for $\mu = 2m_b = 9.4 \text{ GeV}$ we find

$$\begin{aligned} i^{(4c)} \times 10^3 &= (-32.5 - i7.57, 2.81 + i6.42, 7.58 + i1.63, 2.75 - i1.87), \\ j^{(4c)} \times 10^3 &= \begin{bmatrix} -13.2 - i3.10 & 22.7 + i3.31 & 22.6 - i0.45 & 21.0 - i0.16 \\ -1.05 - i3.19 & -2.05 + i1.85 & 1.20 + i1.72 & -0.22 - i1.44 \\ 0.11 + i0.01 & 0.06 + i0.08 & 0.07 - i0.09 & -0.07 + i0.10 \end{bmatrix}, \\ k^{(1c)} \times 10^3 &= (228 + i43.3, 6.8 - i54.7, 195 + i32.5). \end{aligned} \quad (135)$$

From Eq. (133) we observe that these α_s corrections induce imaginary contributions which are often appreciable since the $\alpha_s C_{1,2}$ terms can compete with C_{3-6} . For example, the imaginary part of $j_{00}^{(4c)}$ determined from our result for the one-loop matching given in Eq. (52), is $\sim 30\%$ of the real part.

Because we have neglected terms $\alpha_s C_{3-6}$ we must also neglect the μ dependence of ζ , ζ_J , and the ϕ 's for consistency. These terms induce a $\alpha_s \ln(\mu)$ that multiplies the tree-level penguin coefficients involving C_{3-6} and are hence compensated by $\alpha_s \ln(\mu) C_{3-6}$ corrections to the short-distance coefficients. The dominant coefficients have $\alpha = \beta = 0$. At zeroth order in α_s the central values for the coefficients $i_0^{(4c)}$ and $j_{00}^{(4c)}$ vary by $\pm 30\text{-}50\%$ when we take $\mu = m_b/2$ and $\mu = 2m_b$. We find this change is reduced to $\leq 10\%$ at NLO. At LO the chirally enhanced $k_0^{(1c)}$ varies by $\pm 35\text{-}55\%$, and this is reduced by about a factor of two, to $\pm 20\text{-}25\%$ at NLO. The imaginary parts first appear at $\mathcal{O}(\alpha_s(\mu))$, and exhibit a $\pm 20\text{-}30\%$ range for $i_0^{(4c)}$ and $k_0^{(1c)}$, and $\pm 30\text{-}50\%$ dependence for $j_{00}^{(4c)}$. The LO coefficients $\ell_{00}^{(1c,3c,4c)}$ also have a sizeable μ -dependence (20-50%) and it will be important to compute their α_s corrections in the future. Below we will take this residual scale uncertainty as a way of estimating the size of missing higher order perturbative corrections on our final result.

On the other hand the electroweak coefficients $j_{00}^{(1c)}$ and $\ell_{00}^{(2c)}$ have only $\sim 3\%$ μ -dependence at LO, consistent with our expectations that the NLO corrections to this term are small. This reflects the fact that the corresponding μ dependence occurs in a NLO penguin diagram with photon exchange, whereas the leading order Wilson coefficients are generated by both photon and the larger Z exchange. The corrections to the electroweak coefficient $i_0^{(1c)}$ at LO is larger as a percent (40-50%), however the $i_0^{(1c)}$ is tiny to begin with, since at LO its proportional to

the numerically small combination $C_{10} + C_9/N_c$. Thus we do not expect our neglect of these one-loop electroweak corrections to have a large effect.

In table II we present numbers for the penguin amplitudes in Eq. (120), showing separately the tree-level and α_s corrections. The errors shown in the table include only input parameter uncertainty, and are computed with Gaussian scans for the errors in the model parameters given in section XII. Despite having a number of hadronic parameters, we observe a relatively small model parameter dependence in the first four columns for $\pi\pi$ and $K\pi$. This occurs because there is only a small dependence of the penguin amplitudes on the shape of $\zeta_J^{BM}(z)$ and $\phi^M(u)$. The normalization terms, $i_0^{(4c)}$ and $j_{00}^{(1c,4c)}$, give the dominant contribution to the amplitudes and the corresponding model parameters were fit to independent data to reduce their uncertainty. Furthermore, at LO the only shape parameter dependence comes from $\langle x^{-1} \rangle_M$ and for the pion this parameter is quite well known (which in our error analysis is accounted for by taking into account an important correlation in a_2^π and a_4^π). For example, we find that further doubling the error bars on the shape parameters $A_{i=1,2}^M$ only effects the last quoted digit of the error bars on the penguin amplitudes in table II. Since the second and third rows of $j_{\alpha\beta}^{(4t)}$ are small, the dependence on the shape of $\zeta_J^{BM}(z)$ is very small. Though the coefficients $j_{01}^{(4t)}$, $j_{02}^{(4t)}$ are similar in size to $j_{00}^{(4t)}$, their contributions are suppressed by the small $a_{1,2}^M$. One entry is very sensitive to the a_2^K , namely the $\alpha_s C_{1,2,8g}$ contributions to $\hat{P}_{K\pi}^{\zeta_J}$. Here the dominant term is

$$\begin{aligned} 10^3 \hat{P}_{K\pi}^{\zeta_J} \Big|_{\alpha_s C_i} &\simeq \hat{f}_K \zeta_J^{B\pi} [(2.9 + i4.5) - (10.3 + i4.47) a_1^K \\ &\quad - (10.8 - i0.15) a_2^K], \end{aligned} \quad (136)$$

and exhibits a large cancellation in the real part for the

Penguin Amplitudes, $\hat{P}_{M_1 M_2}^i \times 10^4$						Penguin Annihilation, $\hat{P}_{M_1 M_2}^i \times 10^4$			
	$\hat{P}_{\pi\pi}^\zeta$	$\hat{P}_{\pi\pi}^{\zeta_J}$	$\hat{P}_{\pi\pi}^{\chi\zeta}$	$\hat{P}_{\pi\pi}^{\chi\zeta_J}$	$\hat{P}_{\pi\pi}^{\chi\zeta_\chi}$		$\hat{P}_{\pi\pi}^{\text{Lann}}$	$\hat{P}_{\pi\pi}^{\text{Gann}}$	$\hat{P}_{\pi\pi}^{\text{Lann}\chi}$
C_{3-10} $\alpha_s C_{1,2,8g}$	3.58 ± 1.02 (0.86±0.25) $+i(1.08 \pm 0.32)$	3.34 ± 0.88 (0.32±0.26) $+i(0.53 \pm 0.13)$	4.41 ± 1.78 (1.21±0.37) $+i(1.10 \pm 0.40)$	4.51 ± 1.71 —	0.00 ± 1.03 —	$\alpha_s C_{1-10}$	— -1.46 ± 0.88	— 0.15 ± 0.08	— 0.00 ± 5.00
$\hat{P}_{K\pi}^i \times 10^4$:	$\hat{P}_{K\pi}^\zeta$	$\hat{P}_{K\pi}^{\zeta_J}$	$\hat{P}_{K\pi}^{\chi\zeta}$	$\hat{P}_{K\pi}^{\chi\zeta_J}$	$\hat{P}_{K\pi}^{\chi\zeta_\chi}$		$\hat{P}_{K\pi}^{\text{Lann}}$	$\hat{P}_{K\pi}^{\text{Gann}}$	$\hat{P}_{K\pi}^{\text{Lann}\chi}$
C_{3-10} $\alpha_s C_{1,2,8g}$	4.37 ± 1.25 (0.86±0.40) $+i(1.38 \pm 0.40)$	4.00 ± 1.02 (0.11±0.35) $+i(0.70 \pm 0.18)$	6.02 ± 2.42 (1.66±0.50) $+i(1.50 \pm 0.57)$	6.15 ± 2.33 —	0.00 ± 1.18 —	$\alpha_s C_{1-10}$	— 0.26 ± 0.14	— 0.20 ± 0.11	— 0.00 ± 8.03
$\hat{P}_{\rho\rho}^i \times 10^4$:	$\hat{P}_{\rho\rho}^\zeta$	$\hat{P}_{\rho\rho}^{\zeta_J}$					$\hat{P}_{\rho\rho}^{\text{Lann}}$	$\hat{P}_{\rho\rho}^{\text{Gann}}$	
C_{3-10} $\alpha_s C_{1,2,8g}$	14.8 ± 3.5 (5.59 ^{+3.08} _{-1.61}) $+i(5.39+2.60-1.48)$	1.64 ± 2.99 (0.36±0.66) $+i(0.28 \pm 0.49)$				$\alpha_s C_{1-10}$	$0.65+0.63-0.21$	$0.22+0.22-0.20$	

TABLE II: Numerical predictions for the penguin amplitudes, \hat{P}_{MM} , from the factorization theorem. The results were split into terms generated at $\mathcal{O}(\alpha_s^0)$ and $\mathcal{O}(\alpha_s)$ in the short-distance matching coefficients. In each row the theoretical predictions are broken down by contributions from the ζ^{BM} and ζ_J^{BM} terms in the leading power amplitude, terms ζ^{BM} , ζ_J^{BM} , ζ_χ^{BM} from the chirally enhanced part of the amplitude, and terms from standard penguin annihilation, three-parton annihilation, and chirally enhanced annihilation. The errors shown are uncertainties propagated from input parameters as described in the text.

value $a_2^K = 0.2$ (explaining its large percent uncertainty for $a_2^K = 0.2 \pm 0.2$). Some cancellation is also evident for $\hat{P}_{\pi\pi}^{\zeta_J}$. However, overall these are both small contributions to their respective penguin amplitudes. This type of parameter dependence does not appear in other terms, and we find that it does not significantly effect the final result. Thus even though our model parameters vary over a large range we have fairly robust central values for individual contributions to the leading order penguin amplitudes in table II. The uncertainty in the 3rd and 4th columns for the chirally enhanced amplitudes is also reduced by our knowledge of the normalization of ζ and ζ_J , and is a bit bigger than the first two columns due to the added uncertainty from $\phi_{pp}^M(u)$. The 5th column involves the new form factor $\zeta_\chi^{BM}(z)$, where we do not have information about the sign, and hence zero central values.

In the $\pi\pi$ and $K\pi$ entries in table II we also observe that the contributions from ζ^{BM} and ζ_J^{BM} are similar in size. This is a reflection of the fact that these coefficients are similar numerically, and is in agreement with the power counting $\zeta^{BM} \sim \zeta_J^{BM}$. In determining the errors associated with these parameters it was quite important to take into account the correlations, as already described in section II. Also, as mentioned above, the chirally enhanced penguin amplitudes compete numerically with the leading power amplitudes due to the presence of the enhancement by the $1/u\bar{u}$ momentum fraction factor which generates a numerical factor of six. For example, we have

$$\hat{P}_{\pi\pi}^{\zeta_J} + \hat{P}_{\pi\pi}^{\chi\zeta_J} \Big|_{C_{3-10}} \sim \hat{f}_\pi \zeta_J^{B\pi} \left(28 + 215 \frac{\mu_\pi}{3m_B} \right) + \dots, \quad (137)$$

where the large numerical value 215 is generated by this enhancement.

Examining the annihilation amplitudes we see that $\hat{P}_{\pi\pi}^{\text{Lann}} + \hat{P}_{\pi\pi}^{\text{Gann}}$ is suppressed by a factor of 1/5 relative to $\hat{P}_{\pi\pi}^\zeta + \hat{P}_{\pi\pi}^{\zeta_J}$, and so is of the expected size for this power correction, namely

$$\frac{\hat{P}_{\pi\pi}^{\text{Lann}} + \hat{P}_{\pi\pi}^{\text{Gann}}}{\hat{P}_{\pi\pi}^\zeta + \hat{P}_{\pi\pi}^{\zeta_J}} \sim \frac{\Lambda_{\text{QCD}}}{E} \frac{\alpha_s(m_b)}{\alpha_s(\mu_i)}. \quad (138)$$

The same conclusions hold for $K\pi$. On the other hand the chirally enhanced annihilation terms $\hat{P}_{\pi\pi}^{\text{Lann}\chi}$ and $\hat{P}_{K\pi}^{\text{Lann}\chi}$ have much larger parameter uncertainty, and we are not able to draw definite conclusions about the size of these terms. In fact they provide the dominant parameter uncertainty for the $\pi\pi$ and $K\pi$ channels.

For $B \rightarrow \rho\rho$ decays, our analysis was slightly different from the pseudoscalars as we used a non-polynomial model for $\phi^\rho(x)$. Here the errors are dominated by the uncertainty in $\zeta^{B\rho}$, $\zeta_J^{B\rho}$, and a_ρ . The uncertainty from the shape parameters A_i are negligible in comparison. Since current data prefers a central value for $\zeta_J^{B\rho}$ significantly smaller than that for $\zeta^{B\rho}$ this same hierarchy is observed in the penguin amplitudes. The size of $\hat{P}_{\rho\rho}^\zeta$ is enhanced by f_ρ and the ρ -form factor in comparison to $\hat{P}_{\pi\pi}^\zeta$. Due to the absence of chirally enhanced contributions the dominant parameter uncertainty comes from experimental uncertainties that propagate into the errors for $\zeta^{B\rho}$ and $\zeta_J^{B\rho}$.

In table III we “sum up” the individual contributions from the leading power, chirally enhanced, and annihilation penguin amplitudes, to obtain \hat{P}^{LO} , \hat{P}^χ , and \hat{P}^{ann} respectively. To perform these sums we do separate Gaussian scans for the total penguin amplitude since this provides the simplest way of propagating correlated parameter uncertainties. This also explains why the central

	$\hat{P}^{\text{LO}} \times 10^4$	$\hat{P}^{\text{x}} \times 10^4$	$\hat{P}^{\text{ann}} \times 10^4$	$\hat{P}^{\text{total}} \times 10^4$	$\hat{P}_{\text{ispin}}^{\text{expt}} \times 10^4$ ($\gamma = 59^\circ$)	$\hat{P}_{\text{ispin}}^{\text{expt}} \times 10^4$ ($\gamma = 74^\circ$)	$\hat{P}_{\text{TF}}^{\text{expt}} \times 10^4$ ($\gamma = 59^\circ - 74^\circ$)
$B \rightarrow \pi\pi$	(8.10 ± 0.63) $+i(1.61 \pm 0.21)$	(10.2 ± 2.9) $+i(1.10 \pm 0.39)$	-1.31 ± 5.08	(16.9 ± 5.9) $+i(2.71 \pm 0.45)$	(18 ± 9) $-i(29 \pm 6)$	(44 ± 6) $-i(29 \pm 6)$	
$B \rightarrow K\pi$	(9.34 ± 1.00) $+i(2.08 \pm 0.25)$	(13.8 ± 3.9) $+i(1.49 \pm 0.57)$	0.46 ± 8.03	(23.6 ± 9.0) $+i(3.57 \pm 0.62)$			$\pm(48 \pm 4 \pm 10)$ $-i(22 \pm 7 \pm 4)$
$B \rightarrow \rho\rho$	$22.4^{+3.7}_{-2.3}$ $+i5.68^{+2.45}_{-1.07}$	— —	$0.87^{+0.67}_{-0.29}$	$23.3^{+3.7}_{-2.4}$ $+i5.68^{+2.45}_{-1.07}$	$-(29 \pm 26)$ $-i(8 \pm 18)$	(38 ± 23) $-i(8 \pm 18)$	

TABLE III: Numerical predictions for the short-distance penguin amplitudes at leading power, \hat{P}^{LO} , from chirally enhanced terms \hat{P}^{x} , and from the annihilation amplitudes in Refs. [28, 29]. The sum of these contributions \hat{P}^{total} , is the total short-distance result from the factorization theorems discussed in the text (long-distance terms are discussed in the text). The last three columns show current experimental data. Comparing them with \hat{P}^{total} shows an order of magnitude short-fall for the imaginary part.

values are not precisely the mean from table II, due to small non-linearity effects in the parameter dependences. The correlation in input parameter uncertainties must be taken into account to get the errors shown here. The three amplitudes in the first three columns of table III are then added together to get the total theoretical contribution, \hat{P}^{total} . These total values can be compared to the experimental values in the last three columns. The uncertainty shown only includes the variation of parameters from the Gaussian scans. For the first column the displayed errors are dominated by the uncertainties in $a_2^\pi + a_4^\pi$, $a_{1,2}^K$, $\zeta^{B\pi}$, $\zeta_J^{B\pi}$, and for $B \rightarrow \rho\rho$ those in a_ρ , $\zeta^{B\rho}$, and $\zeta_J^{B\rho}$. The effect of other parameter uncertainties is quite small. Even the dominant uncertainties are small due to our proper account of parameter correlations and use of experimental data. Also due to our fit procedure the errors from ζ and ζ_J will decrease with improved measurements of the tree amplitudes (which come from improved branching ratios and CP-asymmetries). In \hat{P}^{total} the uncertainty from the parameters in the chiral enhanced annihilation by far dominate the errors for $B \rightarrow \pi\pi$ and $B \rightarrow K\pi$.

In addition we can estimate the uncertainty from determining the hard coefficients by varying $\mu \in [m_b/2, 2m_b]$. For the real parts this gives an additional $^{+7\%}_{-9\%}$ uncertainty for $\hat{P}_{\pi\pi}^{\text{total}}$, $^{+15\%}_{-12\%}$ uncertainty for $\hat{P}_{K\pi}^{\text{total}}$, and $^{+9\%}_{-10\%}$ uncertainty for $\hat{P}_{\rho\rho}^{\text{total}}$. For the imaginary parts we find an additional $^{+25\%}_{-19\%}$ uncertainty for $\hat{P}_{\pi\pi}^{\text{total}}$, $^{+26\%}_{-19\%}$ uncertainty for $\hat{P}_{K\pi}^{\text{total}}$, and $^{+30\%}_{-22\%}$ uncertainty for $\hat{P}_{\rho\rho}^{\text{total}}$. Finally we assign a generic 20% uncertainty to the final \hat{P}^{total} results to account for the fact that we have given only a partial treatment of $1/m_b$ corrections, but do not foresee a reason why the untreated corrections should be enhanced over the power counting estimate. Thus with an estimate

for all theoretical uncertainties we find

$$\begin{aligned}
\hat{P}_{\pi\pi}^{\text{total}} &= (16.9 \pm 5.9^{+1.0}_{-1.7} \pm 2.0 \pm 3.4) \\
&\quad + i(2.71 \pm 0.38^{+.68}_{-.51} \pm 0.33 \pm 0.54), \\
\hat{P}_{K\pi}^{\text{total}} &= (23.6 \pm 9.0^{+3.5}_{-2.8} \pm 2.8 \pm 4.7) \\
&\quad + i(3.57 \pm 0.53^{+.93}_{-.68} \pm 0.43 \pm 0.71), \\
\hat{P}_{\rho\rho}^{\text{total}} &= (23.3^{+3.7}_{-2.4} \pm 2.1 \pm 2.8 \pm 4.7) \\
&\quad + i(5.68^{+2.81+1.70}_{-1.75-1.25} \pm 0.68 \pm 1.14). \quad (139)
\end{aligned}$$

The first errors are from input parameters and are dominated by chiral-enhanced annihilation for $B \rightarrow \pi\pi, K\pi$. The second errors are our estimates of higher order perturbative corrections (the μ -variation). The third terms are errors from $|V_{ub}|$ which propagate through the form factors and hence can be added as a $\pm 12\%$ uncertainty.⁴ Finally the fourth errors are a generic 20% that we add for unknown power corrections.

For $\pi\pi$ the real part of the amplitude in Eq. (139) agrees with the data in table III for $\gamma = 59^\circ$. However, the same is not true for $K\pi$, nor even for $\pi\pi$ if $\gamma = 74^\circ$ (which is the value preferred by SU(3) and SCET power counting which predicts $\hat{P}_{\pi\pi} \simeq \hat{P}_{K\pi}$ [15]). Here the disagreement with data in the real part is at the level of factor of two.

On the other hand the imaginary part of the short-distance prediction for $\hat{P}^{\pi\pi}$ and $\hat{P}^{K\pi}$ are much smaller than the corresponding experimental values and have the opposite sign. Due to a numerical enhancement $\hat{P}_{M_1 M_2}^{\chi\zeta}$ and $\hat{P}_{M_1 M_2}^{\chi\zeta_J}$ are of same size as the leading power contributions to the amplitude, but as we have demonstrated by deriving an SCET_I factorization theorem, these terms are real at zeroth order in α_s . After taking into account all theoretical uncertainties in our analysis, we conclude that it is not possible to match the \hat{P} imaginary parts

⁴ We have increased the 7% error on $|V_{ub}|$ quoted by HFAG [1], which we consider to be overly optimistic.

obtained from experimental data. Therefore the large phase of the penguin relative to tree amplitudes can only be explained by long distance charm contribution, $\hat{P}_{c\bar{c}}$, within the standard model, or by contributions from new physics.

If the remainder is generated by long distance charm contributions, then we can determine what values of $\hat{P}_{c\bar{c}}^{M_1 M_2}$ reproduce the experimental data. This gives

$$\hat{P}_{c\bar{c}}^{\pi\pi} = \begin{cases} (1 \pm 11) - i(32 \pm 6) & (\gamma = 59^\circ) \\ (27 \pm 8) - i(32 \pm 6) & (\gamma = 74^\circ) \end{cases},$$

$$\hat{P}_{c\bar{c}}^{K\pi} = (24 \pm 14) - i(26 \pm 8), \quad (140)$$

where we have added the experimental and theoretical errors in quadrature. Thus a long-distance charm penguin with substantial imaginary amplitude is one possibility for reproducing the data. This explanation was favored in Refs. [3, 22, 23], and the analysis here makes the required size of these long-distance terms fairly precise. In the next section we contrast this long distance standard model explanation with the more exciting possibility of a new physics contribution. An additional test of the penguin amplitudes can be made from studying the channels $B^- \rightarrow \bar{K}^0 K^-$, $\bar{B}^0 \rightarrow K^0 \bar{K}^0$, and $\bar{B}^0 \rightarrow K^+ K^-$ which get contributions from penguin and annihilation/exchange type diagrams. Branching ratios for these channels are available [61]. Since for $B \rightarrow KK$ we do not have enough experimental information to fix ζ^{BK} and ζ_J^{BK} we resort to SU(3). We can apply SU(3) directly at the level of SCET amplitudes as discussed in Ref. [15], and it implies that $\hat{P}^{KK} \simeq \hat{P}^{K\pi}$ up to the small penguin annihilation terms. Using the experimental value of $\hat{P}_{TF}^{\text{expt}}(K\pi)$ from table III this value of \hat{P}^{KK} reproduces the data for $Br(B^- \rightarrow \bar{K}^0 K^-) = 1.36 \pm 0.28$ and $Br(\bar{B}^0 \rightarrow K^0 \bar{K}^0) = 0.96 \pm 0.20$ from HFAG [1]. The channel $\bar{B}^0 \rightarrow K^+ K^-$ does not get contributions from the penguin amplitudes \hat{P}^ζ , \hat{P}^{ζ_J} , nor the chirally enhanced penguin amplitudes as can be seen from Table I. It does get contributions from annihilation, but not from the potentially sizeable chirally enhanced penguin annihilation, $\hat{P}^{Lann\chi}$, as is clear from Table IV of Ref. [29]. Hence the small observed value $Br(\bar{B}^0 \rightarrow K^+ K^-) = 0.15 \pm 0.10$ is consistent with the size of the annihilation results for \hat{P}^{Lann} and \hat{P}^{Gann} in table II. The size of these amplitudes is also consistent with the power counting estimate of Λ/m_b suppression relative to leading order terms.

The experimental errors in $\hat{P}^{\rho\rho}$ are too large at this time to draw strong conclusions, but it is interesting to note that the positive sign for the real part of the short-distance standard model penguin prefers values of γ larger than 59° .

Our numerical results for the penguins can also be compared with earlier analyses in the BBNS [17, 27] and KLS [25, 26] approaches where light-cone sum-rules are used for the hadronic parameters. The BBNS analysis also gives numbers where $\hat{P}^\chi \sim \hat{P}^{\text{LO}}$, and gives small short-distance imaginary parts in \hat{P}^{LO} . However, indi-

vidual central values differ from ours due to their different method for dealing with input parameters and their use of an expansion in $\alpha_s(\mu_i)$ at the intermediate scale for the LO penguin and chiral enhanced penguin contributions. Also a larger (complex) range of annihilation amplitudes was adopted in Ref. [27], with a non-perturbative strong phase that can be chosen to fit the data. In the KLS approach it is more difficult to compare individual contributions, but generically the penguin amplitudes are somewhat larger, and have a large strong phase from annihilation graphs. The most prominent feature in both comparisons is that our parameter errors in \hat{P}^{LO} and \hat{P}^χ are significantly smaller than earlier results, due to our use of tree amplitude data to determine the hadronic parameters. From our numerical analysis of annihilation amplitudes, together with power counting arguments it appears that nonperturbative charm loops are the most likely culprit for a missing long-distance contribution to the amplitude.

XIV. PENGUINS CONTRIBUTIONS FROM NEW PHYSICS

There has been a lot of discussion about the possibility of new physics in nonleptonic B -decays (for example [31, 68, 69, 70, 71, 72, 73, 74, 75, 76, 77, 78]). The precision achieved for the computation of the standard model penguin amplitudes in tables II and III, and their lack of concordance with the experimental results, make it interesting to reexamine the role new physics contributions may play. In this section we aim to look at general features the new physics contributions should have, and do not attempt to explore this topic in specific models.

Lets consider adding new physics contributions to the nonleptonic amplitudes. Since new flavor-changing physics is likely to be heavy we can suppose that upon integrating out the short-distance new particles we generate a set of operators whose amplitude is parameterized by a CP-even matrix element N and a CP-violating phase ϕ , $\hat{A}^{NP} = N e^{i\phi}$. Here N contains the strong rescattering phase for the amplitude, and $e^{i\phi}$ has CP violation that need not follow the CKM paradigm.

In order to fit the data, i.e. contribute to $\text{Im}(\hat{P})$, we will demonstrate that $N e^{i\phi}$ must have a non-zero CP-even strong phase. Given this we may ask whether a small strong phase in N can be enhanced by a large new source of CP violation, or by some other new physics effect. We will see that there is a strict bound that prevents us from enhancing $\text{Im}(\hat{P})$ without having large $\text{Im}(N)$.

To study these points we follow Ref. [76] and use the fact that we can decompose any new physics amplitude into terms that simply shift the CP-even standard model amplitudes in Eq. (1). For example, we can decompose any $N e^{i\phi}$ to make it look like terms appearing in $B \rightarrow \pi\pi, K\pi, \rho\rho$:

$$N e^{i\phi} = N_1 + N_2 e^{-i\gamma}, \quad (141)$$

where the first terms acts like the $\lambda_c^{(d,s)}$ term and the second like $\lambda_u^{(d,s)}$. Here only ϕ and the standard model phase γ change sign under CP, while $N_1 = N_1^R + iN_1^I$ and $N_2 = N_2^R + iN_2^I$ are CP-even. Adding $Ne^{i\phi}$ terms to the SM amplitudes, we see that $N_{1,2}$ simply shift the SM amplitude parameters. Eq. (141) was used in Ref. [77] to point out that it is not possible to observe new physics in penguin amplitudes in decays like $B \rightarrow \pi\pi, K\pi$ without having information about the SM penguins that goes beyond isospin. Given the computations of the SM penguins in the previous section, we can use Eq. (141) to explore how new physics effects can appear. To generate large $\text{Im}(\hat{P})$ in our phase convention we need large $\text{Im}(N_1)$ and/or large $\text{Im}(N_2)$.

Being CP-even the parameters $N_{1,2}$ act like strong interaction amplitudes, despite the fact that they contain short-distance CP-violating parameters. Solving Eq. (141) gives

$$\begin{aligned} N_1^I &= \frac{\text{Im}(N)}{\sin\gamma} \sin(\gamma + \phi), & N_2^I &= -\frac{\text{Im}(N)}{\sin\gamma} \sin(\phi), \\ N_1^R &= \frac{\text{Re}(N)}{\sin\gamma} \sin(\gamma + \phi), & N_2^R &= -\frac{\text{Re}(N)}{\sin\gamma} \sin(\phi). \end{aligned} \quad (142)$$

Hence the shift to the imaginary part of the standard model amplitudes is zero if $\text{Im}(N) = 0$. Furthermore we have the bounds

$$|N_1^I| \leq \left| \frac{\text{Im}(N)}{\sin\gamma} \right|, \quad |N_2^I| \leq \left| \frac{\text{Im}(N)}{\sin\gamma} \right|. \quad (143)$$

The SM value of γ is not small ($\sin\gamma \sim 0.9$), so these bounds imply that enhancement in N_1^I or N_2^I requires large $\text{Im}(N)$, and hence a large strong phase for this new physics amplitude. Thus given $\sin\gamma$, no enhancement of the effective strong phase can occur due simply to new sources of CP-violation. This conclusion does not appear to be changed if one or more new physics amplitudes are added in the various standard model decay channels.

The CP-even phase in N will be generated by strong rescattering, and it is useful to consider N as an amplitude generated by new dimension-6 four-quark operators not present in the SM. Our analysis of SM four-quark operators gave power suppressed non-perturbative strong phases and small strong phases from hard penguin loops, so we might speculate that the same would be true for four-quark operators with non-SM symmetry properties. In this case the imaginary part of N will be small, and Eq. (143) implies that adding new physics will not significantly improve the situation with $\text{Im}(\hat{P})$. One might think that the inclusion of new physics into the process of extracting a value for \hat{P} could mollify the need for a large imaginary part. However, a simple analysis, say in the $\pi\pi$ modes, shows that the existence of an N with a small imaginary part can not lead to penguin completion. It will simply shift the meaning of the real parts of the tree and penguin amplitudes in the fit, with only a small change to the meaning of the imaginary parts.

Thus for new physics to play a significant role in the observed $\text{Im}(\hat{P})$ we need to find a large imaginary part for an N from analyzing an operator not generated by the standard model. Though there is no reason to expect an enhanced short-distance contribution, this is a logical possibility which deserves further study. Significant new physics contributions could in fact be obtained by modifying the coefficient of four-quark operators with charm quarks, since then a large long distance charming penguin amplitude could provide the necessary contribution in $\text{Im}(N)$. It might be interesting to attempt to construct explicit new physics models of this type which are not ruled out by other constraints on flavor changing neutral currents. Thus it seems to be quite a challenge to complete the penguin without the aid of a long-distance contribution.

XV. DISCUSSION AND CONCLUSION

Let us now address the question raised in the title. The results in table III show a lack of concordance between the theoretical prediction for the short-distance standard model penguin contributions and the extracted value for the penguin amplitude.⁵ Chirally enhanced operators substantially increase the penguin contributions, but they are not able to generate the necessary imaginary pieces. Thus it would seem that the shortfall must be due to either the long distance charm or new physics.

Before addressing these possibilities we must be assured that the assumptions leading to this conclusion are justified. Our theory predictions for SM penguins assume that the expansion in powers of Λ/m_b is trustworthy, since the convergence of this series is a necessary criteria for factorization to apply. The experimental extraction of $\hat{P}_{\pi\pi}$ and $\hat{P}_{\rho\rho}$ relies on isospin, and hence is quite robust. The penguin extraction for the $K\pi$ system relies slightly more on the factorization (the Λ/m_b expansion) since we use factorization for the tree amplitude $T^{K^+\pi^-}$.

What evidence do we have that the large mass expansion is indeed converging? The factorization theorem for color allowed $B \rightarrow D^{(*)}M^-$ decays (proven in [79]) agrees with data with the expected accuracy. For color suppressed charmed decays, $B \rightarrow D^{(*)}M^0$ the SCET prediction for the strong phases [38, 80] is in good accord with the data for many channels, which provides a non-trivial test of the large energy expansion. The same expansion is also used in analyzing the photon cut dependence of $B \rightarrow X_s\gamma$ [81] and for the analysis of $|V_{ub}|$ from $B \rightarrow X_u\ell\bar{\nu}$ [82], where power corrections appear with the expected size. One might object that these last two examples are inclusive, summing over states up to $\mu^2 \sim m_b\Lambda$. However, our analysis is quite similar, since

⁵ As shown in Eq. (15) for this conclusion uncertainties in the weak phase γ are irrelevant for $\text{Im}(\hat{P}_{\pi\pi})$, but not for $\text{Re}(\hat{P}_{\pi\pi})$.

the factorization theorems we use do not attempt to factorize physics below $\mu^2 \sim m_b \Lambda$, and instead retain it as form factors. Due to experimental cuts an analysis of $B \rightarrow X_s \ell^+ \ell^-$ data will also rely on this type of expansion [83].

More direct evidence for our methodology for analyzing charmless nonleptonic decays comes from successes in the exclusive modes themselves. In [15, 43], a complete list of the predictions for branching ratios and CP asymmetries was given, by using the data to fit the unknown hadronic parameters (including long-distance charm penguin amplitudes). The theory fits the data quite well, with all of the theory points falling within 1-2 σ of the data. (The only significant exception is the ratio of $A_{CP}(K^- \pi^0)/A_{CP}(K^- \pi^+)$ where the sign disagrees with the data.) It is interesting to note that SCET predicts certain asymmetries to be negative while the current experimental central values are positive. The factorization theorem for charmless nonleptonic decays also gives a prediction for $|V_{ub}|f_+(0)$ given in Eq. (20), which is in good agreement with the recent extractions based upon dispersion relations [84, 85] utilizing lattice data [62, 63, 64, 65]. (Using Hill's δ parameter [86] an analogous test will be possible for $\zeta_J^{B\pi}$ with future experimental improvements on the $B \rightarrow \pi \ell \bar{\nu}$ spectrum.) Note that for all of these successes the penguins were fit to the data and any deviation from the short distance prediction was absorbed into the long distance charm piece A_{cc} . Thus these successes do not directly imply convergence of the large energy expansion for the penguin amplitudes. However, from the point of view of QCD there is not much distinction between short distance tree and penguin contributions. Although the pattern of contributions to each of their amplitudes differs, the Λ/m_b expansion for each type of contribution involves very similar hadronic physics. An exception occurs for charm quarks, where the non-relativistic region and poorer convergence of the Λ/m_c expansion may play a role.

For the penguin amplitudes we can see from table III, that the chirally enhanced power correction is of the same order as the leading order penguin contribution. It is interesting to understand the origin of the enhancement for these power corrections. First off, the chiral condensate gives an enhancement of a factor of three [27]. As we discussed the chirally enhanced contribution also has a Wilson coefficient which gives an added numerical enhancement compared to leading order penguins by ~ 6 , coming from a factor of $1/(u\bar{u})$. One should worry that there could be higher dimensional operators which are chirally enhanced as well. However, for these operators to be as large as the leading chirally enhanced contribution they would have to have additional enhancement from their coefficient function. At present no such subleading operators are known to exist, but further investigation is warranted.

From the power counting and form of the factorization formulas for the nonleptonic amplitudes, terms with a long distance phase (outside of long-distance charm am-

plitudes P_{cc}) arise from contributions which are down by $\alpha(\mu_i)/\pi$ relative to the corrections considered in this paper, see [36]. In principle these corrections, which come in at order $\Lambda/m_b \alpha(\mu_i)/\pi$, as well as $\Lambda \mu_M/m_b^2 \alpha(\mu_i)/\pi$ (the chirally enhanced pieces), could account for the penguin deficit. However, this would be in gross violation of the power counting. Even if the expansion in $\alpha(\mu_i)$ were very poorly behaved, which seems not to be the case in the calculations performed to date [40], these contributions could still not make up the deficit, as they would be expected to be the same size as the chirally enhanced penguin annihilation (at best), shown in the last column in table II. Of course if the chirally enhanced annihilation were truly as big as the lower order terms in the power expansion, which our error in the table allows, then we would question the whole power expansion in the penguin sector. However, to push the penguin annihilation to the limits of our errors one needs large deviations from naturalness.

Two possible resolutions are, new physics and long distance charm. Let us consider the former possibility first. As we have shown in the previous section, introducing a large CP violating phase from new physics, does indeed have the effect of mimicking a CP conserving imaginary penguin, however its size is bounded by the strong phase induced by QCD. Thus, given that we have shown that such imaginary pieces (modulo A_{cc}) are small, it would seem to be a challenge to complete the penguin using new physics. One open possibility is that the new physics generates new operators not present in the standard model electro-weak Hamiltonian, that generate large imaginary parts when matching onto SCET₁. However, given our experience matching the standard model operators, there is no compelling reason to believe that such a scenario is likely.

In addition, generically, the new physics is constrained to only arise in certain operators. In particular, we note that the new physics would not fall under the rubric of Minimally Flavor Violation [66, 67], since there are strong constraints on ϵ' in the kaon system. This in itself is not a problem as one might expect the new physics to couple differently to the third generation, given the top quark mass. Furthermore the new physics should leave the $\Delta B = 2$ operators responsible for $B - \bar{B}$ mixing essentially unscathed. It would seem to be an interesting challenge to build a model which accomplishes these goal without fine-tunings.

Long distance charm contributions are perhaps the most compelling explanation for the penguin deficit. As was shown in section XIV current data appears to require a sizeable long-distance strong phase, such as the long-distance charm amplitude described in section IX. Moreover, the long distance charm has the potential to explain another discrepancy with the data [87], namely the deficit of transversely polarized vectors in the decay ϕK^* channel [3]. In SCET one does not generate any leading operators which produce transversely polarized vectors. This suppression follows from simple chi-

rality arguments [31]. To derive an amplitude factorization formula for the long distance charming penguins which generates transverse polarization was beyond the scope of this paper. However, it is simple to see that we would expect transverse polarization by noting that the helicity arguments mentioned above no longer apply because the valence quarks which make up the mesons are no longer produced on the light cone. Moreover, a post-diction of our SCET analysis method would be that one would expect a large transverse polarization fraction in the ϕK^* channel, but not in the $\rho\rho$, simply because the latter is tree dominated while the former is penguin, and hence A_{cc} dominated. Thus it would seem that the long distance charm contribution can explain both the penguin dearth as well as the transverse polarization in ϕK^* . Whereas a new physics scenario would seem to need some organizing principle which would lead to an enhanced $C_{3,4}$ coupling, the generation of a set of new operators to explain the polarization [31], and at the same time not disturb all the successes of the standard model in the B and K sectors. Recent work on the polarization question was done in Ref. [88] and [89].

Note: While this manuscript was in preparation Ref. [35] appeared where $\Delta b_4^{(f)}$ was also computed in the NDR scheme. We have verified that our result for $\Delta b_4^{(f)}$ in the NDR agrees with theirs as a function of u and z (they use a different basis, and the relevant comparison is for $2\Delta b_4^{(f)} - 2\Delta c_4^{(f)}$). Unlike Ref. [35], for the up and charm loops we demonstrated the simplicity of using the offshell UV subtraction procedure, and also presented the

computation in the HV scheme for γ_5 . Ref. [35] includes small $C_{i \geq 3} \alpha_s$ terms in $\Delta b_4^{(f)}$, which we neglected because they are expected to compete with other terms of similar numerical size (such as the complete two-loop corrections with C_1) which remain unknown. We also derived a new factorization theorem for chirally enhanced penguins, and demonstrated that only the short-distance perturbative coefficients give imaginary parts to the corresponding amplitudes. In contrast Ref. [35] includes a complex hadronic parameter in their modeling of the analogous terms which they obtain with an additional expansion in $\alpha_s(\mu_i)$, where $\mu_i^2 \simeq E\Lambda$ is the intermediate scale. Finally our phenomenological analysis differs from Ref. [35]. Our strategy was to avoid expanding in $\alpha_s(\mu_i)$, and to use data on the tree-amplitudes to determine the most important non-perturbative parameters. This allowed us to reduce the model uncertainty considerably while still predicting the penguin amplitudes. In contrast Ref. [35] models all non-perturbative parameters, and hence has larger parameter uncertainty in their final result.

We thank C. Arnesen, Z. Ligeti and J. Zupan for their comments on the manuscript. This work was supported in part by the DOE under DE-FG03-91-ER40683, and by the DOE Office of Nuclear Science under the grant DE-FG02-94ER40818. I.S. was also supported in part by the DOE Outstanding Junior Investigator program and Sloan Foundation.

APPENDIX A: ONE-LOOP FUNCTIONS

In this appendix we quote some of the basic loop integrals used in the text. We work in $d = 4 - 2\epsilon$ dimensions in the $\overline{\text{MS}}$ scheme, and the $(4\pi)^{-1} e^{\gamma_E}$ constant is absorbed in momentum subtraction scale μ^2 . The basic loop integrals J_0 and $I_0(q^2)$ are defined as,

$$\begin{aligned}
J_0(p, q) &= \left(\frac{16\pi^2}{i} \right) \cdot \int \frac{d^d k}{(2\pi)^d} \frac{1}{[k^2 - m_c^2]} \frac{1}{[(k+p)^2 - m_c^2]} \frac{1}{[(k-q)^2 - m_c^2]} \\
&= \frac{1}{2p \cdot q} \left[\text{Li}_2 \left(\frac{2}{1 - \sqrt{1 - 4m_c^2/q^2}} \right) + \text{Li}_2 \left(\frac{2}{1 + \sqrt{1 - 4m_c^2/q^2}} \right) \right. \\
&\quad \left. - \text{Li}_2 \left(\frac{2}{1 + \sqrt{1 - 4m_c^2/(p+q)^2}} \right) - \text{Li}_2 \left(\frac{2}{1 - \sqrt{1 - 4m_c^2/(p+q)^2}} \right) \right], \\
I_0(q^2) &= \left(\frac{16\pi^2}{i} \right) \cdot \int \frac{d^d k}{(2\pi)^d} \frac{1}{(k^2 - m_c^2)} \frac{1}{((k-q)^2 - m_c^2)} = \frac{1}{\epsilon} + \bar{I}_0(q^2) \\
\bar{I}_0(q^2) &= 2 + \ln \left(\frac{\mu^2}{m_c^2} \right) - \theta(q^2 - 4m_c^2) \sqrt{1 - 4m_c^2/q^2} \left\{ \ln \left(\frac{1 + \sqrt{1 - 4m_c^2/q^2}}{1 - \sqrt{1 - 4m_c^2/q^2}} \right) - i\pi \right\} \\
&\quad - 2\theta(4m_c^2 - q^2) \sqrt{4m_c^2/q^2 - 1} \cot^{-1} \left(\sqrt{4m_c^2/q^2 - 1} \right), \tag{A1}
\end{aligned}$$

Some limits for these functions are

$$\begin{aligned}
I_0^{(u)}(q^2) &\equiv \lim_{m_c \rightarrow 0} I_0(q^2) = \frac{1}{\epsilon} + 2 + \ln \left(\frac{\mu^2}{q^2} \right) + i\pi, \\
I_0 &\equiv \lim_{q^2 \rightarrow 0} I_0(q^2) = \frac{1}{\epsilon} + \ln \left(\frac{\mu^2}{m_c^2} \right), \\
\bar{I}_0^{(u)}(q^2) &= 2 + \ln \left(\frac{\mu^2}{q^2} \right) + i\pi, \\
\bar{I}_0 &= \ln \left(\frac{\mu^2}{m_c^2} \right). \tag{A2}
\end{aligned}$$

The combinations of these integrals that appear in the

body of the paper are

$$\begin{aligned} h_0^c(u, z, \rho) &= m_c^2 J_0(p, q), \\ \bar{I}_0(q^2) &= G \left(\frac{q^2}{m_b^2}, \rho \right), \\ \bar{I}_0^{(u)}(q^2) &= G_0 \left(\frac{q^2}{m_b^2} \right), \end{aligned} \quad (\text{A3})$$

where u and z are momentum fractions of quarks in M_1 and M_2 respectively. Notice that functions $h_i^p(u, z)$ are finite and dimensionless. Change of the functional dependence from square of momenta to momentum fractions comes from the relations $q^2 = m_b^2(1-u)z$ and $(p+q)^2 = m_b^2(1-u)$.

We also list some useful Fierz relations. For convenience we define,

$$\begin{aligned} P^{\lambda a} &= [\bar{q}_n \gamma_\perp^\lambda T^a P_L b_v] [\bar{d}_n \not{\eta} P_L q_n] \\ V^{\lambda a} &= [\bar{q}_n T^a P_L b_v] [\bar{d}_n \not{\eta} \gamma_\perp^\lambda P_R q_n]. \end{aligned}$$

Feirzing gives following formulas useful for simplification,

$$\begin{aligned} \epsilon_\perp^{\lambda\mu} [\bar{d}_n \not{\eta} P_L b_v] [\bar{q}_n \gamma_{\perp\mu} T^a q_n] &= -\frac{i}{3} (P^{\lambda a} - V^{\lambda a}), \\ d^{abc} \epsilon_\perp^{\lambda\mu} [\bar{d}_n \not{\eta} P_L T^c b_v] [\bar{q}_n \gamma_{\perp\mu} T^b q_n] &= -\frac{i5}{18} (P^{\lambda a} - V^{\lambda a}), \\ f^{abc} [\bar{d}_n \not{\eta} P_L T^c b_v] [\bar{q}_n \gamma_\perp^\lambda T^b q_n] &= -\frac{i}{2} (P^{\lambda a} + V^{\lambda a}), \\ [\bar{d}_n \not{\eta} P_L \gamma_\perp^\lambda \gamma_\perp^\mu b_v] [\bar{q}_n \gamma_{\perp\mu} T^a q_n] &= -\frac{2}{3} V^{\lambda a}, \\ [\bar{d}_n \not{\eta} P_L \gamma_\perp^\mu \gamma_\perp^\lambda b_v] [\bar{q}_n \gamma_{\perp\mu} T^a q_n] &= -\frac{2}{3} P^{\lambda a}, \\ [\bar{d}_n \not{\eta} P_L b_v] [\bar{q}_n \gamma_\perp^\lambda T^a q_n] &= -\frac{1}{3} (P^{\lambda a} + V^{\lambda a}). \end{aligned} \quad (\text{A4})$$

These results include the minus sign from permuting fermion fields.

APPENDIX B: CHIRALY ENHANCED TERMS IN SCET_{II}

In section VIII we made the statement that the operators $Q_i^{(2\chi)*}$ in Eq. (77) only contribute for B^* decays. The simplest way to verify this statement is to consider the Dirac structures generated by matching the T_2 time-ordered product of these operators onto operators in SCET_{II}. This can be done working to all orders in α_s . From Ref. [3] the most general perturbative matching generates Wilson coefficients given by jet functions J and J_\perp whose form is constrained by RPI, chirality, power counting and dimensional analysis [$\omega_1 = z\omega$,

$$\begin{aligned} \omega_4 &= (1-z)\omega, \bar{x} = 1-x, \chi_{n,\omega} = (W^\dagger \xi_n)_\omega, \\ T [(\bar{\xi}_n W)_{\omega_1} i g \mathcal{B}_{n,\omega_4}^{\perp\alpha} P_{R,L}]^{ia} (0) [i g \mathcal{B}_n^{\perp\alpha} W^\dagger \xi_n]^{jb} (y) \\ &= i \delta^{ab} \delta(y^+) \delta^{(2)}(y_\perp) \frac{1}{\omega} \int_0^1 dx \int \frac{dk^+}{2\pi} e^{+ik^+ y^- / 2} \\ &\times \left\{ -J_\perp(z, x, k_+) \left(\frac{\not{\eta}}{2} P_{R,L} \gamma_\perp^\alpha \gamma_\perp^\beta \right)_{ji} [\bar{\chi}_{n,x\omega}^{L,R} \not{\eta} \gamma_\beta^\perp \chi_{n,-\bar{x}\omega}^{R,L}] \right. \\ &\left. + J(z, x, k_+) \left(\not{\eta} P_{L,R} \gamma_\perp^\alpha \right)_{ji} [\bar{\chi}_{n,x\omega}^{L,R} \not{\eta} \chi_{n,-\bar{x}\omega}^{L,R}] \right\}, \end{aligned} \quad (\text{B1})$$

where $\{i, j\}$ and $\{a, b\}$ are spin and color indices. This result on the RHS includes the sign from antipermuting the fermion fields that are contracted with the spin indices ij . To use this formula other Dirac structures occurring in the T_2 time-ordered product should be grouped with the heavy-quark field h_v and soft-quark field \bar{q}_s . Using Eq. (B1) we find that all the operators $Q_i^{(2\chi)*}$ give the structure $\bar{q}_s \not{\eta} \gamma_\perp^\alpha h_v$ which has a vanishing B -meson matrix element, but would be nonzero for B^* initial states.

In section VIII we used $\zeta_\chi^{BM}(z) \sim z$ which followed from the power counting in SCET_I that indicates that it can not be more singular than $\zeta_J^{BM}(z)$. We also stated that this scaling could be checked by factorizing the SCET_I time-ordered product that defines this form factor using SCET_{II}. To do so we again use Eq. (B1) and take the matrix element of the resulting operators to find

$$\zeta_\chi^{BM}(z) = \frac{f_B f_M}{m_b} \int_0^1 dx \int_0^\infty dk^+ \frac{J_\perp(z, k^+, x)}{1-z} \phi_B^+(k^+) \phi_{pp}^M(x). \quad (\text{B2})$$

Here $J_\perp(z, x, k_+) = \delta(x-z) \pi \alpha_s(\mu) C_F / (N_c \bar{x} k_+)$ at lowest order, so the behavior of $\zeta_\chi^{BM}(z)$ as $z \rightarrow 0$ is inherited from $\phi_{pp}^M(x)$ as $x \rightarrow 0$, giving linear scaling $\propto z$. The one-loop result for J_\perp is also known [40, 41] and the linear scaling is reproduced at this order. The limit $x \rightarrow 0$ corresponds to the collinear quark in the form factor becoming soft, and for this matrix element there is no corresponding diagram with a soft quark at this order. Hence, because we do not expect an overlap with a soft diagram, we do not expect there is a need for any zero-bin subtractions, and hence no endpoint divergences which would result from constant scaling as $z \rightarrow 0$. The other interesting limit is $z \rightarrow 1$, where we expect $\zeta_\chi^{BM}(z) \sim 1$. From the point of view of SCET_{II} this limit is more interesting because there are diagrams with soft antiquarks in the form factor, and we must avoid double counting them. Indeed the tree level jet function appears to give $\zeta_\chi^{BM}(z) \sim \phi_{pp}^M(z) / (1-z)^2$, which would imply singular behavior as $z \rightarrow 1$. However in SCET_{II} to avoid double counting the region where this quark is soft we must make zero-bin subtractions in defining this singular moment [30]. These subtractions modify the distribution, causing scaling behavior of $\phi_{pp}^{0-bin}(z) \sim (1-z)^2$ in the endpoint region (and also generate dependence of this distribution on an additional rapidity parameter). The result is that as $z \rightarrow 1$, $\zeta_\chi^{BM}(z) \sim 1$ as expected from power counting in SCET_I.

APPENDIX C: BETA'S AT $\mu = m_b/2$ AND $\mu = 2m_b$ also required the values at $\mu = m_b/2 = 2.3$ GeV

In Eq. (119) we quoted values for the annihilation moments at $\mu = m_b = 4.7$ GeV. For our error analysis we

$$\begin{aligned}
\beta_{1c}^{\pi\pi} &= (-5.5 \pm 3.0) \times 10^{-2}, & \beta_{3c}^{\pi\pi} &= 1.15 \pm 0.58, & \beta_{4c}^{\pi\pi} &= -0.25 \pm 0.15, & & & & (C1) \\
\beta_{hc1}^{\pi\pi} &= -2.35 \pm 0.78, & \beta_{hc2}^{\pi\pi} &= 0.61 \pm 0.34, & \beta_{hc3}^{\pi\pi} &= (4.4 \pm 5.3) \times 10^{-3}, & \beta_{hc4}^{\pi\pi} &= (-8.6 \pm 2.8) \times 10^{-2}, \\
\beta_{\chi_1}^{\pi\pi} &= 0.0 \pm 9.7, & \beta_{\chi_2}^{\pi\pi} &= 0.0 \pm 9.1, & \beta_{\chi_5}^{\pi\pi} &= 0.0 \pm 0.13, & \beta_{\chi_6}^{\pi\pi} &= 0.0 \pm 0.16, \\
\beta_{4c}^{\pi K} &= -0.27 \pm 0.11, & & & & & & & & \\
\beta_{hc1}^{\pi K} &= -2.45 \pm 0.80, & \beta_{hc2}^{\pi K} &= 0.61 \pm 0.34, & \beta_{hc3}^{\pi K} &= (0.8 \pm 5.5) \times 10^{-3}, & \beta_{hc4}^{\pi K} &= (-8.6 \pm 2.7) \times 10^{-2}, \\
\beta_{\chi_1}^{\pi K} &= 0.0 \pm 12.3, & \beta_{\chi_2}^{\pi K} &= 0.0 \pm 11.2, & \beta_{\chi_5}^{\pi K} &= 0.0 \pm 0.17, & \beta_{\chi_6}^{\pi K} &= 0.0 \pm 0.20, \\
\beta_{1c}^{\rho\rho} &= (9.2_{-2.5}^{+7.6}) \times 10^{-3}, & \beta_{3c}^{\rho\rho} &= -0.19_{-0.05}^{+0.16}, & \beta_{4c}^{\rho\rho} &= (4.3_{-1.2}^{+3.5}) \times 10^{-2}, & & & & \\
\beta_{hc1}^{\rho\rho} &= (-7.0_{-5.3}^{+6.1}) \times 10^{-2}, & \beta_{hc2}^{\rho\rho} &= (-1.4_{-1.1}^{+1.4}) \times 10^{-2}, & \beta_{hc3}^{\rho\rho} &= (-1.4_{-1.0}^{+1.2}) \times 10^{-4}, & \beta_{hc4}^{\rho\rho} &= (2.6_{-2.0}^{+2.2}) \times 10^{-3},
\end{aligned}$$

and at $\mu = 2m_b$

$$\begin{aligned}
\beta_{1c}^{\pi\pi} &= (-1.6 \pm 0.9) \times 10^{-2}, & \beta_{3c}^{\pi\pi} &= 0.35 \pm 0.18, & \beta_{4c}^{\pi\pi} &= -0.089 \pm 0.054, & & & & (C2) \\
\beta_{hc1}^{\pi\pi} &= -0.73 \pm 0.23, & \beta_{hc2}^{\pi\pi} &= -0.015 \pm 0.040, & \beta_{hc3}^{\pi\pi} &= (-4.9 \pm 0.8) \times 10^{-3}, & \beta_{hc4}^{\pi\pi} &= (-3.7 \pm 1.1) \times 10^{-2}, \\
\beta_{\chi_1}^{\pi\pi} &= 0.0 \pm 2.7, & \beta_{\chi_2}^{\pi\pi} &= 0.0 \pm 2.5, & \beta_{\chi_5}^{\pi\pi} &= 0.0 \pm 0.040, & \beta_{\chi_6}^{\pi\pi} &= 0.0 \pm 0.053, \\
\beta_{4c}^{\pi K} &= -0.095 \pm 0.069, & & & & & & & & \\
\beta_{hc1}^{\pi K} &= -0.76 \pm 0.24, & \beta_{hc2}^{\pi K} &= -0.015 \pm 0.040, & \beta_{hc3}^{\pi K} &= (-4.9 \pm 0.8) \times 10^{-3}, & \beta_{hc4}^{\pi K} &= (-3.7 \pm 1.1) \times 10^{-2}, \\
\beta_{\chi_1}^{\pi K} &= 0.0 \pm 3.4, & \beta_{\chi_2}^{\pi K} &= 0.0 \pm 3.0, & \beta_{\chi_5}^{\pi K} &= 0.0 \pm 0.051, & \beta_{\chi_6}^{\pi K} &= 0.0 \pm 0.065, \\
\beta_{1c}^{\rho\rho} &= (2.7_{-0.7}^{+2.2}) \times 10^{-3}, & \beta_{3c}^{\rho\rho} &= -0.06_{-0.02}^{+0.05}, & \beta_{4c}^{\rho\rho} &= (1.5_{-0.4}^{+1.2}) \times 10^{-2}, & & & & \\
\beta_{hc1}^{\rho\rho} &= (-2.2_{-1.7}^{+1.9}) \times 10^{-2}, & \beta_{hc2}^{\rho\rho} &= (1.7_{-1.3}^{+1.3}) \times 10^{-3}, & \beta_{hc3}^{\rho\rho} &= (-2.1 \pm 1.7) \times 10^{-4}, & \beta_{hc4}^{\rho\rho} &= (1.1_{-0.9}^{+1.0}) \times 10^{-3}.
\end{aligned}$$

- [1] A summary of experimental results is given by the Heavy Flavor Averaging Group [HFAG]: <http://www.slac.stanford.edu/xorg/hfag/>
- [2] See Refs. [7,8,11-18,22-29,37-43,71].
- [3] C. W. Bauer, D. Pirjol, I. Z. Rothstein and I. W. Stewart, Phys. Rev. D **70**, 054015 (2004) [arXiv:hep-ph/0401188].
- [4] M. Gronau and J. Zupan, Phys. Rev. D **71**, 074017 (2005) [arXiv:hep-ph/0502139].
- [5] S. Gardner, Phys. Rev. D **59**, 077502 (1999) [arXiv:hep-ph/9806423].
- [6] B. Aubert *et al.* [BABAR Collaboration], Phys. Rev. Lett. **97**, 261801 (2006) [arXiv:hep-ex/0607092]. J. Zhang *et al.* [BELLE Collaboration], Phys. Rev. Lett. **91**, 221801 (2003) [arXiv:hep-ex/0306007]. B. Aubert *et al.* [BABAR Collaboration], arXiv:hep-ex/0607098. A. Somov *et al.*, Phys. Rev. Lett. **96**, 171801 (2006) [arXiv:hep-ex/0601024]. B. Aubert *et al.* [BABAR Collaboration], Phys. Rev. Lett. **98**, 111801 (2007) [arXiv:hep-ex/0612021].
- [7] A. F. Falk, Z. Ligeti, Y. Nir and H. Quinn, Phys. Rev. D **69**, 011502 (2004) [arXiv:hep-ph/0310242].
- [8] J. Charles *et al.* [CKMfitter Group], Eur. Phys. J. C **41**, 1 (2005) [hep-ph/0406184].
- [9] M. Bona *et al.* [UTfit Collaboration], arXiv:hep-ph/0509219; [http://utfit.roma1.infn.it/]
- [10] M. Gronau and D. London, Phys. Rev. Lett. **65**, 3381 (1990).
- [11] C. W. Bauer, I. Z. Rothstein and I. W. Stewart, Phys. Rev. Lett. **94**, 231802 (2005) [arXiv:hep-ph/0412120].
- [12] B. Aubert *et al.* [BABAR Collaboration], arXiv:hep-ex/0703016. K. Abe [Belle Collaboration], Phys. Rev. Lett. **98**, 211801 (2007) [arXiv:hep-ex/0608035]. B. Aubert *et al.* [BABAR Collaboration], Phys. Rev. D **75**, 012008 (2007) [arXiv:hep-ex/0608003]. K. Abe *et al.*, arXiv:hep-ex/0609015; and talk by Y. Unno presented at ICHEP06 (2006). M. Morello [CDF Collaboration], arXiv:hep-ex/0612018.
- [13] Y. Grossman, A. Hocker, Z. Ligeti and D. Pirjol, Phys. Rev. D **72**, 094033 (2005) [arXiv:hep-ph/0506228].
- [14] A. Ali, E. Lunghi and A. Y. Parkhomenko, arXiv:hep-ph/0403275.
- [15] C. W. Bauer, I. Z. Rothstein and I. W. Stewart, Phys.

- Rev. D **74**, 034010 (2006) [arXiv:hep-ph/0510241].
- [16] J.g. Chay and C. Kim, Phys. Rev. D **68**, 071502 (2003); arXiv:hep-ph/0301262.
- [17] M. Beneke, G. Buchalla, M. Neubert and C. T. Sachrajda, Phys. Rev. Lett. **83**, 1914 (1999).
- [18] S. Descotes-Genon, J. Matias and J. Virto, Phys. Rev. Lett. **97** (2006) 061801 [arXiv:hep-ph/0603239]; S. Descotes-Genon, J. Matias and J. Virto, arXiv:0705.0477[hep-ph].
- [19] A. J. Buras, R. Fleischer, S. Recksiegel and F. Schwab, Nucl. Phys. B **697**, 133 (2004) [arXiv:hep-ph/0402112].
- [20] C. W. Chiang, M. Gronau, J. L. Rosner and D. A. Suprun, Phys. Rev. D **70**, 034020 (2004) [arXiv:hep-ph/0404073].
- [21] C.W. Bauer, S. Fleming and M.E. Luke, Phys. Rev. D **63**, 014006 (2001); C.W. Bauer, S. Fleming, D. Pirjol and I.W. Stewart, Phys. Rev. D **63**, 114020 (2001); C.W. Bauer and I.W. Stewart, Phys. Lett. B **516**, 134 (2001); C.W. Bauer, D. Pirjol and I.W. Stewart, Phys. Rev. D **65**, 054022 (2002).
- [22] M. Ciuchini, E. Franco, G. Martinelli and L. Silvestrini, Nucl. Phys. B **501**, 271 (1997); M. Ciuchini et al., Phys. Lett. B **515**, 33 (2001).
- [23] P. Colangelo, G. Nardulli, N. Paver and Riazuddin, Z. Phys. C **45**, 575 (1990).
- [24] C. W. Bauer, D. Pirjol, I. Z. Rothstein and I. W. Stewart, Phys. Rev. D **72**, 098502 (2005) [arXiv:hep-ph/0502094].
- [25] Y.Y. Keum, H.n. Li and A.I. Sanda, Phys. Lett. B **504**, 6 (2001); Phys. Rev. D **63**, 054008 (2001).
- [26] C. D. Lu, K. Ukai and M. Z. Yang, Phys. Rev. D **63**, 074009 (2001).
- [27] M. Beneke, G. Buchalla, M. Neubert and C. T. Sachrajda, Nucl. Phys. B **606**, 245 (2001). M. Beneke and M. Neubert, Nucl. Phys. B **675**, 333 (2003).
- [28] C. M. Arnesen, I. Z. Rothstein and I. W. Stewart, arXiv:hep-ph/0611356.
- [29] C. M. Arnesen, Z. Ligeti, I. Z. Rothstein and I. W. Stewart, arXiv:hep-ph/0607001.
- [30] Aneesh V. Manohar and Iain W. Stewart, hep-ph/0605001.
- [31] A. L. Kagan, Phys. Lett. B **601**, 151 (2004) [arXiv:hep-ph/0405134].
- [32] M. Beneke, J. Rohrer and D. Yang, Phys. Rev. Lett. **96**, 141801 (2006) [arXiv:hep-ph/0512258].
- [33] For a recent review see E. Lunghi, PoS **HEP2005**, 278 (2006).
- [34] G. Bell, talk given at SCET'07, Berkeley, CA, <http://scet07.lbl.gov>, arXiv:0705.3127 [hep-ph].
- [35] M. Beneke and S. Jager, arXiv:hep-ph/0610322.
- [36] M. C. Arnesen, B. Grinstein, I. Z. Rothstein and I. W. Stewart, Phys. Rev. Lett. **95**, 071802 (2005) [arXiv:hep-ph/0504209].
- [37] A. P. Bakulev, S. V. Mikhailov and N. G. Stefanis, Phys. Lett. B **578**, 91 (2004) [arXiv:hep-ph/0303039].
- [38] S. Mantry, D. Pirjol and I.W. Stewart, Phys. Rev. D **68**, 114009 (2003).
- [39] G. Buchalla, A.J. Buras and M.E. Lautenbacher, Rev. Mod. Phys. **68**, 1125 (1996).
- [40] T. Becher and R. J. Hill, JHEP **0410**, 055 (2004) [arXiv:hep-ph/0408344].
- [41] M. Beneke and D. Yang, Nucl. Phys. B **736**, 34 (2006) [arXiv:hep-ph/0508250].
- [42] M. Beneke and S. Jager, Nucl. Phys. B **751**, 160 (2006) [arXiv:hep-ph/0512351].
- [43] A. R. Williamson and J. Zupan, Phys. Rev. D **74**, 014003 (2006) [Erratum-ibid. D **74**, 03901 (2006)] [arXiv:hep-ph/0601214].
- [44] C.W. Bauer, D. Pirjol and I.W. Stewart, Phys. Rev. D **67**, 071502 (2003).
- [45] D. Pirjol and I.W. Stewart, Phys. Rev. D **67**, 094005 (2003); for $B \rightarrow V$ see *ibid.*, arXiv:hep-ph/0309053.
- [46] C.W. Bauer, D. Pirjol and I.W. Stewart, Phys. Rev. D **68**, 034021 (2003).
- [47] A. J. Buras, arXiv:hep-ph/9806471.
- [48] K. G. Chetyrkin, M. Misiak and M. Munz, Nucl. Phys. B **520**, 279 (1998) [arXiv:hep-ph/9711280].
- [49] S. Wandzura and F. Wilczek, Phys. Lett. B **72**, 195 (1977).
- [50] A. Hardmeier, E. Lunghi, D. Pirjol and D. Wyler, Nucl. Phys. B **682**, 150 (2004) [arXiv:hep-ph/0307171].
- [51] J. Chay, C. Kim, A. K. Leibovich and J. Zupan, Phys. Rev. D **74**, 074022 (2006) [arXiv:hep-ph/0607004].
- [52] M. E. Luke, A. V. Manohar and I. Z. Rothstein, Phys. Rev. D **61**, 074025 (2000) [arXiv:hep-ph/9910209].
- [53] C. W. Bauer, S. Fleming, D. Pirjol, I. Z. Rothstein and I. W. Stewart, Phys. Rev. D **66**, 014017 (2002) [arXiv:hep-ph/0202088].
- [54] W. M. Yao *et al.* [Particle Data Group], J. Phys. G **33**, 1 (2006).
- [55] A. Gray *et al.* [HPQCD Collaboration], Phys. Rev. Lett. **95**, 212001 (2005) [arXiv:hep-lat/0507015].
- [56] V. M. Braun *et al.*, Phys. Rev. D **74**, 074501 (2006) [arXiv:hep-lat/0606012].
- [57] P. Ball, V. M. Braun and A. Lenz, JHEP **0605**, 004 (2006) [arXiv:hep-ph/0603063].
- [58] P. Ball and G. W. Jones, JHEP **0703**, 069 (2007) [arXiv:hep-ph/0702100].
- [59] P. Ball and R. Zwicky, JHEP **0110**, 019 (2001).
- [60] C. W. Bauer and D. Pirjol, Phys. Lett. B **604**, 183 (2004) [arXiv:hep-ph/0408161].
- [61] B. Aubert *et al.* [BABAR Collaboration], Phys. Rev. Lett. **97**, 171805 (2006) [arXiv:hep-ex/0608036]; K. Abe *et al.* [Belle Collaboration], arXiv:hep-ex/0608049; and the last reference in [12].
- [62] M. Okamoto *et al.*, Nucl. Phys. Proc. Suppl. **140**, 461 (2005) [arXiv:hep-lat/0409116].
- [63] P. B. Mackenzie *et al.* [Fermilab Lattice, MILC and HPQCD Collaborations], PoS **LAT2005**, 207 (2006).
- [64] Fermilab Lattice, MILC and HPQCD Collaboration, P.B. Mackenzie et. al., PoS **LAT2005**.
- [65] R.S. Van de Water and P. Mackenzie, PoS **LAT2006**, 097 (2006).
- [66] G. D'Ambrosio, G. F. Giudice, G. Isidori and A. Strumia, Nucl. Phys. B **645**, 155 (2002) [arXiv:hep-ph/0207036].
- [67] A. J. Buras, P. Gambino, M. Gorbahn, S. Jager and L. Silvestrini, Phys. Lett. B **500**, 161 (2001) [arXiv:hep-ph/0007085].
- [68] T. Yoshikawa, Phys. Rev. D **68**, 054023 (2003) [arXiv:hep-ph/0306147].
- [69] A. J. Buras, R. Fleischer, S. Recksiegel and F. Schwab, Eur. Phys. J. C **32**, 45 (2003) [arXiv:hep-ph/0309012].
- [70] Y. Grossman, Int. J. Mod. Phys. A **19**, 907 (2004) [arXiv:hep-ph/0310229].
- [71] A. J. Buras, R. Fleischer, S. Recksiegel and F. Schwab, Nucl. Phys. B **697**, 133 (2004) [arXiv:hep-ph/0402112]; Acta Phys. Polon. B **36**, 2015 (2005) [arXiv:hep-ph/0410407].
- [72] A. Datta and D. London, Phys. Lett. B **595**, 453 (2004)

- [arXiv:hep-ph/0404130].
- [73] S. Mishima and T. Yoshikawa, Phys. Rev. D **70**, 094024 (2004) [arXiv:hep-ph/0408090].
- [74] J. L. . Hewett *et al.*, arXiv:hep-ph/0503261.
- [75] K. Agashe, M. Papucci, G. Perez and D. Pirjol, arXiv:hep-ph/0509117.
- [76] F. J. Botella and J. P. Silva, Phys. Rev. D **71**, 094008 (2005) [arXiv:hep-ph/0503136].
- [77] M. Imbeault, D. London, C. Sharma, N. Sinha and R. Sinha, arXiv:hep-ph/0608169.
- [78] L. Silvestrini, arXiv:0705.1624 [hep-ph].
- [79] C. W. Bauer, D. Pirjol and I. W. Stewart, Phys. Rev. Lett. **87**, 201806 (2001) [arXiv:hep-ph/0107002].
- [80] A. E. Blechman, S. Mantry and I. W. Stewart, Phys. Lett. B **608**, 77 (2005) [arXiv:hep-ph/0410312].
- [81] T. Becher and M. Neubert, Phys. Rev. Lett. **98**, 022003 (2007) [arXiv:hep-ph/0610067].
- [82] B. O. Lange, M. Neubert and G. Paz, Phys. Rev. D **72**, 073006 (2005) [arXiv:hep-ph/0504071].
- [83] K. S. M. Lee, Z. Ligeti, I. W. Stewart and F. J. Tackmann, Phys. Rev. D **74**, 011501 (2006) [arXiv:hep-ph/0512191]; K. S. M. Lee and I. W. Stewart, Phys. Rev. D **74**, 014005 (2006) [arXiv:hep-ph/0511334].
- [84] I. W. Stewart, talk on “Dispersion Relations” at CKM’2006, <http://agenda.hepl.phys.nagoya-u.ac.jp/conferenceDisplay.py?confId=2#2>
- [85] J. M. Flynn and J. Nieves, arXiv:0705.3553 [hep-ph].
- [86] R. J. Hill, Phys. Rev. D **73**, 014012 (2006) [arXiv:hep-ph/0505129].
- [87] B. Aubert *et al.* [BABAR Collaboration], Phys. Rev. Lett. **97**, 201801 (2006) [arXiv:hep-ex/0607057]. K. Abe *et al.* [BELLE-Collaboration], Phys. Rev. Lett. **95**, 141801 (2005) [arXiv:hep-ex/0408102]. B. Aubert *et al.* [BABAR Collaboration], Phys. Rev. Lett. **98**, 051801 (2007) [arXiv:hep-ex/0610073]. K. F. Chen *et al.* [BELLE Collaboration], Phys. Rev. Lett. **94**, 221804 (2005) [arXiv:hep-ex/0503013].
- [88] A. Datta, A. V. Gritsan, D. London, M. Nagashima and A. Szykman, arXiv:0705.3915 [hep-ph].
- [89] M. Beneke, J. Rohrer and D. Yang, Nucl. Phys. B **774**, 64 (2007) [arXiv:hep-ph/0612290].